

Centro de Investigación Científica y de Educación Superior de
Ensenada, Baja California



Sciences Postgraduate Program in Electronics and Telecommunications
with orientation in High Frequency Electronics

**The impact of VNA calibration techniques on the load-pull characterization of
microwave power transistors**

Dissertation

submitted in partial fulfillment of the requirements for the degree of

Doctor in Sciences

Presents:

Manuel Alejandro Pulido Gaytán

Ensenada, Baja California, Mexico

2016

Dissertation defended by

Manuel Alejandro Pulido Gaytán

and approved by the following committee

Dr. J. Apolinar Reynoso Hernández

Thesis Advisor

Dra. María del Carmen Maya Sánchez

Dr. José Raúl Loo Yau

Dr. Arturo Velázquez Ventura

Dr. Enrique Mitrani Abenchuchan

Dr. Roberto Stack Murphy Arteaga



Dr. Miguel Ángel Alonso Arévalo

Head of the Postgraduate Programm in
Electronics and Telecommunications

Dra. Rufina Hernández Martínez

Head of the Postgraduate Studies Program

Manuel Alejandro Pulido Gaytán ©2016

Total or partial reproduction of this document without the express authorisation of the author and thesis advisor is prohibited

Resumen de la tesis de **Manuel Alejandro Pulido Gaytán**, presentada como requisito parcial para la obtención del grado de Doctor en Ciencias en Electrónica y Telecomunicaciones con orientación en Electrónica de Altas Frecuencias. Ensenada, Baja California, Agosto 2016.

Impacto de las técnicas de calibración para el ARV en la caracterización de transistores de potencia de microondas mediante sistemas de sintonización de carga

Resumen aprobado por:

Dr. J. Apolinar Reynoso Hernández

Director de Tesis

Los amplificadores de potencia que operan a frecuencias de RF y microondas son una pieza importante en todos los sistemas de comunicación modernos. Estos convierten potencia de corriente directa en complejas ondas de radio que viajan por el espacio para llevar a cabo el proceso de comunicación. El elemento más importante en un amplificador de potencia es el transistor de potencia. Así, la caracterización del comportamiento de los transistores bajo condiciones de gran señal es de vital importancia en el diseño de los amplificadores de potencia usados en los sistemas de telecomunicaciones.

Entre los sistemas de comunicación más utilizados para caracterizar transistores de potencia, tanto en la industria como en la investigación, están los sistemas de sintonización de carga (load-pull). Estos sistemas caracterizan de forma experimental el desempeño de un transistor en función de la carga que le es presentada a la salida.

Los sistemas de load-pull pueden ser implementados usando sintonizadores de impedancia pre-caracterizados o usando sistemas de calibración y sintonización en tiempo real. En cualquier sistema de load-pull, la medición de las ondas incidentes y reflejadas que definen los coeficientes de reflexión, y por lo tanto las impedancias, a la salida del transistor de potencia se realiza utilizando un analizador de redes vectorial (ARV). En esta tesis se evalúa el impacto de diferentes técnicas de calibración para el ARV en la caracterización de transistores de potencia de microondas usando sistemas de load-pull.

Palabras clave: Técnicas de calibración, analizador de redes vectorial, sistemas de sintonización de carga, transistores de potencia de microondas

Abstract of the thesis presented by **Manuel Alejandro Pulido Gaytán**, in partial fulfillment of the requirements of the degree of Doctor in Sciences in Electronics and Telecommunications with orientation in High Frequency Electronics. Ensenada, Baja California, August 2016.

The impact of VNA calibration techniques on the load-pull characterization of microwave power transistors

Abstract approved by:

Dr. J. Apolinar Reynoso Hernández

Thesis Advisor

Power amplifiers operating at RF/microwave frequencies are one of the most important elements in modern communication systems; they convert simple direct-current power into complex radio waves that travel through space to enable the wireless communication process. The most important element in a power amplifier is the power transistor, which operates in its nonlinear regime in such applications. Thus, characterizing the large signal behavior of power transistors is of paramount importance for designing power amplifiers for wireless communications.

Among the most commonly used systems for characterizing power transistors, in both industry and academy, are the load-pull systems. These systems characterize the performance of power transistors as a function of its loading condition for a determined set of bias, frequency and input power conditions.

Load-pull systems may be implemented by using either pre-calibrated impedance tuners or real-time tuning and calibration methods. In every load-pull system, the measurement of the incident and reflected waves defining the reflection coefficients, and thus the impedances, at the output of power transistors is carried out by using a calibrated vector network analyzer (VNA). In this dissertation the impact of different VNA calibration techniques on the characterization of microwave power transistors using load-pull systems is studied.

Keywords: Calibration techniques, vector network analyzer, load-pull systems, microwave power amplifiers

*Dedicated to my mother, my wife, my grandmother,
and to the loving memory of my uncle Alvaro Gaytan.*

Acknowledgements

There are many people I would like to thank for being important part in the work behind this dissertation. I hope I did not miss anyone, otherwise my sincere apologies. First of all, I thank my mother Angelica Gaytan, my wife Raquel Villagrana and my grandmother Eva Martinez for their continuous encouragement, support, love and sacrifice. Thanks to the life for giving me the privilege of being surrounded by so valuable women. I also thank my brother Bernardo Pulido, my aunts Martina, Raquel, Abigail, Lidia and Eva Gaytan, and my uncles Alvaro Gaytan and Manuel Aguiña for their unconditional support.

There are no words to express my gratitude to my thesis advisor, Professor Apolinar Reynoso. I am deeply grateful to him for giving me the opportunity to contribute to his research work. To him, my endless respect and admiration.

I would like to thank the members of my thesis committee, Dr. Carmen Maya, Dr. Enrique Mitrani, Dr. Raul Loo, Dr. Arturo Velazquez and Dr. Roberto Murphy. Their continuous feedback was fundamental to find the direction to this research work.

I also thank Dr. Andres Zarate for always being willing to participate in my research publications and for helping me to expand my professional opportunities.

A special thank to my friend and professional mentor Rodrigo Mendez for all the valuable advices he has given me in order to improve my professional and interpersonal skills.

This work was possible thanks to the support of the Mexican Council for Science and Technology (CONACyT) under scholarship number 242889. In this order, I would like to manifest a special feeling of gratitude to the Mexican people for the opportunity they gave me of being full-time Ph.D. Student during the last four years.

Finally, I thank the Center for Scientific Research and Higher Education of Ensenada, Baja California for the support this institution gave me during the development of this work.

Table of contents

	Page
Abstract in spanish	i
Abstract in english	ii
Dedicatory	iii
Acknowledgements	iv
List of figures	vii
List of tables	xi
1. Introduction	1
1.1 Motivation	1
1.2 State of the art	2
1.3 Problem statement	5
1.4 Objective	6
1.5 Thesis outline	6
1.6 Contributions	7
2. Fundamentals of Microwave Vector Network Analysis	10
2.1 Introduction	10
2.2 Scattering parameters	11
2.3 Measurement of S-parameters	13
2.4 T and ABCD parameters	15
2.4.1 Wave-cascading transmission parameters	16
2.4.2 Voltage-current transmission parameters	17
2.5 Error Models	19
2.5.1 The 3-term error model	20
2.5.2 The 12-term error model	21
2.5.3 Switching Errors Correction	23
2.5.4 The 8-term error model	25
3. VNA Calibration Techniques	26
3.1 Introduction	26
3.2 ABCD-parameters representation of a transmission line	27
3.3 Statement of the general problem of VNA calibration	30
3.4 Measurement of calibration structures	31
3.4.1 Measurement of a transmission line	32
3.4.2 Measurement of a thru	33
3.4.3 Measurement of a pair of loads	34
3.5 The TRL calibration technique	39
3.5.1 TRL calibration procedure	40
3.6 Generalized theory of the TRM calibration technique	42

3.6.1	TRM calibration procedure	43
3.7	The TRRM calibration technique	45
3.7.1	TRRM calibration procedure	46
3.8	The LZZ calibration technique	48
3.8.1	LZZ calibration procedure	49
3.9	LZZM: an extension of the theory of the LZZ technique	57
3.9.1	Contributions of the LZZM procedure to the LZZ technique	57
3.9.2	Advantages of the LZZM procedure over the TRRM technique	58
3.10	The OSM one-port calibration technique	59
3.11	Summary	61
4.	Load-Pull Systems	63
4.1	Load-pull contours	63
4.1.1	Power match condition	63
4.1.2	Cripps' load-line theory	65
4.1.3	Estimation of the load-pull contours	69
4.2	Load-pull systems	74
4.2.1	Passive load-pull systems	76
4.2.2	Active load-pull systems	77
4.2.3	Pre-calibrated and real-time load-pull systems	82
4.3	Load-pull as a tool for power amplifier design	85
4.3.1	Methods based on device's nonlinear models and CAD-tools	86
4.3.2	Methods based on nonlinear measurements	87
5.	Calibration of real-time LP measurement systems	88
5.1	Relative calibration	89
5.2	Power calibration	94
6.	Load-Pull Characterization of Power Transistors	99
6.1	Implementation of a real-time LP measurement system	99
6.2	Characterization of power transistors using LP systems	102
6.2.1	Load-pull contours of constant power, efficiency and gain	102
6.2.2	Large-signal gain under optimal loading condition	105
6.3	Evaluation of the impact of calibration techniques on the LP characteriza- tion of microwave transistors	108
6.3.1	The impact of assuming the line/load used as calibration structures as a non-reflecting element	108
6.3.2	The impact of assuming the load used in the TRM calibration as a symmetrical element	113
6.3.3	The impact of knowing the impedance of the line used in the TRL on the LP characterization of power transistors	118
6.4	Design of a power amplifier based on LP measurements	122
7.	Conclusions and Future work	125
	Bibliographic references	129

List of figures

Figure		Page
1	Structure and organization of the dissertation.	7
2	Wave definitions.	11
3	Incident and scattered waves of a two-port network.	12
4	S-parameters measurement in a) forward direction and b) reverse direction. .	14
5	Two-port network and the incident and reflected waves at its terminals. . . .	16
6	Two-port network and the voltage and current at its terminals.	18
7	Simplified diagram of a VNA.	19
8	a) VNA configuration for one-port measurements and b) signal flow diagram of its error model.	20
9	VNA configuration diagram representing the a) forward and b) reverse measurements.	21
10	Signal flow diagram representing the a) forward and b) reverse measurements.	22
11	VNA configuration for the correction of the switching errors in the a) forward and b) reverse directions.	23
12	a) VNA configuration diagram a b) signal flow diagram of the 8-terms error model.	25
13	Measurement of a two-port DUT.	31
14	Equivalent structure of the through connection of ports one and two of the VNA.	33
15	Equivalent two-port structure of a shunted load.	35
16	Equivalent structures of the measurement of loads connected at: a) port 1 y b) port 2 of the VNA.	35
17	TRL calibration structures: a) thru, b) line and c) reflecting load.	39
18	TRM calibration structures: a) thru, b) reflecting load and c) symmetrical/nonsymmetrical load of arbitrary impedance.	42
19	TRRM calibration structures: a) thru, b) a symmetrical load of very high impedance , c) a symmetrical load of very low impedance and d) a one-port load of known impedance.	45
20	LZZ calibration structures: a) line, b) offset-open, c) offset-short.	49
21	Equivalent structure of the offset loads connected at: a) port 1 and b) port 2 of the VNA.	50

Figure	Page
22	LZZM calibration structures: a) one transmission line, b) two pairs of highly reflecting loads and c) one broadband load (match). 57
23	OSM calibration structures : a) an offset load of very high impedance (open, O), b) an offset load of very low impedance (short, S) and c) an offset load of impedance close to the measuring system impedance (match, M). 60
24	Illustration of the limiting mechanisms of output voltage and current swings of FETs: a) input junction forward conduction, b) channel pich-off, c) ohmic region and d) breakdown. 64
25	Illustration of the concept of load line for a loading condition for maximum output power. The load lines corresponding to the loading conditions for reduced voltage and current swings are also shown. 65
26	Simplified model of a field effect transistor: a) model and b) I-V curves. . . . 66
27	FET device loaded with a load of arbitrary impedance and biased using ideal DC blocking and RF choke networks. 66
28	RF waveforms for a typical class-A biasing condition: a) voltage and b) current, at their amplitude reduction due to non-optimum loading conditions. . . 67
29	Example of the location of the optimum resistance and the estimation of LP power contours. In a) the addition of a series reactance to a suboptimum resistance is depicted and in b) the addition of a susceptance in parallel with a suboptimum conductance is depicted. 68
30	Impedance at the package Z_L^{PK} plane that has to be generated by an impedance tuner to synthesize an impedance Z_L^{CS} at the current source: a) parasitics considered in the analysis and b) equivalent circuit. 72
31	Impedance at the package Z_L^{PK} plane of a transistor when: a) a shunted capacitance of 1.3 pF is considered and b) when a series inductance of 1.0 nH is considered. For compactness, only the impedance for maximum power and the LP contour for 1 dBm of power below the maximum power are shown. . . 73
32	Load-Pull contours as a method for reporting the results of an active device characterization using load-pull systems. 75
33	Principle of operation of a passive LP systems and the reflection coefficient synthesis. In this type of tuners, the vertical movements of a probe vary mostly the magnitude of Γ_{LOAD} and the horizontal movements vary mostly the phase of Γ_{LOAD} 77
34	Generic diagram of an active LP system using the open-loop active LP concept. 78
35	Generic diagram of an active LP system using the feed-forward active LP concept. 80
36	Generic diagram of an active LP system using the closed-loop active LP concept. 81

Figure	Page	
37	Generic diagram of a LP system using pre-calibrated impedance tuners.	83
38	Generic diagram of a real-time LP system.	84
39	Power amplifier design cycles methods based on device's nonlinear models/CAD-tools and using nonlinear measurements(AM-AM, AM-PM, load-pull) [Ghanouchi (2013)].	86
40	Measurement setup of a real-time load-pull system (neither driver amplifier nor networks for DUT biasing are depicted).	88
41	Measurement setup configuration for the relative calibration (networks for DUT biasing are not depicted).	90
42	Model for the measurement setup configuration for the relative calibration.	91
43	Measurement setup configuration for the absolute power calibration (networks for DUT biasing are not depicted).	95
44	Model for the measurement of the a) coaxial loads and b) the power meter.	95
45	Measurement setup of the implemented passive real-time LP system.	100
46	Measurement setup of the implemented closed-loop active real-time LP system.	101
47	a) Test fixture and calibration structures used to implement the TRL, TRM, TRRM and LZZ techniques: b) thru, c) 50 Ω transmission line, d) short, e) open and f) 50 Ω load.	102
48	Large-signal gain of a thru: a) voltage gain (G_v), b) ratio of transmitted to incident waves (G_d), c) current gain (G_i) and d) power gain (G_p), as a function of the magnitude of the load reflection coefficient Γ_{LD}	103
49	Measured LP contours of constant: a) output power, b) drain efficiency, c) power added efficiency and d) large-signal gain of the transistor used as DUT ($V_{GS} = -2.6$ V; $V_{DS} = 28$ V).	104
50	Measured LP contours of constant output power using: a) a passive load-pull system and b) using an active load-pull system of the transistor used as DUT ($V_{GS} = -2.6$ V; $V_{DS} = 28$ V).	105
51	Measured large-signal gain as a function of input power of the transistor used as DUT ($V_{GS} = -2.6$ V; $V_{DS} = 28$ V): a) magnitude, b) angle.	106
52	Measured large-signal gain for different bias conditions: a) magnitude and b) angle of $ G_d $ as a function of V_{GS} , a) magnitude and b) angle of $ G_d $ as a function of V_{DS}	107
53	Error in the calculation of Z_{LD} due to assuming the line/load used as calibration structure in the a) TRL, b) LZZ, c) TRM and d) TRRM calibrations as non-reflecting elements.	109

Figure	Page
54	Measured LP contours of constant: a) output power, b) drain efficiency, c) power added efficiency and d) large-signal gain of the transistor used as DUT ($V_{GS} = -2.6$ V; $V_{DS} = 28$ V). 110
55	Measured LP contours of constant: a) output power, b) drain efficiency, c) power added efficiency and d) large-signal gain of the transistor used as DUT ($V_{GS} = -2.6$ V; $V_{DS} = 28$ V). 111
56	Measured large signal gain calculated using different calibration techniques: a) magnitude, b) phase when the correct values of Z_L and Z_M are used in the calibration. The results obtained when Z_L and Z_M are assumed as non reflecting elements are shown in c) magnitude and d) phase. 113
57	Microstrip structures used to implement the TRM calibration with asymmetrical loads: a) thru, b) reflecting load (short circuit) and c) asymmetrical load. The dotted line indicates that the calibration reference plane is located at the center of the thru. 114
58	Contours of constant output power calculated using in the relative calibration: a) TRL (used as a reference), b) TRM $Z_A = Z_{M1}$, $Z_B = Z_{M2}$ 115
59	Contours of constant output power calculated using in the relative calibration: a) TRM $Z_A = Z_{M1}$, $Z_B = Z_{M2}$, b) TRM $Z_A = 50 \Omega$, $Z_B = 25 \Omega$, c) TRM $Z_A = Z_B = Z_{M1}$, d) TRM $Z_A = Z_B = 50 \Omega$, e) TRM $Z_A = Z_B = Z_{M2}$, f) TRM $Z_A = Z_B = 25 \Omega$ 116
60	Large-signal voltage gain of the transistor used as DUT calculated using the TRM technique ($V_{GS} = -2.6$ V; $V_{DS} = 28$ V): a) magnitude and b) angle. . . 117
61	Microstrip structures used to implement the TRL calibration with lines of low impedance: a) DUT in test fixture, b) thru, c) line and d) symmetrical reflecting load (Open circuit). The dotted line indicates that the calibration reference plane is located at the center of the thru. 118
62	Contours of constant output power of a CGH40045 power transistor ($V_{DS}=20$ V, $V_{GS}=-2.5$ V) using a) $Z_L = 5 \hat{I}\odot$, b) $Z_L = 10 \hat{I}\odot$, c) $Z_L = 20 \hat{I}\odot$, d) $Z_L = 50 \hat{I}\odot$ in the calibration procedure. 119
63	Input impedance of the DUT calculated using different values of Z in the calibration. The load impedance was fixed at $Z_{LD}=Z_{opt}$ 120
64	Gain of the DUT calculated using different values of Z in the calibration: a) magnitude and b) phase. The load impedance was fixed at $Z_{LD}=Z_{opt}$ 121
65	a) I-V curves of the transistor used in the design of the power amplifier. b) LP contours of constant output power and LP contours of constant drain effiecy. 122
66	Fabricated power amplifier. 123
67	a) Measured performance of the fabricated PA. b) LP contours of constant output power and LP contours of constant drain efficiency of the fabricated PA 123

List of tables

Table	Page
I Calculation of the calibration terms using the calibration structures of different calibration techniques. The corresponding values of the impedances Z_A and Z_B are also presented.	62

1. Introduction

This chapter gives an introduction to the work presented in this dissertation. First, the driving factors that motivated the research conducted in this work are presented. Then, the problem statement is outlined in order to introduce the aim of this work. Finally, the main outcomes of this research work are summarized.

1.1 Motivation

While most of the advances in wireless communications are mainly motivated by new developments in digital coding and modulation techniques and by the liberation of new fragments of the electromagnetic spectrum [Ha (2010); McCune (2010)], the element which remains present in every communication system, since the early era of radio broadcasting and up to modern wireless communication systems, is the power amplifier (PA) [Aaen (2007); Yifeng (2006)].

Power amplifiers commonly used in modern communication systems are specified in terms of linearity, bandwidth, output power and efficiency. Hence, PA designers have to deal with a multidimensional design problem, in which tradeoffs between some of the variables make the design of PAs a difficult task.

At the heart of a PA there is always a power transistor. In this order, the demands in the accuracy of methods for characterizing power transistors for optimum design of PAs have increased mainly motivated by the requirements imposed by regulatory agencies in the electrical characteristics of PAs for wireless communications (e.g., creation of undesired spectral components, power consumption) [Calvillo-Cortes (2014); De Groote (2008)].

The characterization of the large-signal behavior of microwave transistors using only scattering parameters (S-parameters) is often inadequate [Pirola (2007); Hashmi (2011)], since S-parameters are defined only for input power levels far from the stimulus for device's satu-

ration [Root (2013)]. Hence, the representation of the performance of power transistors by means of S-parameters is only valid when describing its small-signal behavior.

The increased demand for enhanced performance from microwave transistors requires to operate these devices nearer to compression, in their nonlinear regime. In those conditions, nonlinear phenomena such as gain compression, phase distortion or the generation of harmonic frequencies and intermodulation distortion products play an important role in the characterization of high power transistors [Pedro (2002); Camarchia (2007)].

The measurement of devices operating in the nonlinear regime requires large-signal measurement systems. For PA design, load-pull (LP) systems are essential for the accurate measurement of transistors' performance. In generic terms, LP refers to present a set of impedances to a device under test (DUT) in a controlled fashion, while the DUT's performance is evaluated. The DUT's performance is assessed by varying the DUT load impedance, along with frequency and bias, to accurately establish the conditions under which optimal performance from the DUT can be obtained [Hashmi (2013, 2011)]. The performance of the DUT is evaluated in terms of a determined set of metrics; the most commonly used are output power (P_{OUT}), drain efficiency (η_D), power added efficiency (PAE) and adjacent channel power ratio ($ACPR$). Due to the increase in the requirements of PAs for wireless communications, the optimization of transistors' performance is of paramount importance [Ferrero (2011)]. Thus, optimizing the accuracy in the characterization of power transistors using LP systems becomes important when few percentage of η_D or some tenths of watt of P_{OUT} determine the success or failure in the design of a PA.

1.2 State of the art

Since this work covers two closely related topics, namely VNA calibration techniques and LP systems, a brief review of the state-of-the-art in these two topics is presented.

VNA calibration techniques

Short-Open-Load-Thru (SOLT) is the most popular technique based on the 12-term error model [Rytting (2004)]. It has been the most widely used calibration for coaxial-based measurements. However, SOLT is not suggested for VNA calibration using planar calibration structures (e.g., microstrip structures, coplanar waveguide structures) for high frequency applications, since it is quite difficult to fabricate planar calibration structures meeting the requirements of the SOLT technique.

This work is devoted to the characterization of microwave power transistors, which in order to be measured have to be either mounted in coaxial-to-microstrip test fixtures (packaged devices) or contacted using coplanar probes (on-wafer devices). In these cases the use of planar calibration structures is required.

For applications in which planar calibration structures have to be used, calibration techniques based on the 8-term error model are preferred [Reynoso-Hernandez (2015)]. Among them, the thru-reflect-line (TRL) technique [Engen (1979)] is considered as a reference calibration technique. It allows referring S-parameters [Reynoso-Hernandez (2013)] and LP measurements [Aaen (2000)] to the measuring system impedance (Z_0) as long as the characteristic impedance of the line used as calibration structure is known. The main issue in the TRL is that multiple lines of different length are required [Marks (1991)] to obtain a wide measurement bandwidth. The measurement ports have to be moved several times in order to accommodate structures of different size, reducing the measurement repeatability in both S-parameters and LP measurements.

Thru-reflect-match (TRM) [Eul (1988)] replaces the line used in the TRL by a load of known impedance in order to achieve a broadband calibration. As originally proposed, the TRM required that the impedance of the load used as match standard be symmetrical and identical to Z_0 . These two conditions are difficult to achieve when using planar calibration structures. In this order, one of the contributions of this research work is the development of a generalized theory of the TRM technique allowing the use of symmetrical and nonsymmetrical

loads of arbitrary impedance as match standard [Pulido-Gaytan (2015d)]. The thru-reflect-reflect-match (TRRM) [Davidson (1989)] calibration is a variation of TRM, where only one known load is used. In general, TRM and TRRM involve the use of at least one broadband load which has to be known prior to the calibration.

The Line, Offset-open, Offset-short (LZZ) calibration technique [Pulido-Gaytan (2013)], which is another contribution of this work, uses as standards: a transmission line and two pairs of offset reflecting loads. Unlike TRM and TRRM, in the LZZ calibration the use of a characterized load is not required. Moreover, since the LZZ calibration does not use multiple transmission lines for calculating the error calibration terms, it may be implemented using fixed spacing structures.

Load-pull systems

The LP concept was introduced for the first time more than forty years ago [Cusack (1974)]. The first works regarding LP systems [Cusack (1974); Secci (1983); Tucker (1984); Pierpoint (1986)] are considered now as pioneering, since they introduced a paradigm in the characterization of power transistors. Since the early beginnings of the use of LP systems as a tool for characterizing power transistors, a number of advances have been reported; the most relevant ones are summarized in the following paragraphs.

The most important element in a LP system is the impedance tuning method [Maury-Microwave (2002)]. In this sense, the introduction of computer controlled passive impedance tuners in [Secci (1983)] was an important advance three decades ago. Nowadays, there are important organizations, whose primary business is the development of impedance tuners [Maury-Microwave (2009); Focus-Microwave (1994)].

Impedance tuning systems using active elements developed in the late 1970's and early 1980's [Takayama (1976); Van der Puije (1978); Bava (1982)], were very important advances to the LP theory. They were mainly motivated by the limitations of passive systems to synthesize the low-impedance loads required in the characterization of power transistors.

The most important advances in the LP characterization of microwave devices in the latest twenty five years are: hybrid LP systems [Simpson (2011)] combining active and passive systems, the use of state-of-the-art instruments allowing LP measurements under pulsed conditions [Nuttinck (2001)], and the extension of the LP concept to the multi-harmonic characterization of transistors [Stancliff (1979); Ferrero (2008)].

While advances in low impedance tuning systems, thermal management capabilities, and harmonic tuning capabilities of LP systems are very important, accurate calibration of them is always a must. Some previously reported works have dealt with the evaluation of residual VNA calibration errors in the accuracy of the LP measurements [Ferrero (2001); Teppati (2007, 2012)]. However, to the best of the author's knowledge, an exhaustive study of the impact of the different VNA calibration procedures on the LP characterization of microwave power transistors has not been reported in the literature.

1.3 Problem statement

The objective behind the LP characterization of power transistors is the evaluation of the device's performance under different loading conditions for a determined set of bias, frequency and power conditions. However, errors due to uncalibrated measurement system, cause errors in the measurement of the impedances and nonlinear behavior at the DUT plane, thereby defeating the LP's primary objective.

All of the LP systems are based on the use of a VNA. The accuracy of a measurement using a VNA is enhanced when it is accurately calibrated. In this sense, calibration techniques allowing the use of calibration elements of arbitrary impedance, and allowing the measurement results to be referred to a standard and frequency-independent impedance are required. In order to compare the impact that different calibration techniques have in the calculation of these measurement results, a unified theory for different calibration techniques is also required.

1.4 Objective

The objective of this work is to evaluate the impact of different VNA calibration techniques on the LP characterization of microwave power transistors. Since to accurately perform measurements using a VNA, the instrument has to be calibrated, the method used for calibrating it plays an important role in the precision of the DUT characterization.

The impact of different calibration techniques for calibrating the VNA used in the LP characterization of power transistors is studied. The study of the classical calibration techniques, the development of new calibration procedures, the design of test fixtures and the implementation of LP test benches are the main focus of this work.

1.5 Thesis outline

The theory presented in Chapters 2 to 7, describes the most relevant theoretical and technical aspects to be considered in the development of accurate LP measurements for characterizing microwave power transistors. This document is organized as follows:

- In chapter 2 the fundamentals of vector network analysis of microwave circuits is presented. Some basic concepts which will help the reader to comprehend the math and analysis developed in chapters 3 and 4 are presented.
- Chapter 3 presents a unified theory of the most popular VNA calibration techniques (TRL, TRM and TRRM) using the ABCD-parameters matrix formalism. An original calibration technique, referred to as the LZZ, is also presented.
- Chapter 4 gives a description and classification of the different types of LP systems commonly used for characterizing microwave power transistors. The theoretical foundations of the load-pull concept are also presented.
- In chapter 5 the calibration procedure of a real-time load-pull system is presented.

- In chapter 6 some experimental results involving the LP characterization of microwave power transistors are presented. The evaluation of the impact of different VNA calibration procedures on the LP characterization of microwave transistors is described.
- Finally, in chapter 7 the conclusions of this dissertation along with some recommendations for future research work are presented.

A schematic diagram representing the dissertation structure is shown in Figure 1.

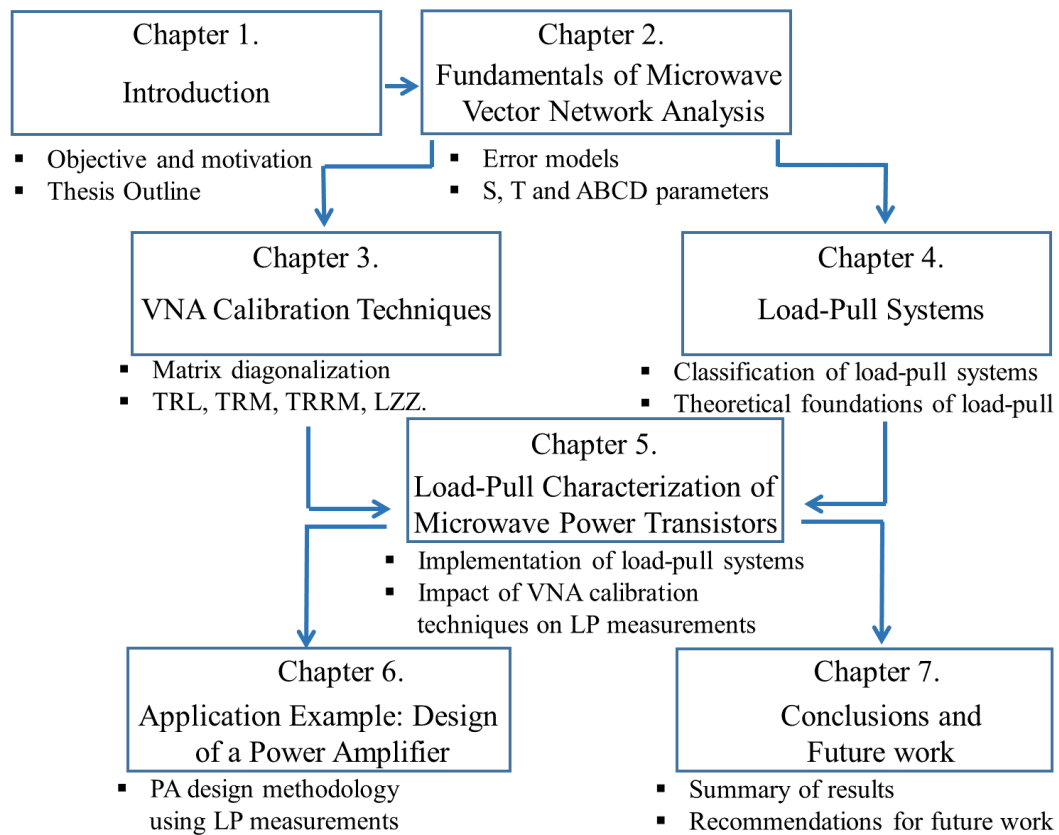


Figure 1. Structure and organization of the dissertation.

1.6 Contributions

The main contributions of this research work are reflected in a list of papers published during the time period in which the author was member of the High Frequency Electronics Group of CICESE Research Center. The list of journal and conference papers is presented below:

Pulido-Gaytan, M.A.; Reynoso-Hernandez, J.A.; Zarate-de Landa, A.; Loo-Yau, J.R.; Maya-Sanchez, M. C., “Vector Network Analyzer Calibration Using a Line and Two Offset Reflecting Loads,” *Microwave Theory and Techniques, IEEE Transactions on* , vol.61, no.9, pp. 3417-3423, Sep. 2013.

Pulido-Gaytan, M.A.; Reynoso-Hernandez, J.A.; Zarate-de Landa, A.; Loo-Yau, J.R.; Maya-Sanchez, M. C., “Generalized theory of the thru-reflect-match calibration technique. *Microwave Theory and Techniques, IEEE Transactions on* , vol.63, no.9, pp. 3417-3423, Sep. 2015.

Pulido-Gaytan, M.A.; Reynoso-Hernandez, J.A.; Zarate-de Landa, A.; Loo-Yau, J.R.; Maya-Sanchez, M. C., “LZZM: An Extension of the Theory of the LZZ Calibration Technique,” *84th ARFTG Microwave Measurement Conference Digest*, pp.1-5. Dec. 2014. Boulder, CO, USA.

Pulido-Gaytan, M.A.; Reynoso-Hernandez, J.A.; Maya-Sanchez, M. C.; Zarate-de Landa, A.; Loo-Yau, J.R., “On the Implementation of the LZZ Calibration Technique in the S-Parameters Measurement of Devices Mounted in Test Fixtures,” *85th ARFTG Microwave Measurement Conference Digest*, pp.1-5. May. 2015. Phoenix, AZ, USA.

Pulido-Gaytan, M.A.; Reynoso-Hernandez, J.A.; Maya-Sanchez, M. C.; Loo-Yau, J.R., “The Impact of Knowing the Impedance of the Lines Used in the TRL Calibration on the Load-Pull Characterization of Power Transistors,” *86th ARFTG Microwave Measurement Conference Digest*, pp.1-5. Dec. 2015. Atlanta, GA, USA.

Pulido-Gaytan, M.A.; Reynoso-Hernandez, J.A.; Maya-Sanchez, M. C.; Loo-Yau, J.R., “Calibration of a Real-Time Load-Pull System Using the Generalized Theory of the TRM Technique,” *87th ARFTG Microwave Measurement Conference Digest*, pp.1-5. May. 2016. San Francisco, CA, USA.

Reynoso-Hernandez, J.A.; **Pulido-Gaytan, M.A.**; Maya-Sanchez, M.C.; Loo-Yau, J.R., “What can the ABCD parameters tell us about the TRL?,” 79th ARFTG Microwave Measurement Conference Digest, pp.1-4, Jun. 2012. Montreal, QB, Canada.

Reynoso-Hernandez, J.A.; **Pulido-Gaytan, M.A.**; Zarate-de Landa, A.; Zuñiga-Juarez, J.E.; Monjardin-Lopez, J.R.; Garcia-Osorio, A.; Orozco-Navarro, D.; Loo-Yau, J.R.; Maya-Sanchez, M.C., “Using lines of arbitrary impedance as standards on the TRL technique,” 81st ARFTG Microwave Measurement Conference Digest, pp.1-4, Jun. 2013. Seattle, WA, USA.

The theoretical and experimental study conducted in this work, regarding the measurements and characterization of power devices, will be useful in the immediate future of the research activities of the High Frequency Electronics Group of CICESE Research Center. Hence, the developed LP test bench, fully described in chapter 5, is considered to be a contribution to the CICESE’s RF/Microwave Laboratory.

2. Fundamentals of Microwave Vector Network Analysis

2.1 Introduction

Microwave network analysis is the formalism by which the electrical performance of microwave components and circuits are studied. It is a method for characterizing microwave circuits by evaluating their response in amplitude and phase to swept-frequency and swept-power test signals. Measuring both magnitude and phase of signals coming to and emerging from components is important for a number of applications in RF and microwave research; some of these applications, which are repeatedly recalled throughout this document, are summarized below:

- **Characterization:** both magnitude and phase are required to fully characterize linear and nonlinear networks.
- **Design:** to design the matching networks for RF power amplifiers, the optimum complex impedance at the output of the transistors must be determined by using either load-pull systems or nonlinear models of the device.
- **Modeling:** the development and verification of accurate models for computer-aided design requires magnitude and phase measurement data.
- **Calibration:** vector error correction, used to improve measurement accuracy by removing the effects of measurement system errors, requires both magnitude and phase data.

In this chapter, the fundamental principles of vector network analysis will be reviewed. The discussion includes the common parameters that can be measured at high frequencies, S-parameters, and other important parameters that will be useful for the readership in the

following chapters, T-parameters and ABCD-parameters. The most commonly used error models in VNA calibration are also presented.

2.2 Scattering parameters

Since more than half a century, S-parameters [Kurokawa (1965)] have been one of the most important foundations of microwave theory and techniques. S-parameters are easy to measure at high frequencies with a VNA, provided that systematic measurement errors have been removed by using appropriate calibration procedures.

The term *scattering* refers to the relationship between incident and scattered (reflected and transmitted) traveling waves. We can distinguish between an incident wave a and a scattered wave b [Rahola (2008)]. These wave variables are defined as simple linear combinations of the voltage at (v) and the current flowing through (i) the same port (Figure 2) according to the following expressions:

$$a = \frac{v + iZ_0}{2\sqrt{Z_0}}, \quad (1)$$

$$b = \frac{v - iZ_0}{2\sqrt{Z_0}}. \quad (2)$$

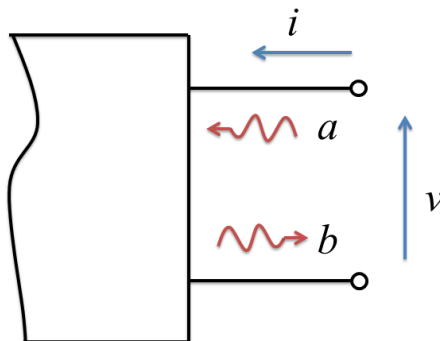


Figure 2. Wave definitions.

The reference impedance for a given port, Z_0 , is in general a complex quantity. Nevertheless,

for most practical cases in microwave engineering it is desired that Z_0 be purely real and frequency independent.

Analogously, by solving (1)-(2) for v and i , the current and voltage can be recovered from the wave parameters as follows

$$v = \sqrt{Z_0}(a + b), \quad (3)$$

$$i = \frac{1}{\sqrt{Z_0}}(a - b). \quad (4)$$

The variables in equations (1)-(4) are complex numbers representing the RMS phasor description of sinusoidal signals in the frequency-domain. Thus, a , b , v , i are vectors, the components of which indicate the values associated with sinusoidal signals at a particular port i , $i = 1, 2, \dots, N$, with N defined as the total number of ports in the network. Figure 3 shows a graphical representation of the description of these waves for the case of a two port network.

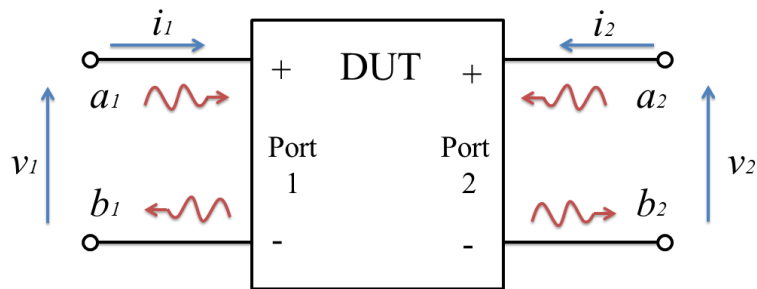


Figure 3. Incident and scattered waves of a two-port network.

The assumption behind the S-parameters formalism is that the system being described is linear and therefore there is a linear relationship between the phasor representation of incident and scattered waves, as expressed bellow

$$b_i = \sum_{j=1}^N S_{ij} a_j, \forall i \in 1, 2, \dots, N. \quad (5)$$

The set of complex coefficients S_{ij} in (5) defines the S-parameters of an N -ports device. The summation in (5) is over all port indices, so that incident waves at each port j , contribute in general to the overall scattered wave at each output port i . For the particular case of a two-port network, the scattered waves at ports one and two of the the network are expressed as

$$b_1 = S_{11}a_1 + S_{12}a_2, \quad (6)$$

$$b_2 = S_{21}a_1 + S_{22}a_2. \quad (7)$$

S-parameters can be grouped to obtain the S-parameters matrix as follows

$$\begin{bmatrix} b_1 \\ b_2 \end{bmatrix} = \begin{bmatrix} S_{11} & S_{12} \\ S_{21} & S_{22} \end{bmatrix} \begin{bmatrix} a_1 \\ a_2 \end{bmatrix}. \quad (8)$$

Thus far, the concept of S-parameters as a linear combination of incident and scattered waves has been presented. In the following section, the procedure for S-parameters measurement is described.

2.3 Measurement of S-parameters

Most of the common tasks in microwave research involve the analysis of circuits [Hiebel (2007)]. A network analyzer is an instrument that handles this job with a great precision through the measurement of S-parameters. By setting all incident waves to zero in (5), except for a_j , one can deduce the simple relationship between a given S-parameters matrix element and a particular ratio of scattered to incident waves as

$$S_{ij} = \frac{b_i}{a_j} \Big|_{a_k=0, k \neq j}. \quad (9)$$

Equation (9) may be used to analyze the measurement of a two-port network. For a two-port network, the measurement of S-parameters is carried out in two steps: a) forward

direction, in which the incident signal is set at port one and b) reverse direction, in which the signal source is set at port two, as depicted in Figure 4.

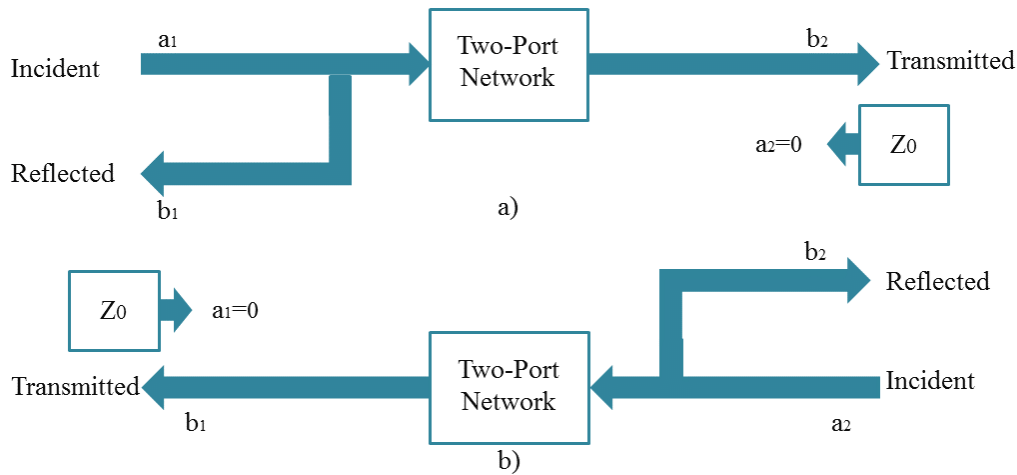


Figure 4. S-parameters measurement in a) forward direction and b) reverse direction.

In Figure 4a, the stimulus is an incident wave at port 1. The fact that a_2 is not present ($a_2 = 0$) is interpreted to mean that the b_2 wave scattered and traveling away from port 2 is not reflected back into the device at port 2. Under this condition, the device is said to be perfectly matched at port 2. Two of the four complex S-parameters, namely S_{11} and S_{21} , can be identified from (9) as

$$S_{11} = \frac{b_1}{a_1} \Big|_{a_2=0}, \quad (10)$$

$$S_{21} = \frac{b_2}{a_1} \Big|_{a_2=0}. \quad (11)$$

In reverse direction the stimulus is an incident wave at port 2 (Figure 4b). In this case, the fact that a_1 is not present ($a_1 = 0$) is interpreted to mean that the b_1 wave scattered and traveling away from port 1 is not reflected back into the device at port 1. Under this condition, the device is said to be perfectly matched at port 1. Two of the four S-parameters, S_{12} and S_{22} , can be identified from (9) as

$$S_{22} = \frac{b_2}{a_2} \Big|_{a_1=0}, \quad (12)$$

$$S_{12} = \frac{b_1}{a_2} \Big|_{a_1=0}. \quad (13)$$

In practice, the ratio on the right-hand side of (9) may vary with the magnitude of the incident wave. Nevertheless, the identification of this ratio with the S-parameters of a device is valid only if the incident wave allow the DUT to operate in its linear region. For nonlinear components, such as transistors biased at a fixed voltage, the scattered waves eventually increase nonlinearly with the incident wave as the latter becomes larger in magnitude. A better and more complete definition of S-parameters for a nonlinear component is given by [Root (2013)]

$$S_{ij} = \lim_{a_j \rightarrow 0} \frac{b_i}{a_j} \Big|_{a_k=0, k \neq j}. \quad (14)$$

That is, for a general active component biased at a constant DC stimulus, S-parameters are defined as ratios of output responses to input stimuli in the limit of small input signals. This emphasizes that S-parameters apply to nonlinear components only in the small-signal limit.

2.4 T and ABCD parameters

Thus far, the concept of S-parameters of two-port active and passive devices has been presented. In this section, other matrix representations commonly used in vector analysis of microwave networks, namely T- and ABCD- parameters, are described. These two representations will be very useful in chapter 3 for developing VNA calibration techniques.

2.4.1 Wave-cascading transmission parameters

T-parameters are a modified version of S-parameters, which facilitates the representation of the cascading connection of two or more networks, as outlined next. By rearranging the terms in equations (6)-(7), such that the variables at the left hand side of the equal sign are the waves at port one, a_1 and b_1 , and the variables at the right hand side of the equal sign are the waves at port two, a_2 and b_2 , one has

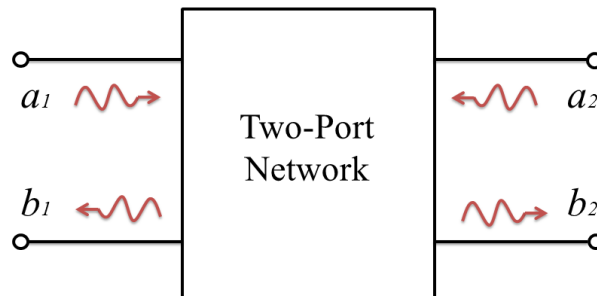


Figure 5. Two-port network and the incident and reflected waves at its terminals.

$$\begin{bmatrix} b_1 \\ a_1 \end{bmatrix} = \begin{bmatrix} T_{11} & T_{12} \\ T_{21} & T_{22} \end{bmatrix} \begin{bmatrix} a_2 \\ b_2 \end{bmatrix}, \quad (15)$$

where

$$\begin{bmatrix} T_{11} & T_{12} \\ T_{21} & T_{22} \end{bmatrix} = \frac{1}{S_{21}} \begin{bmatrix} -\det(S) & S_{11} \\ -S_{22} & 1 \end{bmatrix}. \quad (16)$$

Thus, for a two-port network, such as the one depicted in Figure 5, the T-parameters are represented as a function of incident and reflected waves as

$$T_{11} = \left. \frac{b_1}{a_2} \right|_{b_2=0}, \quad (17)$$

$$T_{12} = \left. \frac{b_1}{b_2} \right|_{a_2=0}, \quad (18)$$

$$T_{21} = \frac{a_1}{a_2} \Big|_{b_2=0}, \quad (19)$$

$$T_{22} = \frac{a_1}{b_2} \Big|_{a_2=0}. \quad (20)$$

The T-parameters network representation allow representing the cascading connection of N networks by simple multiplication of their individual T-parameters as

$$\begin{bmatrix} b_{1T} \\ a_{1T} \end{bmatrix} = \begin{bmatrix} T1_{11} & T1_{12} \\ T1_{21} & T1_{22} \end{bmatrix} \begin{bmatrix} T2_{11} & T2_{12} \\ T2_{21} & T2_{22} \end{bmatrix} \cdots \begin{bmatrix} TN_{11} & TN_{12} \\ TN_{21} & TN_{22} \end{bmatrix} \begin{bmatrix} b_{2T} \\ a_{2T} \end{bmatrix}, \quad (21)$$

where a_{iT} and b_{iT} , $i = 1, 2$, represent the incident and reflected waves at the input and output ports of the overall structure.

2.4.2 Voltage-current transmission parameters

ABCD-parameters, also referred to as chain parameters in some classical textbooks of microwave circuit analysis [Gonzalez (1997)], are the natural analogy of T-parameters for voltages and currents instead of incident and scattered waves. The ABCD-parameters representation a of two-port network allows relating the voltage at and the current flowing through port one with the corresponding voltages and currents existing at port two of a two-port network, as shown in Figure 6. The following equation represents what is known as the ABCD parameters matrix of a two-port network

$$\begin{bmatrix} v_1 \\ i_1 \end{bmatrix} = \begin{bmatrix} A & B \\ C & D \end{bmatrix} \begin{bmatrix} v_2 \\ i_2 \end{bmatrix}, \quad (22)$$

where

$$\begin{bmatrix} A & B \\ C & D \end{bmatrix} = \begin{bmatrix} (1 + S_{11})(1 - S_{22}) + S_{12}S_{21} & Z_0((1 + S_{11})(1 + S_{22}) - S_{12}S_{21}) \\ \frac{1}{Z_0}((1 - S_{11})(1 - S_{22}) - S_{12}S_{21}) & (1 - S_{11})(1 + S_{22}) + S_{12}S_{21} \end{bmatrix}. \quad (23)$$

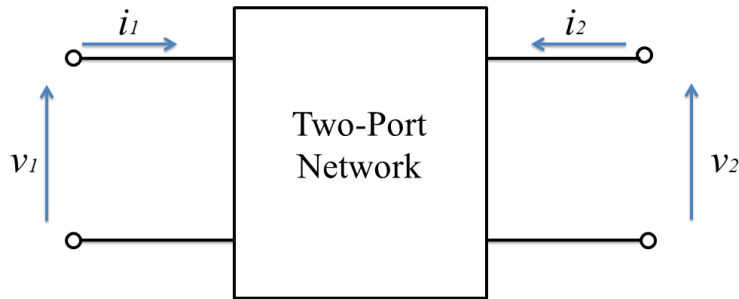


Figure 6. Two-port network and the voltage and current at its terminals.

The four parameters of this matrix can be expressed as function of the voltages at and currents flowing through ports one and two, under open circuit (zero current) and short circuit (zero voltage) conditions at port two:

$$A = \frac{v_1}{v_2} \Big|_{i_2=0}, \quad (24)$$

$$B = \frac{v_1}{i_2} \Big|_{v_2=0}, \quad (25)$$

$$C = \frac{i_1}{v_2} \Big|_{i_2=0}, \quad (26)$$

$$D = \frac{i_1}{i_2} \Big|_{v_2=0}. \quad (27)$$

As in the case of T-parameters, the ABCD-parameters allow representing the cascading connection of N networks by multiplying their individual ABCD-parameters matrix representation as

$$\begin{bmatrix} V_{1T} \\ I_{1T} \end{bmatrix} = \begin{bmatrix} A_1 & B_1 \\ C_1 & D_1 \end{bmatrix} \begin{bmatrix} A_2 & B_2 \\ C_2 & D_2 \end{bmatrix} \cdots \begin{bmatrix} A_N & B_N \\ C_N & D_N \end{bmatrix} \begin{bmatrix} V_{2T} \\ I_{2T} \end{bmatrix}, \quad (28)$$

with V_{iT} and I_{iT} , $i = 1, 2$, representing the voltages at and the currents flowing through the ports one and two of the overall structure.

Finally, it is worth mentioning that, unlike S- and T-parameters, ABCD-parameters are not defined as a function of a reference impedance.

2.5 Error Models

A network analyzer is an instrument that internally encompasses an RF source, a switch to route the signal from the source to either port one or port two of a DUT, a pair of directional couplers to separate the incident and scattered waves at the DUT ports, and the port receivers (detectors) for measuring those waves, as depicted in Figure 7.

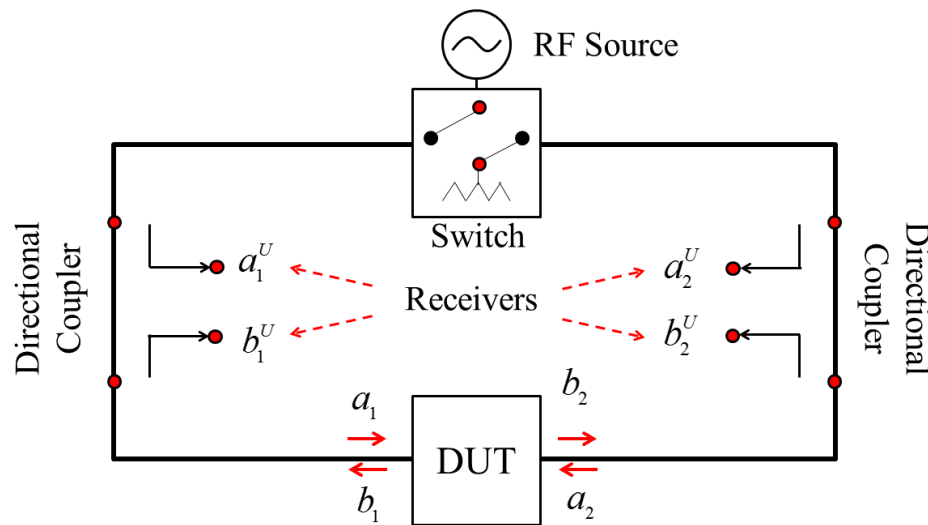


Figure 7. Simplified diagram of a VNA.

Imperfections of the VNA's elements (e.g., ports and source mismatch, low directivity of directional couplers, losses in transmission lines) along with effects introduced by other elements of the measurement setup (e.g., cables, adapters, connectors, bias tees and test fixtures) introduce errors in the measurement of the incident and scattered waves at the DUT ports. In order to determine the contribution of these errors and to remove their effects from the DUT's measurements, a calibration procedure has to be carried out. In a calibration procedure, there are two necessary elements: a calibration technique and an error model. This section is devoted to describe the most commonly used error models in VNA calibration.

2.5.1 The 3-term error model

The 3-term error model is a model suited for one-port calibration. Figure 8a shows the VNA configuration and signal flow diagram representation of the 3-term error model. In this model, the VNA is represented by a perfect reflectometer with an error adapter between the VNA's receivers and the DUT. The error adapter links the waves (a_1^U, b_1^U) and reflection coefficient $(\Gamma_1^U = b_1^U/a_1^U)$ at the plane of the VNA receivers with the waves (a_1, b_1) and reflection coefficient $(\Gamma_1 = b_1/a_1)$ at the DUT plane.

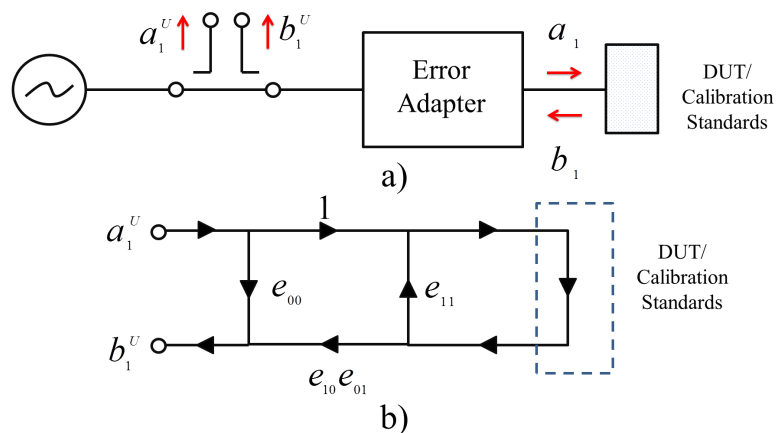


Figure 8. a) VNA configuration for one-port measurements and b) signal flow diagram of its error model.

The error adapter contains three error terms, which are referred to as: directivity, (e_{00}), source match (e_{11}) and reflection response ($e_{10}e_{01}$) errors. From the diagram shown in Figure 8b, the following expression relating Γ_1^U with Γ_1 , may be derived

$$\Gamma_1^U = \frac{b_1}{a_1} = \frac{e_{00} - \Delta_e \Gamma_1}{1 - e_{11} \Gamma_1}. \quad (29)$$

Then, after some algebra, the following expression may be obtained

$$e_{00} - \Delta_e \Gamma_1 + e_{11} \Gamma_1 \Gamma_1^U = \Gamma_1^U. \quad (30)$$

The objective of a one-port calibration is to determine the error terms by using the measurement of (at least) three loads of known reflection coefficient.

2.5.2 The 12-term error model

Unlike one-port measurements, in two-port measurements there are separate forward and reverse VNA measurements. Figure 9 shows the VNA configuration corresponding to the forward and reverse measurements, where independent two-port adapters are used to relate traveling waves at the DUT plane with traveling waves measured at the VNA receivers plane.

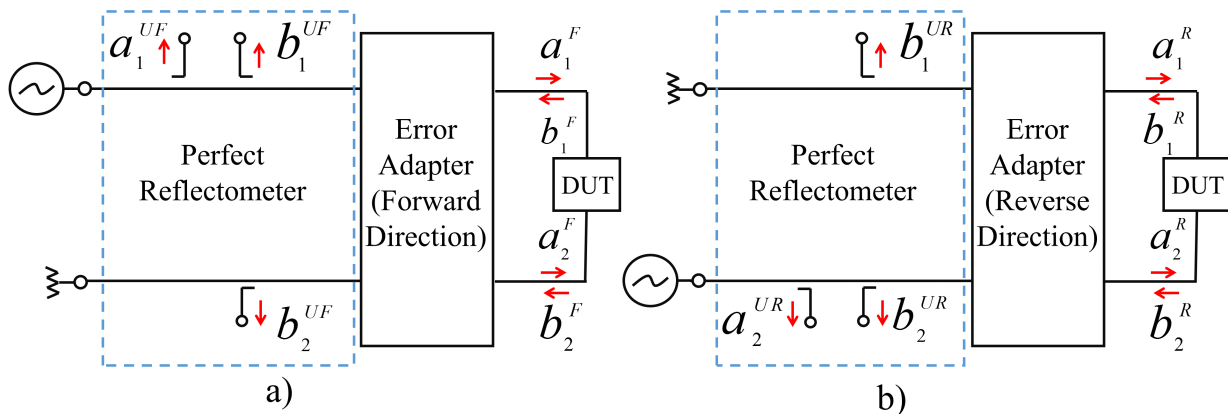


Figure 9. VNA configuration diagram representing the a) forward and b) reverse measurements.

These adapters are represented by independent signal flow graphs. Figure 10 shows the signal flow diagrams representing the forward and reverse measurements. Each signal flow graph is composed of six terms: directivity (e_{00} and e_{33}), source match (e_{11}^F and e_{22}^R), load match (e_{22}^F and e_{11}^R), transmission response ($e_{10}e_{32}$ and $e_{01}e_{23}$), reflection response ($e_{10}e_{01}$ and $e_{23}e_{32}$) and isolation (e_{30} and e_{03}).

A set of calibration structures of known electrical characteristics, typically open circuits, short circuits, matched loads and the connection of the calibration planes, have to be measured at the VNA ports in order to calculate the twelve error terms. Forward and reverse directivity, source match and reflection response at ports one and two of the VNA may be determined by using the one-port calibration procedure described in the preceding section at both VNA ports. The connection of the VNA ports through a two-port structure of known electrical behavior is used to determine the forward and reverse transmission response and load match terms; these terms assess the frequency response of the transmission signal path

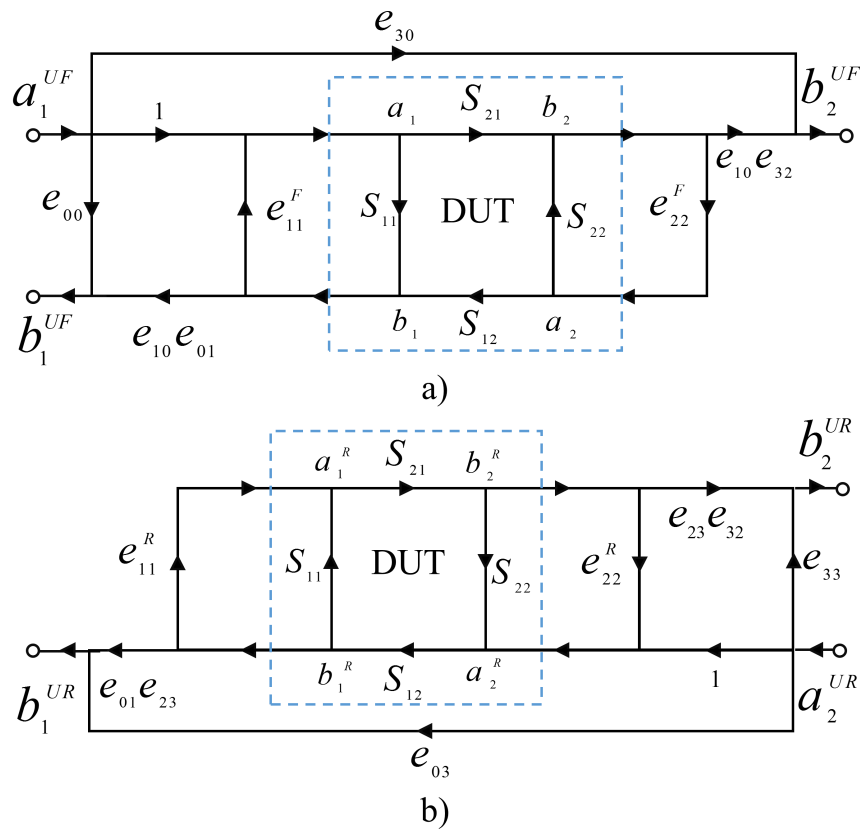


Figure 10. Signal flow diagram representing the a) forward and b) reverse measurements.

and the impedance of the ports. Finally, the connection of a load of very low reflection coefficient (match) is used to determine the isolation terms [Reynoso-Hernandez (2015)].

In most cases, the isolation terms are smaller than the connector repeatability and can be neglected [Wartenberg (2002)]. Furthermore, note that the forward source match and the reverse load match terms should be identical; meanwhile, the forward load match and the reverse source match should be identical. These four terms can be reduced to two as long as errors due to mismatches between the source and the terminating load every time the switch depicted in Figure 9 changes position (*switching errors*) are removed. The following section describes the procedure to correct the switching errors.

2.5.3 Switching Errors Correction

As described in section 2.3, the S-parameters of a two-port DUT are measured by capturing the ratio of the scattered to the incident waves at the DUT ports when one of the ports is terminated with a load of impedance Z_0 . In ideal conditions, the instrument's switch routes the signal from the source to one of the DUT ports while terminates the other port with a load of impedance Z_0 . However, due to mismatches between the source and the terminating load every time the switch changes position, the measured S-parameters are erroneous [Rytting (2004); Zarate-de Landa (2012)].

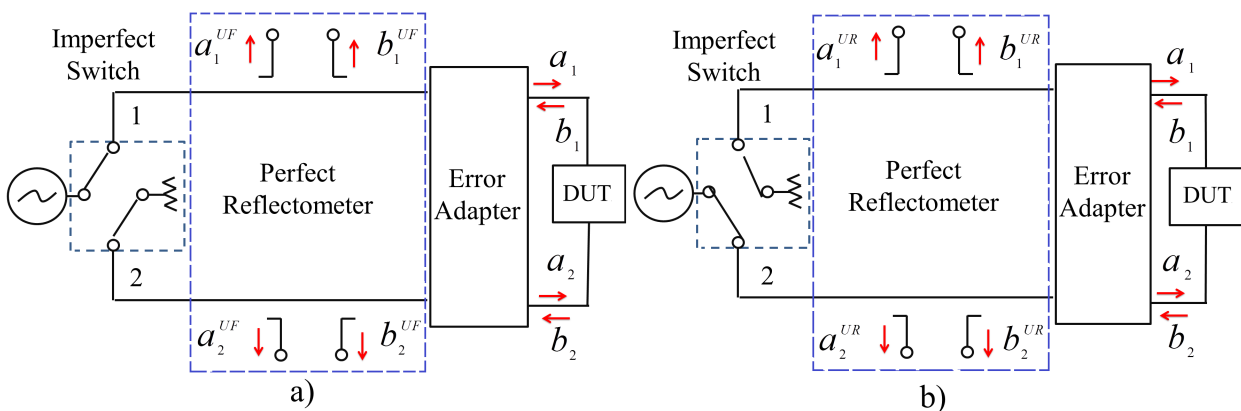


Figure 11. VNA configuration for the correction of the switching errors in the a) forward and b) reverse directions.

The procedure for correcting these *switching errors* uses two sets of incident and scattered waves measured using an uncalibrated VNA. One set of incident, (a_1^{UF}, a_2^{UF}) and scattered (b_1^{UF}, b_2^{UF}) waves is measured by configuring the VNA as shown in Figure 11a. These wave quantities are related by using (8) as

$$\begin{bmatrix} b_1^{UF} \\ b_2^{UF} \end{bmatrix} = \begin{bmatrix} S_{11m} & S_{12m} \\ S_{21m} & S_{22m} \end{bmatrix} \begin{bmatrix} a_1^{UF} \\ a_2^{UF} \end{bmatrix}. \quad (31)$$

A second set of incident, (a_1^{UR}, a_2^{UR}) and scattered (b_1^{UR}, b_2^{UR}) waves is measured by configuring the VNA as shown in Figure 11b. These wave quantities may be related as

$$\begin{bmatrix} b_1^{UR} \\ b_2^{UR} \end{bmatrix} = \begin{bmatrix} S_{11m} & S_{12m} \\ S_{21m} & S_{22m} \end{bmatrix} \begin{bmatrix} a_1^{UR} \\ a_2^{UR} \end{bmatrix}. \quad (32)$$

In (31) and (32), S_{ijm} , $i, j = 1, 2$, represent the measured S-parameters of a DUT free from switching errors. By combining (31)-(32), the following equation may be derived

$$\begin{bmatrix} S_{11m} & S_{12m} \\ S_{21m} & S_{22m} \end{bmatrix} = \begin{bmatrix} b_1^{UF} & b_1^{UR} \\ b_2^{UF} & b_2^{UR} \end{bmatrix} \begin{bmatrix} a_1^{UF} & a_1^{UR} \\ a_2^{UF} & a_2^{UR} \end{bmatrix}^{-1}. \quad (33)$$

Equation (33) allows determining the DUT S-parameters even though the system has not been terminated with a load of impedance Z_0 and therefore removes the effect of the switch. The accuracy of VNA measurements is enhanced when the ratio of signals are measured instead of unratiod quantities. In this sense, by developing (33) and equating the terms at the right and left hand sides, one has

$$S_{11m} = (S_{11_{raw}} - S_{12_{raw}}S_{21_{raw}}G_2) / D \quad (34)$$

$$S_{21m} = (S_{21_{raw}} - S_{22_{raw}}S_{21_{raw}}G_2) / D \quad (35)$$

$$S_{22m} = (S_{22_{raw}} - S_{21_{raw}}S_{12_{raw}}G_1) / D \quad (36)$$

$$S_{12m} = (S_{12_{raw}} - S_{11_{raw}}S_{12_{raw}}G_1) / D, \quad (37)$$

where $D = 1 - S_{12_{raw}}S_{21_{raw}}G_1G_2$. In these expressions, $S_{11_{raw}} = b_1^{UF}/a_1^{UF}$, $S_{21_{raw}} = b_2^{UF}/a_1^{UF}$, $S_{12_{raw}} = b_1^{UR}/a_2^{UR}$, $S_{22_{raw}} = b_2^{UR}/a_2^{UR}$, represent the S-parameters of a DUT before the switching error correction. $G_1 = a_1^{UR}/b_1^{UR}$ and $G_2 = a_2^{UF}/b_2^{UF}$ are ratioed quantities that are measured under reverse and forward conditions, respectively, and are independent of the DUT. Thus, they can be measured only once by using the measurement of an arbitrary device; in practice it is recommended to use a thru or a transmission line for measuring these quantities.

2.5.4 The 8-term error model

Once the switching errors are removed and the isolation errors are either neglected or removed before the calibration procedure, the 12-term error model is reduced to an error model comprising eight terms, four at each port. As shown in Figure 12, it allows representing the measurement system as the cascade connection of three two-port networks, representing the DUT and error adapters at each VNA port.

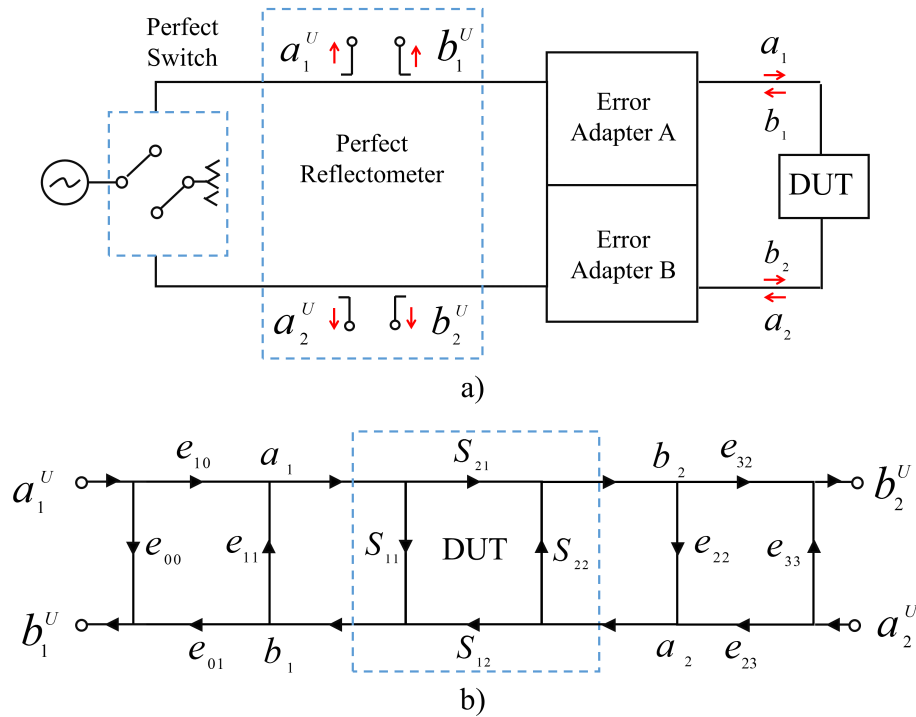


Figure 12. a) VNA configuration diagram a b) signal flow diagram of the 8-terms error model.

The representation of the VNA as the cascade connection of two-port networks allows using mathematical tools for circuit analysis, such as the T-parameters and ABCD-parameters to analyze the measurements performed in a two-port VNA. As a consequence, advanced calibration techniques, such as TRL, TRM or TRRM may be implemented to determine the VNA systematic errors. The advantage of using this family of calibration techniques is that the calibration structures used to determine the error terms do not have to be fully known and some their electrical characteristics are self-calculated in the calibration process. The mathematical procedures of these techniques are fully described in chapter 3.

3. VNA Calibration Techniques

3.1 Introduction

Using a calibrated VNA to evaluate the small-signal behavior of a device under test (DUT) by means of S-parameters is a well known concept in the microwave community [Hiebel (2007); Rumiantsev (2008)]. Since linear VNA calibration is the first part of the calibration of nonlinear measurement systems, such as load-pull systems [Ferrero (1993); Pisani (1996); Roblin (2011)], this chapter is devoted to describe the most important features of VNA calibration techniques.

The mathematical procedures of most of the calibration techniques reported in the literature have been developed using the T-parameters formalism, which as described in section 2.4, are defined as a function of a reference impedance. When measuring S-parameters using an uncalibrated VNA, the reference impedance is identical to the measuring system impedance Z_0 . Nonetheless, calibration techniques developed using T-parameters refer the calibrated measurements to the impedance of one of the calibration structures [Williams (1991)], typically the impedance of a broadband load or the characteristic impedance of a transmission line.

Although the value of the impedance of the transmission lines and loads commonly used as calibration structures are close to Z_0 at low RF frequencies, their values are usually frequency-dependent and may differ from Z_0 at microwave frequencies. Therefore, the measurements calibrated using a calibration technique implemented using T-parameters are referred to a frequency-dependent impedance.

On the other hand, the representation of the linear behavior of a device using ABCD-parameters, is not dependent of a reference impedance [Dobrowolsky (1991); Qian (2007)]. Thus, from a mathematical point of view, the use of ABCD-parameters in the development of calibration algorithms allows eliminating the problem of determining the impedance to

which the calibration is referred. When using the ABCD-parameters formalism, the unique impedance to which the calibration is referred is Z_0 .

In the literature, only a version of the TRRM calibration [Hayden (2006)] and the LL de-embedding method [Zuñiga-Juarez (2009)] have been developed using the ABCD-parameters formalism. In this chapter, the ABCD-parameters are used to develop a unified formulation of the TRL (thru-reflect-line), TRM (thru-reflect-match) and TRRM (thru-reflect-reflect-match) techniques. Moreover, the line, offset-open, offset-short (LZZ) technique, which is a contribution of this dissertation, is also developed using the ABCD-parameters matrix formalism. The one-port OSM (Open-Short-Match) technique is also described.

3.2 ABCD-parameters representation of a transmission line

All of the two-port calibration techniques use as calibration element the connection of the VNA ports. Such a connection is typically carried out by using the measurement of a uniform transmission line¹.

The electrical behavior of a uniform transmission line may be fully described by its characteristic impedance Z_L , propagation constant γ and length l . The ABCD-parameters representation of a uniform transmission line \mathbf{T}_L is denoted as

$$\mathbf{T}_L = \begin{bmatrix} \cosh(\gamma l) & Z_L \sinh(\gamma l) \\ Z_L^{-1} \sinh(\gamma l) & \cosh(\gamma l) \end{bmatrix}. \quad (38)$$

In this section, one of the most powerful tools of linear algebra, matrix diagonalization, is applied to the analysis of the properties of a uniform transmission line. First, some important concepts about the matrix diagonalization are reviewed. Then, matrix diagonalization is used to decompose the ABCD parameters matrix of a transmission line as a matrix product, with several important implications in the analysis of VNA calibration techniques.

¹The short-open-load-reciprocal (SOLR) [Ferrero (1992)] is the only technique that allows using an arbitrary reciprocal two-port device as calibration element, not strictly a uniform transmission line.

One of the most important problems in linear algebra, the eigenvalue problem, is first presented. Let \mathbf{A} be a $n \times n$ matrix. A number λ is called an eigenvalue of \mathbf{A} if there exists a nonzero vector \mathbf{x} such that

$$\mathbf{A}\mathbf{x} = \lambda\mathbf{x}. \quad (39)$$

Every nonzero vector \mathbf{x} satisfying (39) is then called an eigenvector of \mathbf{A} associated to the eigenvalue λ . The eigenvalues of a matrix \mathbf{A} may be determined as follows. Let \mathbf{I}_n be the $n \times n$ identity matrix. Then, equation (39) can be written as $\lambda\mathbf{I}_n\mathbf{x} = \mathbf{A}\mathbf{x}$ and after some algebra the following expression may be obtained

$$(\lambda\mathbf{I}_n - \mathbf{A})\mathbf{x} = 0. \quad (40)$$

This homogeneous equation has a nonzero solution if and only if the determinant of $\lambda\mathbf{I}_n - \mathbf{A}$ equals zero. Equation 40 is known as the characteristic equation of \mathbf{A} , while the expression obtained from the calculation its determinant is known as its characteristic polynomial. An eigenvalue of \mathbf{A} is a scalar λ , such that $|\lambda\mathbf{I}_n - \mathbf{A}| = 0$ and the eigenvectors associated to λ are the nonzero solutions to (40).

Related to the determination of the eigenvalues of a matrix \mathbf{A} is the diagonalization of such a matrix. It consist in investigating if for a nonsingular square matrix \mathbf{A} there exist a nonsingular matrix \mathbf{P} such that $\mathbf{P}^{-1}\mathbf{A}\mathbf{P}$ is identical to a diagonal matrix \mathbf{D} . Two matrices \mathbf{A} and \mathbf{D} are said to be similar if there exist a nonsingular matrix \mathbf{P} such that $\mathbf{D} = \mathbf{P}^{-1}\mathbf{A}\mathbf{P}$. Two similar matrices \mathbf{A} and \mathbf{D} have the following properties:

$$\det(\mathbf{A}) = \det(\mathbf{D}), \quad (41)$$

$$\text{tr}(\mathbf{A}) = \text{tr}(\mathbf{D}), \quad (42)$$

$$\text{eig}(\mathbf{A}) = \text{eig}(\mathbf{D}), \quad (43)$$

where the operators $det(\cdot)$, $tr(\cdot)$ and $eig(\cdot)$, denote the determinant, the trace and the eigenvalues of matrices \mathbf{A} and \mathbf{D} . A $n \times n$ matrix \mathbf{A} may be diagonalized if and only if it has n linearly dependent associated eigenvectors. If \mathbf{A} and \mathbf{D} are two similar matrices, then the n eigenvalues $\lambda_1, \lambda_2, \lambda_3, \dots, \lambda_n$, are the elements of the diagonal matrix \mathbf{D} ,

$$\mathbf{D} = \begin{bmatrix} \lambda_1 & 0 & \cdots & 0 \\ 0 & \lambda_2 & \cdots & 0 \\ \vdots & \vdots & \ddots & \vdots \\ 0 & 0 & \cdots & \lambda_n \end{bmatrix}. \quad (44)$$

Let $\mathbf{x}_1, \mathbf{x}_2, \mathbf{x}_3, \dots, \mathbf{x}_n$ be the eigenvectors associated to a set of eigenvalues $\lambda_1, \lambda_2, \lambda_3, \dots, \lambda_n$. If these eigenvectors form a set of linearly independent vectors, then the $n \times n$ matrix \mathbf{P} ,

$$\mathbf{P} = \begin{bmatrix} \mathbf{x}_1 & \mathbf{x}_2 & \mathbf{x}_3 & \cdots & \mathbf{x}_n \end{bmatrix}, \quad (45)$$

is a matrix such that the identity $\mathbf{D} = \mathbf{P}^{-1}\mathbf{A}\mathbf{P}$ holds.

The ABCD-parameters matrix representation of a uniform transmission line denoted in (38) may be diagonalized [Reynoso-Hernandez (2012)]. Thus, it is possible to express the matrix \mathbf{T}_L as a product of the form

$$\mathbf{T}_L = \mathbf{T}_Z \mathbf{T}_\lambda \mathbf{T}_Z^{-1}. \quad (46)$$

A transmission line is a reciprocal device; an implication of this fact is that its determinant equals the unity. From (38) it is possible to verify that $det(\mathbf{T}_L) = 1$. Since two similar matrices have identical determinant, $det(\mathbf{T}_\lambda) = 1$. Therefore, its eigenvalues λ_1 and λ_2 are related as $\lambda_1 = 1/\lambda_2$.

Using the theory presented in the preceding section, the eigenvalues of \mathbf{T}_L may be calculated and expressed as $\lambda_1 = e^{-\gamma l}$ and $\lambda_2 = e^{\gamma l}$. Thus, the matrix of eigenvalues \mathbf{T}_λ is expressed as follows

$$\mathbf{T}_\lambda = \begin{bmatrix} \lambda_L & 0 \\ 0 & \lambda_L^{-1} \end{bmatrix}, \quad (47)$$

where $\lambda_L = e^{-\gamma l}$, $\gamma = \alpha + j\beta$, with α and β as the per-unit-length losses and phase constants of a transmission line. The eigenvectors associated to λ_1 and λ_2 are

$$\mathbf{x}_1 = \begin{bmatrix} -Z_B \\ 1 \end{bmatrix}, \quad (48)$$

$$\mathbf{x}_2 = \begin{bmatrix} Z_A \\ 1 \end{bmatrix}, \quad (49)$$

where $Z_A = Z_B = Z_L$. Then, one can express the matrix of eigenvectors \mathbf{T}_Z as follows

$$\mathbf{T}_Z = \begin{bmatrix} \mathbf{x}_1 & \mathbf{x}_2 \end{bmatrix} = \begin{bmatrix} -Z_B & Z_A \\ 1 & 1 \end{bmatrix}. \quad (50)$$

The diagonalization of the ABCD-parameters matrix representation of a transmission line is very useful in the development of calibration algorithms for the TRL and LZZ techniques allowing the use of lines of arbitrary impedance as calibration structures. In the case of a zero-length thru, \mathbf{T}_λ is identical to the 2x2 identity matrix \mathbf{I}_2 . In such a case $\mathbf{T}_L = \mathbf{I}_2 = \mathbf{T}_Z \mathbf{T}_Z^{-1}$, independently of the values of Z_A and Z_B in (50). Hence, when using a thru instead of a line as calibration element, the identity $\mathbf{I}_2 = \mathbf{T}_Z \mathbf{T}_Z^{-1}$ holds even though Z_A and Z_B are different from Z_L . This is useful to develop calibration algorithms for the TRM and TRRM techniques allowing the use of loads of arbitrary impedance.

3.3 Statement of the general problem of VNA calibration

The calibration procedures described in this section are based on the use of the 8-term error model; this means that the isolation errors and errors due to source mismatch (switching errors) are either ignored or have been corrected in a step different from the calibration.

When using the 8-term error model and the ABCD-parameters, the measurement of a DUT (Figure 13) can be mathematically expressed as

$$\mathbf{M}_D = \mathbf{T}_A \mathbf{T}_D \mathbf{T}_B. \quad (51)$$

In (51), \mathbf{M}_D and \mathbf{T}_D are ABCD-parameters matrices modeling the uncorrected and the actual behavior of a DUT, respectively. Meanwhile, \mathbf{T}_A and \mathbf{T}_B are matrices modeling the errors in ports one and two of the VNA, respectively.



Figure 13. Measurement of a two-port DUT.

The problem to solve in calibration is to calculate the elements of the matrices \mathbf{T}_A and \mathbf{T}_B , or some modified version of them, using information provided by the measurement of a determined set of calibration structures. Once these terms are known, the ABCD parameters of a DUT may be determined by solving (51) for \mathbf{T}_D .

3.4 Measurement of calibration structures

In this section, the mathematical analysis of the measurement of different calibration structures used in VNA calibration techniques is presented. The information provided by the measurement of these structures is used in the following section to explain how different calibration techniques determine the calibration error terms.

3.4.1 Measurement of a transmission line

As previously presented, the ABCD-parameters matrix of a uniform transmission line may be represented by the matrix product $\mathbf{T}_L = \mathbf{T}_Z \mathbf{T}_\lambda \mathbf{T}_Z^{-1}$. Hence, the measurement of a transmission line may be expressed as

$$\mathbf{M}_L = \mathbf{T}_A \mathbf{T}_L \mathbf{T}_B = \mathbf{T}_X \mathbf{T}_\lambda \mathbf{T}_Y, \quad (52)$$

where

$$\mathbf{T}_X = \mathbf{T}_A \mathbf{T}_Z \triangleq D_X \overline{\mathbf{T}}_X = D_X \begin{bmatrix} \overline{A}_X & \overline{B}_X \\ \overline{C}_X & 1 \end{bmatrix}, \quad (53)$$

$$\mathbf{T}_Y = \mathbf{T}_Z^{-1} \mathbf{T}_B \triangleq D_Y \overline{\mathbf{T}}_Y = D_Y \begin{bmatrix} \overline{A}_Y & \overline{B}_Y \\ \overline{C}_Y & 1 \end{bmatrix}. \quad (54)$$

Solving (51) for \mathbf{T}_D one has

$$\mathbf{T}_D = \mathbf{T}_A^{-1} \mathbf{M}_D \mathbf{T}_B^{-1}. \quad (55)$$

Then, by solving (53) and (54) for \mathbf{T}_A and \mathbf{T}_B , respectively, and substituting the resultant expressions in (55), the following expression for \mathbf{T}_D is obtained

$$\mathbf{T}_D = \mathbf{T}_Z \mathbf{T}_X^{-1} \mathbf{M}_D \mathbf{T}_Y^{-1} \mathbf{T}_Z^{-1}. \quad (56)$$

In order to determine the ABCD parameters of a DUT, provided that the matrix \mathbf{T}_Z is known, seven terms have to be calculated during the calibration process: three elements of the matrix \mathbf{T}_X , namely \overline{A}_X , \overline{B}_X , \overline{C}_X , three elements of the matrix \mathbf{T}_Y , namely \overline{A}_Y , \overline{B}_Y , \overline{C}_Y , and the product $D_X D_Y$.

Using the measurement of a transmission line, it is possible to determine expressions for four of the seven calibration terms. Solving (52) for \mathbf{T}_Y and using (53)-(54), the following expressions may be obtained

$$\overline{A}_Y = \frac{1}{\overline{C}_X} \frac{p_{11} - \overline{B}_X p_{21}}{-p_{12} + \frac{\overline{A}_X}{\overline{C}_X} p_{22}} \lambda_L^{-2}, \quad (57)$$

$$\overline{B}_Y = \frac{1}{\overline{C}_X} \frac{p_{12} - \overline{B}_X p_{22}}{-p_{12} + \frac{\overline{A}_X}{\overline{C}_X} p_{22}} \lambda_L^{-2}, \quad (58)$$

$$\overline{C}_Y = \frac{-p_{11} + \frac{\overline{A}_X}{\overline{C}_X} p_{21}}{-p_{12} + \frac{\overline{A}_X}{\overline{C}_X} p_{22}}, \quad (59)$$

$$D_X D_Y = \frac{\frac{\overline{A}_X}{\overline{C}_X} p_{22} - p_{12}}{\frac{\overline{A}_X}{\overline{C}_X} - \overline{B}_X} \lambda_L. \quad (60)$$

Note that for calculating these terms $\frac{\overline{A}_X}{\overline{C}_X}$, \overline{B}_X and \overline{C}_X have to be known. The following sections show how to determine $\frac{\overline{A}_X}{\overline{C}_X}$, \overline{B}_X and \overline{C}_X by combining the measurements of different sets of calibration structures.

3.4.2 Measurement of a thru

A special case of the measurement of the connection of the VNA ports is when it is achieved by using the through connection of the VNA ports, as depicted in Figure 14. This connection is commonly referred to as the *thru*.

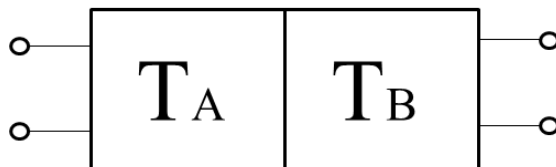


Figure 14. Equivalent structure of the through connection of ports one and two of the VNA.

The TRL, TRM and TRRM techniques use the thru measurement as one of the calibration structures. The thru structure shown in Figure 14 may be mathematically analyzed as a zero-length transmission line as follows.

Let \mathbf{T}_T , defined as

$$\mathbf{T}_T = \mathbf{I}_2 = \mathbf{T}_Z \mathbf{T}_Z^{-1}, \quad (61)$$

be an ABCD-parameters matrix denoting the through connection of the VNA ports. Then, the measurement of the structure shown in Figure 14 may be represented as

$$\mathbf{M}_T = \mathbf{T}_A \mathbf{T}_T \mathbf{T}_B. \quad (62)$$

By substituting (61) in (62), it is possible to express \mathbf{M}_T as

$$\mathbf{M}_T = \mathbf{T}_X \mathbf{T}_Y. \quad (63)$$

It is worth mentioning that in the case of a thru ($l = 0$), the terms $\overline{A_Y}$, $\overline{B_Y}$, $\overline{C_Y}$ and $D_X D_Y$ can still be calculated from (57)-(60) by using $\lambda_L = 1$.

3.4.3 Measurement of a pair of loads

All of the VNA calibration techniques use the measurement of at least one pair of loads which have to be connected at ports one and two of the VNA. The loads commonly used as calibration elements are: loads of very low impedance (ideally short circuits), loads of very high impedance (ideally open circuits) and loads of impedance value close to Z_0 (commonly referred to as the *match* standard). In the analysis developed in the following sections O , S and M will denote the use of an open circuit, a short circuit and a load of impedance close to Z_0 , respectively.

In this section, general expressions for the impedance at the input of port P ($P = 1, 2$) of the VNA Z_{KP}^m ($K = O, S, M$), when it is loaded with a load of impedance Z_{KP} are obtained and the information provided by the measurement of these loads is studied.

According to [Dobrowolsky (1991)], the equivalent ABCD-parameters matrix of a shunted load of impedance Z_{KP} (Figure 15) is expressed as

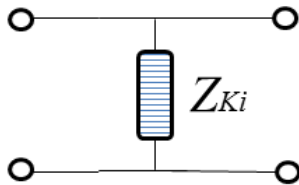


Figure 15. Equivalent two-port structure of a shunted load.

$$\mathbf{T}_{\mathbf{KP}} = \begin{bmatrix} 1 & 0 \\ Z_{KP}^{-1} & 1 \end{bmatrix}. \quad (64)$$

The loads used as calibration elements in VNA calibration techniques are not two-port networks, but one port terminations. Thus, they have no ABCD-parameters matrix representation. Nevertheless, it is possible to analyze these one-port structures by means of the ABCD-parameters matrix shown in (64) using the concept of *impedance at the input of a two port network under output open-circuit condition* [Dobrowolsky (1991); Gonzalez (1997)], as presented next.

Measurement of a load at port 1

The equivalent ABCD-parameters matrix of the structure enclosed in dotted lines in Figure 16a, $\mathbf{M}_{\mathbf{K1}}$, may be expressed as

$$\mathbf{M}_{\mathbf{K1}} = \mathbf{T}_{\mathbf{A}} \mathbf{T}_{\mathbf{K1}}. \quad (65)$$

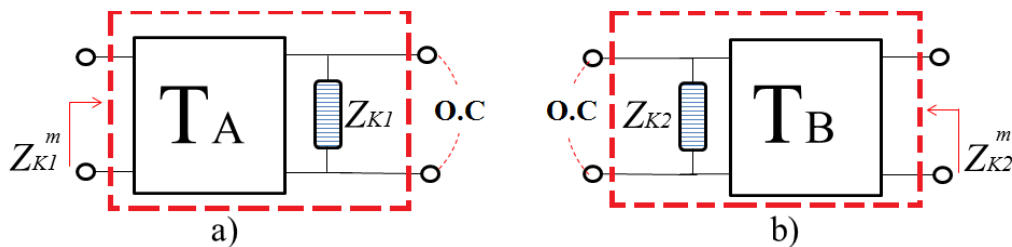


Figure 16. Equivalent structures of the measurement of loads connected at: a) port 1 y b) port 2 of the VNA.

To be consistent with the nomenclature used in (63) for the measurement of the thru

structure, it is necessary to express $\mathbf{M}_{\mathbf{K1}}$ as a function of $\mathbf{T}_{\mathbf{X}}$. By solving (53) for $\mathbf{T}_{\mathbf{A}}$ and substituting the resulting expression in (65), $\mathbf{M}_{\mathbf{K1}}$ may be expressed as

$$\mathbf{M}_{\mathbf{K1}} = \mathbf{T}_{\mathbf{X}}\mathbf{T}_{\mathbf{Z}}^{-1}\mathbf{T}_{\mathbf{K1}}. \quad (66)$$

Then, by developing (66) and calculating the impedance at the input of the structure shown in Figure 16a under output open-circuit condition, one has

$$Z_{K1}^m = \frac{\overline{A_X}(Z_{K1} - Z_A) - \overline{B_X}(Z_{K1} + Z_B)}{\overline{C_X}(Z_{K1} - Z_A) - (Z_{K1} + Z_B)}. \quad (67)$$

Measurement of a load at port 2

The equivalent ABCD-parameters matrix of the structure shown in Figure 16b, $\mathbf{M}_{\mathbf{K2}}$, may be expressed as

$$\mathbf{M}_{\mathbf{K2}} = \widetilde{\mathbf{T}}_{\mathbf{B}}\mathbf{T}_{\mathbf{K2}}. \quad (68)$$

$\widetilde{\mathbf{T}}_{\mathbf{B}}$ is the reverse cascading ABCD parameters matrix corresponding to the matrix $\mathbf{T}_{\mathbf{B}}$, which according to [Pulido-Gaytan (2013)], may be defined as

$$\widetilde{\mathbf{T}}_{\mathbf{B}} = \mathbf{X}\mathbf{T}_{\mathbf{B}}^{-1}\mathbf{X}, \quad (69)$$

where

$$\mathbf{X} = \begin{bmatrix} \pm 1 & 0 \\ 0 & \mp 1 \end{bmatrix}. \quad (70)$$

By substituting (69)-(70) in (68), $\mathbf{M}_{\mathbf{K2}}$ may be expressed as

$$\mathbf{M}_{\mathbf{K2}} = \mathbf{X}\mathbf{T}_{\mathbf{B}}^{-1}\mathbf{X}\mathbf{T}_{\mathbf{K2}}. \quad (71)$$

To be consistent with the nomenclature used in (63) for the measurement of the thru, it is necessary to express $\mathbf{M}_{\mathbf{K}2}$ as a function of $\mathbf{T}_{\mathbf{Y}}$. By solving (54) for $\mathbf{T}_{\mathbf{B}}$ and substituting the resultant expression in (71), $\mathbf{M}_{\mathbf{K}2}$ may be expressed as

$$\mathbf{M}_{\mathbf{K}2} = \mathbf{X}\mathbf{T}_{\mathbf{Y}}^{-1}\mathbf{T}_{\mathbf{Z}}^{-1}\mathbf{X}\mathbf{T}_{\mathbf{K}2}. \quad (72)$$

Finally, by developing (72) and calculating the impedance at the input of the structure shown in Figure 16b under output open-circuit condition, one has

$$Z_{K2}^m = \frac{\overline{B}_Y (Z_{K2} - Z_B) + (Z_{K2} + Z_A)}{\overline{A}_Y (Z_{K2} - Z_B) + \overline{C}_Y (Z_{K2} + Z_A)}. \quad (73)$$

Loading the VNA ports with a pair of reflecting loads

The TRL, TRM, TRRM and LZZ calibration techniques use at least one pair of symmetrical reflecting loads connected at ports one and two of the VNA², for determining the \overline{C}_X term. In order to determine an expression for \overline{C}_X , the expressions shown in (67) and (73) are analyzed as follows.

The loads commonly used as reflecting loads in VNA calibration techniques are either loads of very low impedance or loads of very high impedance. Thus, the subindex K in (67) and (73) is substituted here by the subindex $R=O,S$ in this analysis in order to denote the use of a highly reflecting load.

Regarding VNA port one, by solving (67) for Z_{K1} ($\equiv Z_{R1}$) one has

$$Z_{R1} = \frac{Z_A \overline{C}_X + Z_B \eta_{R1}}{\overline{C}_X - \eta_{R1}}, \quad (74)$$

where

²The symmetry condition recalls to the condition in which the load connected at port one is identical to the load connected at port two.

$$\eta_{R1} = \frac{Z_{R1}^m - \overline{B_X}}{Z_{R1}^m - \frac{\overline{A_X}}{C_X}}. \quad (75)$$

Then, regarding the port two of the VNA, by solving (73) for Z_{K2} ($\equiv Z_{R2}$) the following expression is obtained

$$Z_{R2} = \frac{Z_B \overline{A_Y} + Z_A \eta_{R2}}{\overline{A_Y} - \eta_{R2}}, \quad (76)$$

where

$$\eta_{R2} = \frac{1 - Z_{R2}^m \overline{C_Y}}{Z_{R2}^m - \frac{\overline{B_Y}}{A_Y}}. \quad (77)$$

For a symmetrical load, the impedance of the load connected a port one has to be identical to the impedance of the load connected at port two ($Z_{R1} = Z_{R2}$). Thus, by equating (74) to (76) the following quadratic equation may be obtained

$$\overline{C_X} = \frac{-c_1 \pm \sqrt{c_1^2 - 4c_2c_0}}{2c_2}, \quad (78)$$

where

$$c_0 = -Z_B \eta_{R1} (\overline{A_Y} \cdot \overline{C_X}), \quad (79)$$

$$c_1 = \frac{1}{2} (\overline{A_Y} \cdot \overline{C_X} + \eta_{R1}, \eta_2) (Z_B - Z_A), \quad (80)$$

$$c_2 = Z_A \eta_{R2}. \quad (81)$$

In most of the calibration techniques $Z_A = Z_B$, and then (78) reduces to

$$\overline{C_X} = \pm \sqrt{(\overline{A_Y} \cdot \overline{C_X}) \eta_{R1} / \eta_{R2}}. \quad (82)$$

From (78) and (82) it is possible to observe that for calculating $\overline{C_X}$ it is necessary to know the value of $\frac{\overline{A_X}}{C_X}$ and $\overline{B_X}$. In the following sections it is described how to determine these

terms by using the measurements of the calibration structures corresponding to different calibration techniques.

3.5 The TRL calibration technique

The Thru-Reflect-Line (TRL) calibration technique uses as calibration elements the through connection of the VNA ports, a transmission line of characteristic impedance Z_L and a pair of loads of impedance $Z_R \neq Z_L$ connected at both ports of the VNA³, as shown in Figure 17.

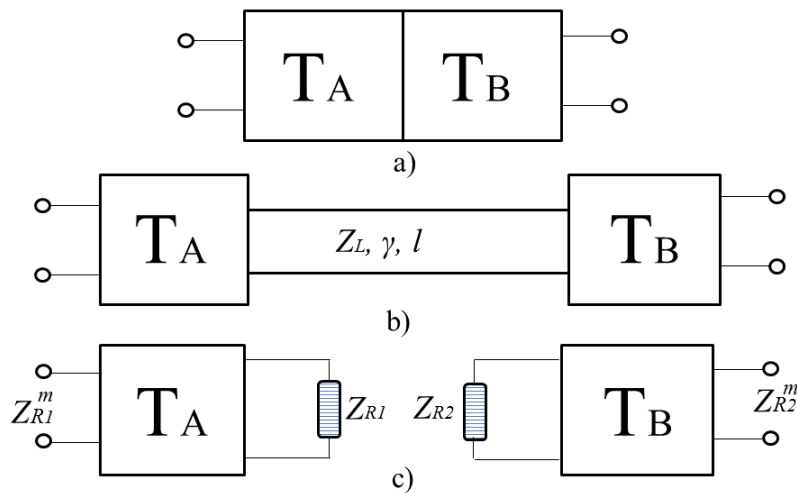


Figure 17. TRL calibration structures: a) thru, b) line and c) reflecting load.

The TRL was introduced in [Engen (1979)] using T-parameters for representing the VNA and the calibration elements. The TRL procedure of [Engen (1979)] assumes that the line used as calibration element is a non reflecting line. It implies that the calibration reference impedance is identical to Z_L . Then, in [Marks (1991)] a procedure for transforming the calibration reference impedance of the TRL from Z_L to Z_0 in a step after the calibration, was introduced.

The procedure for implementing the TRL developed in this work uses the ABCD-parameters to represent the VNA and the calibration structures. It is demonstrated that the unique

³The TRL can also be implemented by using two lines of different length and of identical characteristic impedance and propagation constant. This method is known as LRL (Line-Reflect-Line).

impedance to which the calibration is referred is Z_0 , without the use of reference impedance transformations after the calibration.

3.5.1 TRL calibration procedure

The TRL calibration technique determines the $\frac{\overline{A_X}}{\overline{C_X}}$ and $\overline{B_X}$ terms using the thru-line pair combination, as presented next.

The use of the thru-line pair combination

According to the analysis presented in section 3.4, the ABCD-parameters matrix of the structure shown in Figure 17a (thru) may be denoted as $\mathbf{M}_T = \mathbf{T}_X \mathbf{T}_Y$. Meanwhile, according to the analysis presented in section 3.4, the ABCD-parameters matrix of the structure shown in Figure 17b (line) may be denoted as $\mathbf{M}_L = \mathbf{T}_X \mathbf{T}_\lambda \mathbf{T}_Y$. Then, by calculating the matrix product $\mathbf{M}_{LT} = \mathbf{M}_L \mathbf{M}_T^{-1}$ one has

$$\mathbf{M}_{LT} = \mathbf{T}_X \mathbf{T}_\lambda \mathbf{T}_X^{-1} = \begin{bmatrix} m_{11} & m_{12} \\ m_{21} & m_{22} \end{bmatrix}, \quad (83)$$

with \mathbf{T}_λ previously defined in section 3.2.

Then, by substituting (47) and (53) in (83) and developing the resulting expression, the following equations may be derived

$$\frac{\overline{A_X}}{\overline{C_X}}, \overline{B_X} = \frac{(m_{11} - m_{22}) \pm \sqrt{(m_{11} - m_{22})^2 - 4(m_{12}m_{21})}}{2m_{21}}, \quad (84)$$

$$\lambda = \frac{\frac{\overline{A_X}}{\overline{C_X}} m_{11} + m_{21} - \frac{\overline{A_X}}{\overline{C_X}} \overline{B_X} m_{21} - \overline{B_X} m_{22}}{\frac{\overline{A_X}}{\overline{C_X}} - \overline{B_X}}. \quad (85)$$

In (84) one of the roots corresponds to $\frac{\overline{A_X}}{\overline{C_X}}$ and the other root corresponds to $\overline{B_X}$. The values of $\frac{\overline{A_X}}{\overline{C_X}}$ and $\overline{B_X}$ have to be chosen in such a way that they allow calculating a continuous value of λ using (85) [Reynoso-Hernandez (2003, 2012)].

The $\overline{C_X}$ term is calculated as presented in section 3.4 using the measurement of a pair of reflecting loads of identical impedance.

Limitations of the TRL technique

The frequency bandwidth of the measurements corrected using the TRL is limited since the equations characterizing the TRL are ill-conditioned at frequencies where the phase shift of the thru-line pair combination is $k \cdot 180^\circ$, $k \in \mathbb{N}$. According to (56), to determine the ABCD-parameters of a DUT, it is required that the matrices $\mathbf{T_X}$ and $\mathbf{T_Y}$ are nonsingular matrices. The matrix $\mathbf{T_X}$ is nonsingular if its determinant,

$$\det(\mathbf{T_X}) = \overline{A_X} - \overline{B_X C_X} = \overline{C_X} \left(\frac{\overline{A_X}}{\overline{C_X}} - \overline{B_X} \right), \quad (86)$$

is different from zero, which implies that $\frac{\overline{A_X}}{\overline{C_X}} \neq \overline{B_X}$.

By multiplying both sides of (83), by the right hand side, by $\mathbf{T_X}$ and equating term by term the resultant equation the following expressions may be obtained

$$\frac{\overline{A_X}}{\overline{C_X}} = \frac{m_{12}}{\lambda - m_{11}}, \quad (87)$$

$$\overline{B_X} = \frac{m_{12}}{\lambda^{-1} - m_{11}}. \quad (88)$$

From (87) and (88) it can be noted that $\frac{\overline{A_X}}{\overline{C_X}} = \overline{B_X}$ when $\lambda = e^{\gamma l} = 1$, which occurs when βl is a multiple of 180° and αl is close to zero. Hence, a very short transmission line is useful to avoid βl be close to a multiple of 180° at high frequencies, meanwhile long transmission lines are useful to avoid that βl be close to 0° at low frequencies. The use of different lines for covering a wide frequency bandwidth is known in the literature as the multi-line TRL technique (mTRL) [Marks (1991)].

3.6 Generalized theory of the TRM calibration technique

By replacing the line used in the TRL by a load, a broadband calibration technique, the Thru-Reflect-Match (TRM), is achieved. The TRM technique uses as calibration structures the through connection of the VNA ports (thru), a symmetrical reflecting load (reflect) and a pair of loads of impedance close to the measuring system impedance (match), as shown in Figure 18.

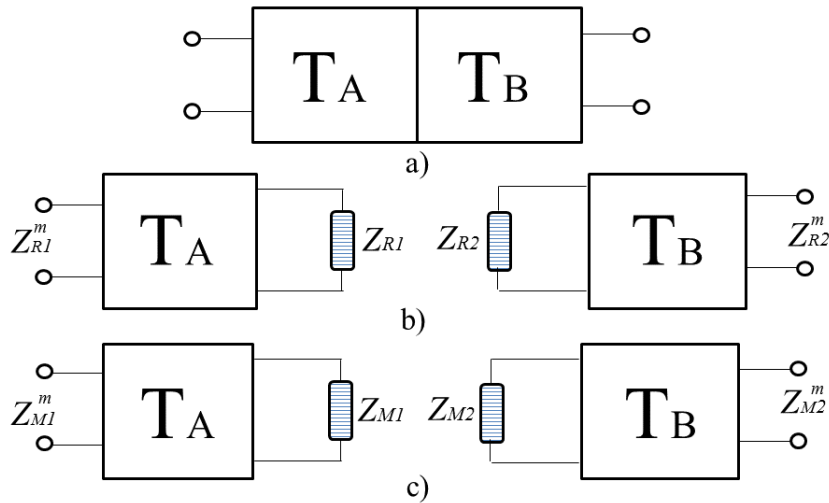


Figure 18. TRM calibration structures: a) thru, b) reflecting load and c) symmetrical/nonsymmetrical load of arbitrary impedance.

The TRM calibration technique was reported in [Eul (1988, 1991)] using the T-parameters formalism. In [Eul (1988, 1991)] the loads used as match standard were assumed as symmetrical loads of impedance identical to Z_0 ; thus, referring the calibration to the impedance of the load used as calibration element.

When dealing with planar structures such as microstrip and coplanar waveguide structures, the value of the load impedance is frequency-dependent [Williams (1995)]. Furthermore, as the frequency increases, the symmetry condition of the loads used as match standard may become difficult to preserve, thus affecting the reference impedance definition and reducing the accuracy of the calibration [Heuermann (1995)].

The TRM calibration implemented using symmetrical loads of frequency-dependent impedance as the match standard was reported in [Williams (1995)]. The TRM of [Williams (1995)]

uses the theory reported in [Marks (1991)] to transform the calibration reference impedance from a frequency-dependent impedance Z_M to the frequency-independent impedance Z_0 in a step after the calibration.

Experimental results regarding the implementation of a TRM-like calibration technique (LRM+), in which the use of nonsymmetrical loads as the match standard is allowed, have been reported in [Scholz (2004); Doerner (2005)]. Nevertheless, a comprehensive analysis of its theory has not yet been published.

A procedure for calibrating the VNA, which uses a known transmitting calibration standard (thru), a symmetrical unknown double one-port standard (reflect) and a double (symmetrical or nonsymmetrical) one-port standard (match) was patented in [Simon (2010)]. Nevertheless, in the procedure of [Simon (2010)] the value of the reflection coefficient of the match standard must be different from zero. Therefore, it does not allow the use of loads of impedance identical to Z_0 .

The TRM procedure developed in this work has been published in [Pulido-Gaytan (2015d)]. It uses the ABCD-parameters matrix formalism to develop a generalized TRM calibration theory, allowing the use of either symmetrical or nonsymmetrical loads of arbitrary impedance as the match standard. This procedure is one of the contributions of this work to the theory of calibration techniques.

3.6.1 TRM calibration procedure

The TRM calibration technique determines the $\overline{\frac{A_X}{C_X}}$ and $\overline{B_X}$ terms by combining the measurements of the thru with the measurement of a symmetrical/nonsymmetrical broadband load of arbitrary impedance.

In this TRM procedure, the non-unity elements of the matrix \mathbf{T}_Z , Z_A and Z_B , are identical to the impedance of the loads used as *match* standards in ports one and two of the VNA, respectively ($Z_A = Z_{M1}$ and $Z_B = Z_{M2}$), which may be either identical or different and of arbitrary value.

The use of the broadband loads

According to the analysis presented in section 3.4, the impedance at the input of port P ($P = 1, 2$) of the VNA Z_{MP}^m when it is loaded with a load of impedance Z_{MP} , may be expressed as

$$Z_{M1}^m = \frac{\overline{A}_X (Z_{M1} - Z_A) - \overline{B}_X (Z_{M1} + Z_B)}{\overline{C}_X (Z_{M1} - Z_A) - (Z_{M1} + Z_B)}, \quad (89)$$

$$Z_{M2}^m = \frac{\overline{B}_Y (Z_{M2} - Z_B) + (Z_{M2} + Z_A)}{\overline{A}_Y (Z_{M2} - Z_B) + \overline{C}_Y (Z_{M2} + Z_A)}. \quad (90)$$

By substituting $Z_A = Z_{M1}$ and $Z_B = Z_{M2}$ in equations (89) and (90), the following expressions may be derived

$$\overline{B}_X = Z_{M1}^m, \quad (91)$$

$$\overline{C}_Y = \frac{1}{Z_{M2}^m}. \quad (92)$$

The value of $\frac{\overline{A}_X}{\overline{C}_X}$ may be determined by substituting (59) in (92) as

$$\frac{\overline{A}_X}{\overline{C}_X} = \frac{p_{12} - p_{11}Z_{M2}^m}{p_{22} - p_{21}Z_{M2}^m}. \quad (93)$$

In the TRM technique, the \overline{C}_X term is calculated as presented in section 3.4 by using the measurement of a pair of reflecting loads, using either equation (78) if the loads used as match standard are symmetrical or equation (82) if these loads are nonsymmetrical.

Limitations of the TRM technique

The accuracy of the TRM technique for calibrating the VNA strongly depends on the knowledge of the complex, frequency-dependent, impedance of the loads used as calibration structures. The impedance of these loads may be determined by using either information obtained

from electromagnetic simulations [Scholz (2004)] combined with information of the loads' fabrication process or by using information obtained from the measurement of the loads using a reference VNA calibration technique [Williams (1995)]. Hence, the main limitation of the TRM technique is imposed by the accuracy with which the impedance of the broadband loads are known.

3.7 The TRRM calibration technique

The Thru-Reflect-Reflect-Match (TRRM) calibration technique uses as calibration elements the through connection of the VNA ports (thru), a pair of symmetrical loads of very low-impedance (short-circuits), a pair of symmetrical loads of very high impedance (open-circuits) and a one-port load of impedance close to Z_0 (match). Figure 19 depicts the set of calibration structures used in the TRRM calibration.

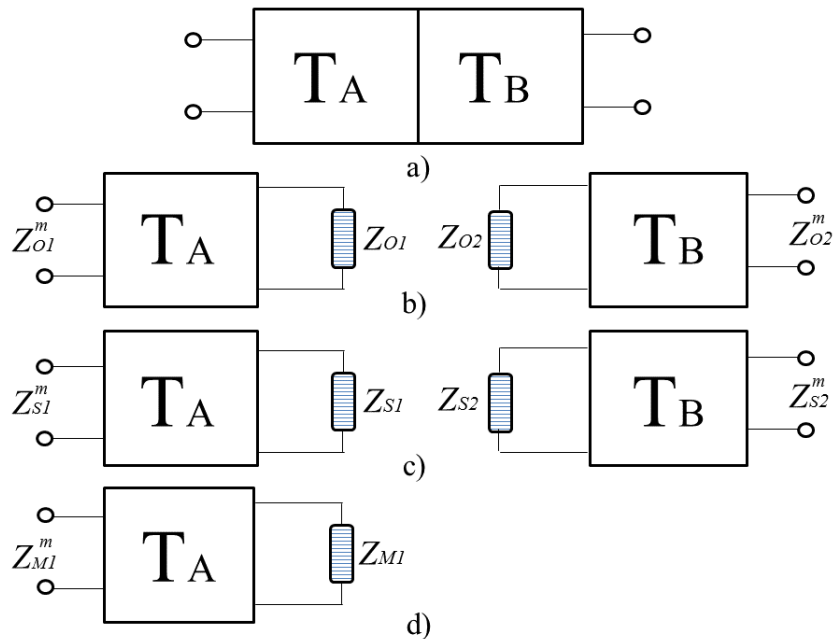


Figure 19. TRRM calibration structures: a) thru, b) a symmetrical load of very high impedance , c) a symmetrical load of very low impedance and d) a one-port load of known impedance.

Unlike the TRM technique, in which it is required to know the impedance of two loads over the frequency band of interest, TRRM only uses one load of known impedance connected at one of the VNA ports; thus, eliminating the problems due to asymmetry between the loads

used as match standards in the TRM.

The TRRM technique was reported for the first time in [Davidson (1990)]; nevertheless, the first TRRM mathematical formulation was presented in [Purroy (2001)]. The TRRM procedure reported in [Purroy (2001)] was developed using T-parameters; it allowed referring the calibration to either the impedance of the load used as match standard or to Z_0 . Then, in [Hayden (2006)] a TRRM procedure using ABCD-parameters was developed (ABCD-parameters are not defined as a function of a reference impedance).

A well known result in the VNA calibration community is that the TRRM technique is more accurate in the port at which the load is connected [Safwat (2001); Pulido-Gaytan (2012)] than in the other port. The mathematical formulation of the TRRM technique reported in this dissertation clearly explains the root of such a result.

3.7.1 TRRM calibration procedure

In this section the TRRM procedure is presented. This procedure assumes that the one-port load (match) shown in Figure 19 is connected at port one of the VNA.

The use of the broadband one-port load (*match*)

As in the TRM, the TRRM uses the measurement of a load of known impedance Z_{M1} connected at port one of the VNA for determining the \overline{B}_X term. Equation (94) denotes the impedance at the input of port one of the VNA, Z_{M1}^m , when it is loaded with a load of impedance Z_{M1}

$$Z_{M1}^m = \frac{\overline{A}_X (Z_{M1} - Z_A) - \overline{B}_X (Z_{M1} + Z_B)}{\overline{C}_X (Z_{M1} - Z_A) - (Z_{M1} + Z_B)}. \quad (94)$$

Unlike the TRM technique, in which the non-unity elements of the matrix \mathbf{T}_Z (Z_A and Z_B) correspond to the impedance of the loads connected at ports one and two of the VNA, in the TRRM these terms are chosen to be identical to the impedance of the load connected at port one. By substituting $Z_A = Z_{M1}$ in (94), the following expression is obtained

$$\overline{B}_X = Z_{M1}. \quad (95)$$

Since in the TRRM only one broadband load is used, $\frac{\overline{A}_X}{\overline{C}_X}$ cannot be determined by using the measurement of a load connected at port two as in the TRM. Instead, $\frac{\overline{A}_X}{\overline{C}_X}$ is calculated by using the thru and two pairs of reflecting loads, as presented next.

The use of the reflecting loads

According to the theory presented in section 3.4, by using the measurement of a symmetrical reflecting load, the following expression may be derived

$$\overline{C}_X^{-2} = (\overline{A}_Y \cdot \overline{C}_X) \eta_{R1} / \eta_{R2}, \quad (96)$$

where $R=O,S$ represent either the use of a load of very high impedance or a load of very low impedance. Then, by combining (57) with (96) the following expression may be derived

$$\overline{C}_X^{-2} = \frac{h_R}{\left(\frac{\overline{A}_X}{\overline{C}_X}\right)^2 \cdot a_{2,R} + \left(\frac{\overline{A}_X}{\overline{C}_X}\right) \cdot a_{1,R} + a_{0,R}}, \quad (97)$$

where

$$\begin{aligned} h_R &= (Z_{R1}^m - \overline{A}_X) (Z_{R2}^m - \overline{B}_Y / \overline{A}_Y) (p_{11} - \overline{B}_X p_{21}), \\ a_{0,R} &= Z_{R1}^m (Z_{R2}^m p_{11} - p_{12}), \\ a_{1,R} &= Z_{R1}^m (Z_{R2}^m p_{21} - p_{22}) + (Z_{R2}^m p_{11} - p_{12}), \\ a_{2,R} &= Z_{R2}^m p_{21} - p_{22}. \end{aligned}$$

Since TRRM uses two types of reflecting loads, it is possible to generate two expressions similar to (97). In the case of a load of very high impedance one has

$$\overline{C}_X^{-2} = \frac{h_O}{\left(\frac{\overline{A}_X}{\overline{C}_X}\right)^2 \cdot a_{2,O} + \left(\frac{\overline{A}_X}{\overline{C}_X}\right) \cdot a_{1,O} + a_{0,O}}. \quad (98)$$

Meanwhile, for a load of very low impedance one obtains the following expression

$$\overline{C}_X^{-2} = \frac{h_S}{\left(\frac{\overline{A}_X}{\overline{C}_X}\right)^2 \cdot a_{2,S} + \left(\frac{\overline{A}_X}{\overline{C}_X}\right) \cdot a_{1,S} + a_{0,S}}. \quad (99)$$

To be consistent, the value of \overline{C}_X in (98) has to be identical to the value of \overline{C}_X in (99). Thus, by equating (98) to (99) and after some algebra, the following quadratic equation may be obtained

$$\left(\frac{\overline{A}_X}{\overline{C}_X}\right)^2 \left(a_{2,S} \frac{h_O}{h_S} - a_{2,O}\right) + \left(\frac{\overline{A}_X}{\overline{C}_X}\right) \left(a_{1,S} \frac{h_O}{h_S} - a_{1,O}\right) + \left(a_{0,S} \frac{h_O}{h_S} - a_{0,O}\right) = 0. \quad (100)$$

The value of $\frac{\overline{A}_X}{\overline{C}_X}$ can then be determined from (100) as

$$\frac{\overline{A}_X}{\overline{C}_X} = \frac{-\kappa_1 \pm \sqrt{\kappa_1^2 - 4\kappa_0\kappa_2}}{2\kappa_2} \quad (101)$$

where $\kappa_i = a_{i,S} \left(\frac{h_O}{h_S}\right) - a_{i,O}$; $i = 0, 1, 2$.

As in the TRL and TRM, the value of \overline{C}_X may be determined using the measurement of a pair of symmetrical reflecting loads.

3.8 The LZZ calibration technique

A number of VNA calibration techniques have been reported in the literature. Among them, the TRL, TRM and TRRM, previously presented, are the most commonly used. TRL is acknowledged as the most accurate technique. Nevertheless, as explained in section 3.5, in order to carry out a broadband calibration using the TRL, multiple transmission lines of different lengths have to be used [Marks (1991); Zuñiga-Juarez (2011)]. It implies that the measurement ports have to be moved several times in order to accommodate structures of different size. TRM and TRRM involve the use of at least one load which has to be known over a wide frequency bandwidth. Therefore, the use of either high technology to fabricate loads of known impedance or the use of complex procedures to characterize them are required.

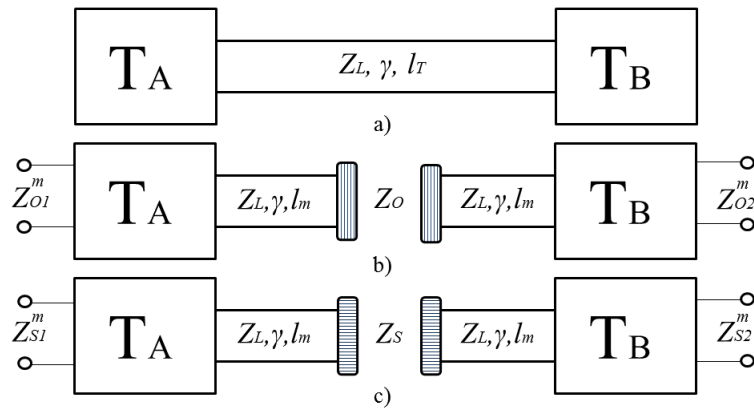


Figure 20. LZZ calibration structures: a) line, b) offset-open, c) offset-short.

The line, offset-open, offset-short (LZZ) calibration technique [Pulido-Gaytan (2013)] uses as standards: a known transmission line, a pair of unknown offset-open circuits and a pair of unknown offset-short circuits (Figure 20). Unlike TRM and TRRM, in the LZZ calibration the use of a precisely characterized load is not required. Moreover, since the LZZ calibration does not use multiple transmission lines for calculating the calibration terms, it may be implemented using fixed spacing structures.

3.8.1 LZZ calibration procedure

As the TRL, TRM and TRRM procedures, the LZZ calibration procedure is developed using 8-term error model and the ABCD-parameters matrix formalism.

According to the theory presented in section 3.4, the value of the non-unity elements of the \mathbf{T}_z matrix (Z_A and Z_B) are identical to the impedance of one of the structures used as calibration elements in a determined calibration. The unique requirement is that the value of Z_A and Z_B allow the matrix \mathbf{T}_z to be nonsingular. In this order, Z_A and Z_B cannot be neither the impedance of a short circuit (ideally zero) nor the impedance of an open circuit (ideally infinity). In the LZZ, Z_A and Z_B are then chosen to be identical to the characteristic impedance of the transmission line ($Z_A = Z_B = Z_L$).

The use of the transmission line

According to the analysis presented in section 3.5.1, the ABCD-parameters representation of the line structure shown in Figure 20a may be expressed as

$$\mathbf{M}_L = \mathbf{T}_X \mathbf{T}_\lambda \mathbf{T}_Y, \quad (102)$$

with the matrices \mathbf{T}_X and \mathbf{T}_Y previously defined in (53)-(54).

Four of the seven terms of the matrices \mathbf{T}_X and \mathbf{T}_Y may be determined from (57)-(60) using the measurement of the transmission line, as long as $\overline{\frac{A_X}{C_X}}$, $\overline{B_X}$ and $\overline{C_X}$ are known. The following sections describe the procedure for determining $\overline{\frac{A_X}{C_X}}$, $\overline{B_X}$ and $\overline{C_X}$ by combining the measurements of a line and two offset reflecting loads.

Measurement of the offset reflecting loads

The LZZ technique, as reported in [Pulido-Gaytan (2013)], considers the loads used as calibration elements as offset loads, as shown in Figure 21.

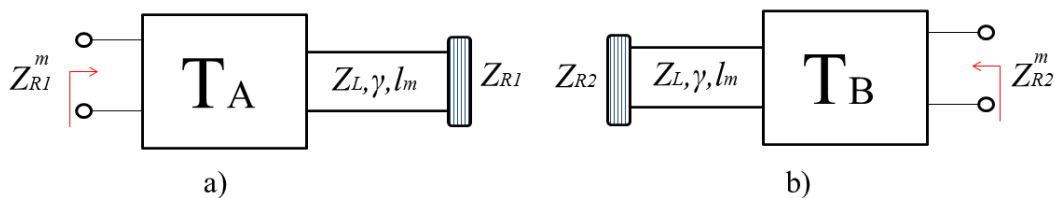


Figure 21. Equivalent structure of the offset loads connected at: a) port 1 and b) port 2 of the VNA.

In this analysis, an offset load connected at port $P = 1, 2$ is represented by a transmission line of length l_m terminated in a load of impedance Z_{RP} , with $R = O, S$ (open-circuit or short-circuit)⁴. The equivalent ABCD-parameters matrix of an offset load connected at port one of the VNA, \mathbf{M}_{R1} , may be expressed as

⁴The characteristic impedance and propagation constant of this line has to be identical to the impedance of the line used as line standard, as shown in Figure 20.

$$\mathbf{M}_{\mathbf{R1}} = \mathbf{T}_{\mathbf{A}}\mathbf{T}_{\mathbf{L}_m}\mathbf{T}_{\mathbf{R1}}. \quad (103)$$

Meanwhile, the equivalent ABCD-parameters matrix of an offset load connected at port two of the VNA, $\mathbf{M}_{\mathbf{R2}}$, may be expressed as

$$\mathbf{M}_{\mathbf{R2}} = \widetilde{\mathbf{T}}_{\mathbf{B}}\mathbf{T}_{\mathbf{L}_m}\mathbf{T}_{\mathbf{R2}}, \quad (104)$$

with $\mathbf{T}_{\mathbf{RP}}$ previously defined in (64). Then, by substituting (69) in (104), $\mathbf{M}_{\mathbf{R2}}$ may be expressed as follows

$$\mathbf{M}_{\mathbf{R2}} = \mathbf{X}\mathbf{T}_{\mathbf{B}}^{-1}\mathbf{X}\mathbf{T}_{\mathbf{L}_m}\mathbf{T}_{\mathbf{R2}}. \quad (105)$$

In (103)-(105), $\mathbf{T}_{\mathbf{L}_m}$ represents the ABCD-parameters matrix of a uniform transmission line of length l_m , which after diagonalization may be expressed as

$$\mathbf{T}_{\mathbf{L}_m} = \mathbf{T}_{\mathbf{Z}}\mathbf{T}_{\lambda_m}\mathbf{T}_{\mathbf{Z}}^{-1}, \quad (106)$$

with $\mathbf{T}_{\mathbf{Z}}$ defined in (50) and \mathbf{T}_{λ_m} defined as

$$\mathbf{T}_{\lambda_m} = \begin{bmatrix} \lambda_{L_m} & 0 \\ 0 & \lambda_{L_m}^{-1} \end{bmatrix}, \quad (107)$$

where, $\lambda_m = e^{-\gamma l_m}$. By solving (53) and (54) for $\mathbf{T}_{\mathbf{A}}$ and $\mathbf{T}_{\mathbf{B}}$, respectively, and substituting the resulting expressions in (103) and (105) one has

$$\mathbf{M}_{\mathbf{K1}} = \mathbf{T}_{\mathbf{X}}\mathbf{T}_{\lambda_m}\mathbf{T}_{\mathbf{Z}}\mathbf{T}_{\mathbf{R1}}, \quad (108)$$

$$\mathbf{M}_{\mathbf{K2}} = \mathbf{X}\mathbf{T}_{\mathbf{Y}}^{-1}\mathbf{T}_{\mathbf{Z}}^{-1}\mathbf{X}\mathbf{T}_{\mathbf{L}_m}\mathbf{T}_{\mathbf{R2}}. \quad (109)$$

Then, by substituting (106) in (108)-(109) and after some algebra, the impedance at the input of port $P = 1, 2$, Z_{RP}^m , when it is loaded with an offset load of impedance Z_{RP} may be expressed as

$$Z_{R1}^m = \frac{\overline{A_X} (Z_{R1} - Z_L) \lambda_m - \overline{B_X} (Z_{R1} + Z_L) \lambda_m^{-1}}{\overline{C_X} (Z_{R1} - Z_L) \lambda_m - (Z_{R1} + Z_L) \lambda_m^{-1}}, \quad (110)$$

$$Z_{R2}^m = \frac{\overline{B_Y} (Z_{R2} - Z_L) \lambda_m + (Z_{R2} + Z_L) \lambda_m^{-1}}{\overline{A_Y} (Z_{R2} - Z_L) \lambda_m + \overline{C_Y} (Z_{R2} + Z_L) \lambda_m^{-1}}. \quad (111)$$

Note that in the case in which the loads are measured at the calibration reference plane (non offset loads) the unique difference is that $\lambda_m = 1$.

Calculation of $\frac{\overline{A_X}}{\overline{C_X}}$ y $\overline{B_X}$

In the LZZ procedure the $\frac{\overline{A_X}}{\overline{C_X}}$ and $\overline{B_X}$ terms are determined as follows. By comparing the value of Z_L to the value of Z_{RP} , two cases may be distinguished:

1. The following expressions may be obtained from (110)-(111) when a load of impedance Z_{RP} , such that $|Z_{RP}| \gg |Z_L|$, $R = O$ (open circuit), is connected at the VNA ports

$$\overline{C_X} = \frac{1}{\lambda_m^2} \frac{Z_{O1}^m - \overline{B_X}}{Z_{O1}^m - \frac{\overline{A_X}}{\overline{C_X}}}, \quad (112)$$

$$\overline{A_Y} = \frac{1}{\lambda_m^2} \frac{Z_{O2}^m \overline{C_Y} - 1}{\frac{\overline{B_Y}}{\overline{A_Y}} - Z_{O2}^m}. \quad (113)$$

2. Similarly, the following expressions may be derived from (110)-(111) when a load of impedance Z_{RP} , such that $|Z_{RP}| \ll |Z_L|$, $R = S$ (short circuit), is connected at the VNA ports

$$\overline{C_X} = -\frac{1}{\lambda_m^2} \frac{Z_{S1}^m - \overline{B_X}}{Z_{S1}^m - \frac{\overline{A_X}}{\overline{C_X}}}, \quad (114)$$

$$\overline{A_Y} = -\frac{1}{\lambda_m^2} \frac{Z_{S2}^m \overline{C_Y} - 1}{\frac{\overline{B_Y}}{\overline{A_Y}} - Z_{S2}^m}. \quad (115)$$

By equating (112) and (114) the following expression may be derived

$$\eta_1 a_1 + \eta_2 a_2 = W_a, \quad (116)$$

where

$$\eta_1 = \frac{\overline{A_X}}{\overline{C_X}} + \overline{B_X}, \quad (117)$$

$$\eta_2 = \frac{\overline{A_X}}{\overline{C_X}} \cdot \overline{B_X}, \quad (118)$$

$$a_1 = Z_{C1}, \quad (119)$$

$$a_2 = -2, \quad (120)$$

$$W_a = 2Z_{D1}. \quad (121)$$

A second expression, similar to (116), may be derived by equating (113) with (115) and using (57)-(59) as

$$\eta_1 b_1 + \eta_2 b_2 = W_b, \quad (122)$$

where

$$b_1 = 2(Z_{D2} p_{11} p_{22} + p_{12} p_{22}) - Z_{C2} (p_{11} p_{22} + p_{12} p_{21}), \quad (123)$$

$$b_2 = -2(Z_{D2} p_{21}^2 + p_{22}^2 - Z_{C2} p_{21} p_{22}), \quad (124)$$

$$W_b = 2(Z_{D2} p_{11}^2 + p_{12}^2 - Z_{C2} p_{11} p_{12}), \quad (125)$$

with Z_{CP} and Z_{DP} defined as follows

$$Z_{CP} = Z_{OP}^m + Z_{SP}^m, \quad (126)$$

$$Z_{DP} = Z_{OP}^m \cdot Z_{SP}^m. \quad (127)$$

The expressions shown in (116) and (122) form a system of linear simultaneous equations with two unknowns, η_1 and η_2 . Solving this set of equations one has

$$\eta_1 = \frac{W_a b_2 - W_b a_2}{a_1 b_2 - a_2 b_1}, \quad (128)$$

$$\eta_2 = \frac{W_b a_1 - W_a b_1}{a_1 b_2 - a_2 b_1}. \quad (129)$$

Then, by using the definitions for η_1 and η_2 given in (117)-(118), the following quadratic equations with roots $\frac{\overline{A_X}}{\overline{C_X}}$ and $\overline{B_X}$ result

$$\left(\frac{\overline{A_X}}{\overline{C_X}}\right)^2 + \frac{\overline{A_X}}{\overline{C_X}}\eta_1 + \eta_2 = 0, \quad (130)$$

$$(\overline{B_X})^2 + \overline{B_X}\eta_1 + \eta_2 = 0, \quad (131)$$

with solutions given by

$$\frac{\overline{A_X}}{\overline{C_X}}, \overline{B_X} = \frac{\eta_1 \pm \sqrt{\eta_1^2 - 4\eta_2}}{2}. \quad (132)$$

As explained in section 3.5, it is mandatory that $\frac{\overline{A_X}}{\overline{C_X}} \neq \overline{B_X}$. Therefore, one of the roots of (132) corresponds to $\frac{\overline{A_X}}{\overline{C_X}}$ and the other root corresponds to $\overline{B_X}$. The appropriate root for $\frac{\overline{A_X}}{\overline{C_X}}$ and $\overline{B_X}$ may be chosen by using the following criterion

$$Re \{ \overline{B_X} \} > Re \left\{ \frac{\overline{A_X}}{\overline{C_X}} \right\}. \quad (133)$$

This criterion has been heuristically identified based on observations of the typical values of the roots of $\frac{\overline{A_X}}{\overline{C_X}}$ and $\overline{B_X}$. At high frequencies, when performing a one-tier calibration, this

criterion may fail. A more robust procedure for choosing the appropriate root for $\frac{\overline{A_X}}{\overline{C_X}}$ and $\overline{B_X}$ is presented in section 3.9.

Regarding the $\overline{C_X}$ term, it is calculated as in the TRL, TRM and TRRM procedures, by using the measurement of a symmetrical reflecting load. By solving (110) and (111) for Z_{R1} and Z_{R2} , respectively, and equating the resulting expressions, using (57)-(59), the following expression may be obtained

$$\overline{C_X} = \pm \frac{\lambda_{R2}}{\lambda_{R1}} \sqrt{(\overline{A_Y} \cdot \overline{C_X}) \eta_{R1} / \eta_{R2}}. \quad (134)$$

Since the offset reflecting loads used as calibration elements in the LZZ technique are typically equally shifted ($\lambda_{R1} = \lambda_{R2}$), (134) reduces to

$$\overline{C_X} = \pm \sqrt{(\overline{A_Y} \cdot \overline{C_X}) \eta_{R1} / \eta_{R2}}. \quad (135)$$

Note that (135) is identical to the expression shown in (82), even though for obtaining (82) the loads were assumed to be non-offset loads.

Limitations of the LZZ technique

The validity of the assumptions $|Z_{OP}| \gg |Z_L|$ and $|Z_{SP}| \ll |Z_L|$, $P = 1, 2$, made to derive (112)-(115) is very important in the LZZ procedure. Since the impedance of an open-circuit is complex and capacitive, as the frequency increases $|Z_{OP}|$ decreases. Regarding the offset short circuit, its impedance is complex and of inductive nature; thus, $|Z_{SP}|$ increases with frequency. Hence, at a given high frequency, which value depends on the capacitance of the open circuit and the inductance of the short circuit used as calibration elements, the assumptions $|Z_{OP}| \gg |Z_L|$ and $|Z_{SP}| \ll |Z_L|$, $P = 1, 2$ are no longer valid. Low capacitance open circuits and low inductance short circuits provide a broader bandwidth in the LZZ calibration.

The LZZ technique was reported in [Pulido-Gaytan (2013)] by using calibration structures fabricated in coplanar waveguide technology on alumina substrates [Pulido-Gaytan

(2013)]. Then, in [Pulido-Gaytan (2014)] and [Pulido-Gaytan (2015c)] the LZZ procedure was implemented using microstrip structures fabricated on alumina and on hydrocarbon-ceramic substrates, respectively. In all the cases, the obtained results have been probed to be accurate over the respective frequency range of interest.

Design considerations in the LZZ calibration structures

The accuracy of the LZZ technique strongly depends on the knowledge of the characteristic impedance of the transmission line. The use of a thru is not recommended in the LZZ technique, since it is difficult to define the impedance of a zero-length transmission line [Pulido-Gaytan (2013)]. The line has to be long enough in the frequency range of interest to allow a good propagation.

A second consideration which has to be taken into account is related with the reflecting loads. Although the theory of the LZZ is not limited to the use of offset loads, it has been observed that the use of offset loads improves the accuracy of this technique. According to the microwave circuit theory [Hiebel (2008)], ideal short- and an open-circuits have reflection coefficients of magnitude identical to unity but phases located 180° apart. In the case of offset reflecting loads, their phases vary with frequency, such that if the line used to shift both open- and short- circuits is identical, the difference between its phases will always be 180° .

Nevertheless, if due to fabrication errors, the offset of the reflecting loads are different, at a given frequency their phase offsets may be identical. This will cause that the reflection coefficients (and impedances) of both loads be close to each other. In such a case, the system of equations formed by (116) and (122) is inconsistent and the calibration fails. Hence, care must be taken in the fabrication of the reflecting loads to assure that the open- and short-circuits are equally shifted [Pulido-Gaytan (2015c)].

3.9 LZZM: an extension of the theory of the LZZ technique

In this section, the theory of the LZZ technique is extended to develop a calibration procedure comparable to the LRRM technique: the line, open, short, unknown load (LZZM) [Pulido-Gaytan (2014)]. The LZZM uses as standards a known transmission line, two pairs of unknown reflecting loads and a load of unknown impedance (match) connected at port one of the VNA, as shown in Figure 22.

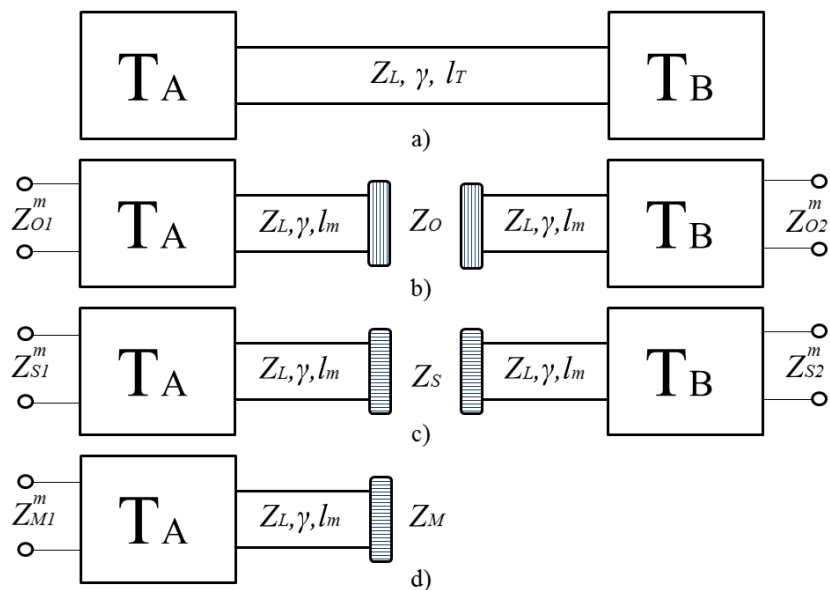


Figure 22. LZZM calibration structures: a) one transmission line, b) two pairs of highly reflecting loads and c) one broadband load (match).

3.9.1 Contributions of the LZZM procedure to the LZZ technique

In the LZZ technique the calculation of the terms $\overline{\frac{A_X}{C_X}}$ and $\overline{B_X}$ implies appropriate choosing the sign of a root of a quadratic equation. The root selection for $\overline{\frac{A_X}{C_X}}$ and $\overline{B_X}$ in (132) by using the criterion given in (133) may fail when one-tier measurements performed at high frequencies are considered [Pulido-Gaytan (2014)]. The use of a load of impedance value close to the impedance of the transmission line used as standard in the LZZM allows developing an analytic procedure to determine the appropriate root.

In (136) an expression for the impedance at the input of port one of the VNA Z_{M1}^m when it is loaded with an offset load is presented

$$Z_{M1}^m = \frac{\overline{A_X}(Z_M - Z_L)\lambda_m - \overline{B_X}(Z_M + Z_L)\lambda_m^{-1}}{\overline{C_X}(Z_M - Z_L)\lambda_m - (Z_M + Z_L)\lambda_m^{-1}}. \quad (136)$$

Whether the value of Z_M is close to Z_L , it is possible to note that Z_{M1}^m is close to the value of $\overline{B_X}$; thus, the following criterion may be derived

$$|Z_{M1}^m - \overline{B_X}| < |Z_{M1}^m - \overline{A_X}/\overline{C_X}|. \quad (137)$$

3.9.2 Advantages of the LZZM procedure over the TRRM technique

The TRRM/LRRM calibration procedure⁵, is one of the most commonly used techniques for correcting VNA systematic errors [Pulido-Gaytan (2012)]. As demonstrated in section 3.7, in order to accurately calibrate the VNA by using the TRRM/LRRM technique, the impedance of a load (Z_M) connected at one of the ports of the VNA, *match*, has to be known prior to the calibration.

Existing TRRM/LRRM procedures [Purroy (2001)], [Hayden (2006), Davidson (1990)] use the real part of Z_M for calculating its imaginary part during the calibration process [Pulido-Gaytan (2012)]. They assume that the real part of Z_M is frequency-independent. Nevertheless, when highly dispersive loads are used as calibration structures, assuming the real part of Z_M as frequency independent may introduce errors in the calibration. The LZZM differs from these methods in the sense that it allows using loads of unknown frequency-dependent impedance.

As in the LZZ procedure, in the LZZM the $\frac{\overline{A_X}}{\overline{C_X}}$ and $\overline{B_X}$ terms are calculated from (128)-(129) and (132), by combining the measurements of the transmission line and the offset reflecting loads. Then, the $\overline{C_X}$ term is calculated by using the measurement of a load of impedance Z_M connected at port one of the VNA, as follows.

From (136), the following expression may be obtained

⁵LRRM is the variation of TRRM in which a transmission line is used instead of a thru.

$$\overline{C}_X = \frac{1}{\lambda_m} \frac{Z_M/Z_L - 1}{Z_M/Z_L + 1} \cdot \frac{Z_{M1}^m - \overline{B}_X}{Z_{M1}^m - \frac{\overline{A}_X}{\overline{C}_X}}. \quad (138)$$

It is possible to observe that for determining the value of \overline{C}_X it is necessary to know the ratio Z_M/Z_L . This ratio may be determined by combining the measurement of a load with the measurement of an open circuit as presented next. By equating (138) with (112) one has

$$\frac{Z_M}{Z_L} = \frac{1 + \xi}{1 - \xi}, \quad (139)$$

$$\xi = \frac{(Z_{O1}^m - \overline{B}_X) \left(Z_{M1}^m \frac{\overline{A}_X}{\overline{C}_X} \right)}{(Z_{O1}^m - \overline{B}_X) \left(Z_{M1}^m \frac{\overline{A}_X}{\overline{C}_X} \right)}. \quad (140)$$

Note that Z_M has to be different from Z_L , otherwise the use of the load provides redundant information (i.e., $Z_{M1}^m = \overline{B}_X$) and the value of \overline{C}_X cannot be determined from (138). In such a case, \overline{C}_X has to be determined from the measurement of a symmetrical reflecting load.

3.10 The OSM one-port calibration technique

The Open-Short-Match (OSM) calibration is based on the three terms error model and uses the measurement of three loads of different (known) impedance at one port of the VNA. In this section the OSM technique is developed using the same ABCD-parameters matrix formalism used in previous sections. For compactness, the case in which the loads are measured at port one is only shown.

The OSM technique is mostly implemented by using coaxial loads. As a matter of fact, this type of loads may be represented as offset loads [Agilent (2011)], as shown in Figure 23. In order to be consistent with the theory used in section 3.8, an offset load is represented as a transmission line of impedance Z_L , propagation constant γ and length l_{K1} terminated in a load of impedance Z_{K1} , $K = O, S, M$. Hence, as described in section 3.8, the impedance at the input of port one when it is loaded with an offset load may be represented as

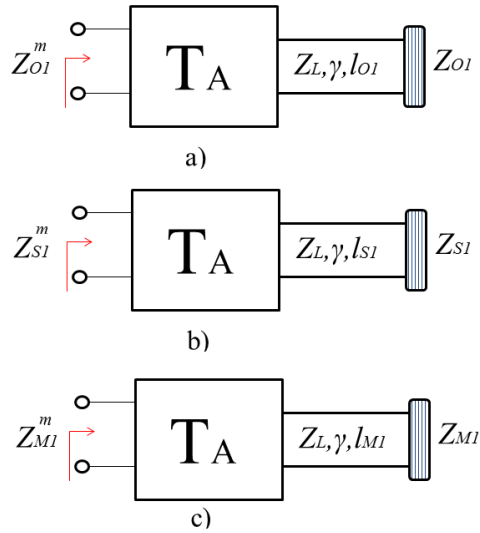


Figure 23. OSM calibration structures : a) an offset load of very high impedance (open, O), b) an offset load of very low impedance (short, S) and c) an offset load of impedance close to the measuring system impedance (match, M).

$$Z_{K1}^m = \frac{\overline{A}_X (Z_{K1} - Z_L) \lambda_{K1} - \overline{B}_X (Z_{K1} + Z_L) \lambda_{K1}^{-1}}{\overline{C}_X (Z_{K1} - Z_L) \lambda_{K1} - (Z_{K1} + Z_L) \lambda_{K1}^{-1}}, \quad (141)$$

where $\lambda_{K1} = e^{-\gamma l_{K1}}$ represent the phase shift of the offset load connected at port one. After some algebra, equation (141) can be rearranged as

$$\overline{A}_X (G_{K1} \lambda_{K1}^2) - \overline{B}_X - \overline{C}_X (Z_{K1}^m G_{K1} \lambda_{K1}^2) = -Z_{K1}^m, \quad (142)$$

where $G_{K1} = (Z_{K1} - Z_L) / (Z_{K1} + Z_L)$. The three unknowns \overline{A}_X , \overline{B}_X and \overline{C}_X may be determined by using the measurement of three loads, as follows.

By using the measurement of a load of very high impedance (open-circuit, O), a load of very low impedance (short-circuit, S) and a load of impedance value close to the measuring system impedance (matched load, M), the following matrix solution for \overline{A}_X , \overline{B}_X and \overline{C}_X may be derived

$$\begin{bmatrix} \overline{A}_X \\ \overline{B}_X \\ \overline{C}_X \end{bmatrix} = \begin{bmatrix} G_{O1} \lambda_{O1}^2 & -1 & -Z_{O1}^m G_{O1} \lambda_{O1}^2 \\ G_{S1} \lambda_{S1}^2 & -1 & -Z_{S1}^m G_{S1} \lambda_{S1}^2 \\ G_{M1} \lambda_{M1}^2 & -1 & -Z_{M1}^m G_{M1} \lambda_{M1}^2 \end{bmatrix}^{-1} \begin{bmatrix} -Z_{O1}^m \\ -Z_{S1}^m \\ -Z_{M1}^m \end{bmatrix}. \quad (143)$$

Once $\overline{A_X}$, $\overline{B_X}$ and $\overline{C_X}$ are known, the impedance of any load connected at port one may be determined by solving (141) for Z_{K1} . It is important to note that although the impedance of a one-port DUT may be determined using this procedure, the terms $\overline{A_X}$, $\overline{B_X}$ and $\overline{C_X}$ are not elements of the matrix \mathbf{T}_A connecting the measurement port to the DUT. Instead, $\overline{A_X}$, $\overline{B_X}$ and $\overline{C_X}$ are three of the four elements of the matrix \mathbf{T}_X , previously defined in section 3.4 as

$$\mathbf{T}_X = \mathbf{T}_A \mathbf{T}_Z = D_X \overline{\mathbf{T}}_X = D_X \begin{bmatrix} \overline{A_X} & \overline{B_X} \\ \overline{C_X} & 1 \end{bmatrix}. \quad (144)$$

Three elements of the matrix \mathbf{T}_A , defined as

$$\mathbf{T}_A = D_A \begin{bmatrix} \overline{A_A} & \overline{B_A} \\ \overline{C_A} & 1 \end{bmatrix}, \quad (145)$$

may be determined by solving (144) for \mathbf{T}_A and developing the resultant expression

$$\overline{A_A} = \frac{\overline{B_X} - \overline{A_X}}{Z(\overline{C_X} + 1)}, \quad (146)$$

$$\overline{B_A} = \frac{\overline{B_X} + \overline{A_X}}{\overline{C_X} + 1}, \quad (147)$$

$$\overline{C_A} = \frac{1 - \overline{C_X}}{Z(\overline{C_X} + 1)}. \quad (148)$$

3.11 Summary

In this chapter, the procedures for the TRL, TRM and TRRM calibration techniques, allowing the use of calibration structures of arbitrary impedance, were described. Moreover, an original calibration procedure, the LZZ calibration was presented. These techniques will be used in chapter 6 for the relative calibration of real-time LP systems. Table I summarizes the calibration structures used for calculating the seven calibration terms of the two-port calibration procedures presented above.

Table I. Calculation of the calibration terms using the calibration structures of different calibration techniques. The corresponding values of the impedances Z_A and Z_B are also presented.

	\overline{B}_X	$\frac{\overline{A}_X}{\overline{C}_X}$	\overline{C}_X	$\overline{A}_Y, \overline{B}_Y, \overline{C}_Y, D_X D_Y$
TRL $Z_A = Z_B = Z_L$	Thru-Line	Thru-Line	Open P1-Open P2/ Short P1-Short P2	Thru
TRM $Z_A = Z_{M1}, Z_B = Z_{M2}$	Load P1	Thru-Load P2	Open P1-Open P2/ Short P1-Short P2	Thru
TRRM $Z_A = Z_B = Z_{M1}$	Load P1	Thru, Open P1-Open P2, Short P1-Short P2	Open P1-Open P2/ Short P1-Short P2	Thru
LZZ $Z_A = Z_B = Z_L$	Line, Open P1-Short P1, Open P2-Short P2	Line, Open P1-Short P1, Open P2-Short P2	Open P1-Open P2/ Short P1-Short P2	Line
LZZM $Z_A = Z_B = Z_L$	Line, Open P1-Short P1, Open P2-Short P2	Line, Open P1-Short P1, Open P2-Short P2	Open P1-Open P2/ Short P1-Short P2	Line

4. Load-Pull Systems

The foundations of the LP concept based on the Cripps' load-line theory along with the most important features and applications of the various types of LP systems for characterizing microwave transistors are presented in this chapter. The advantages and disadvantages of using LP measurements as a tool for PA design are also reviewed.

4.1 Load-pull contours

Microwave solid-state devices are about to enter their half a century of age. Similarly to what was the common procedure in the early days of microwave solid state PAs, power amplifier design is still focused on observing the LP contours of output power, efficiency, or any other metric, to then select a load impedance that maximizes some compromise between these metrics.

The work reported in [Cripps (1983)] is intended to help in this LP-based PA design process. There, Cripps proposed an intuitive and simple explanation for the dependence of delivered output power of a device on its terminating load. Despite its simplicity, this model has survived for more than thirty years of research. It has proved to be capable of estimating the PA output power LP contours, something thirty years ago believed to be extremely difficult because of its nonlinear nature [Pedro (2015)]. This approach, known as the Cripps' load-line theory, is presented next.

4.1.1 Power match condition

The LP approach for characterizing active devices is independent of the device's technology; the LP principle is the same for bipolar transistors (BJTs, HBTs) and field effect transistors, FETs (JFETs, MESFETs, HEMTs, MOSFETs). Nevertheless, due to the fact that FETs are the predominant technology in microwave applications, the analysis presented here is

focused in these type of devices.

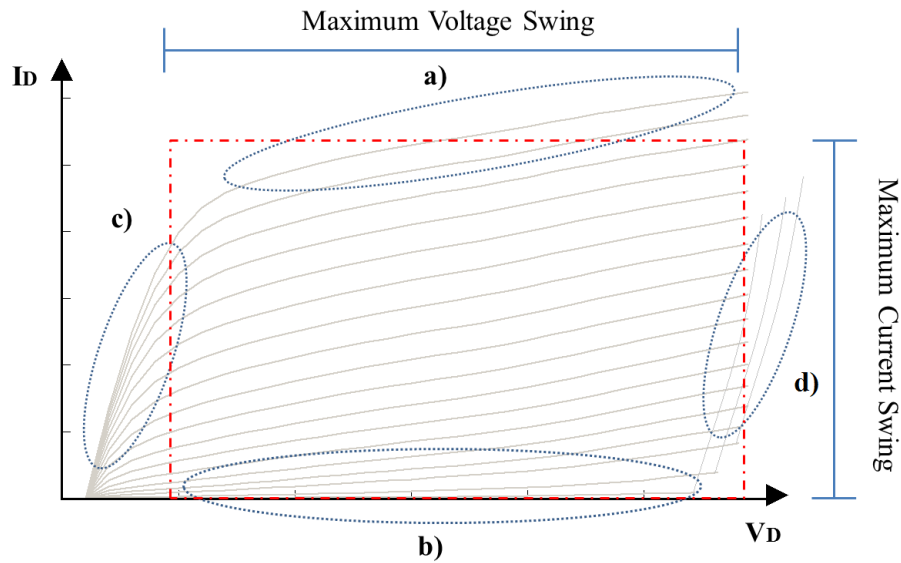


Figure 24. Illustration of the limiting mechanisms of output voltage and current swings of FETs: a) input junction forward conduction, b) channel pinch-off, c) ohmic region and d) breakdown.

In order to describe the principles of the variation of delivered output power in microwave FETs on its loading condition, it is important to analyze first the mechanisms by which transistors deliver a finite amount of power. The limitations in terms of output RF power of microwave transistors are determined by limited output voltage swing and/or limited output current swing. The voltage and current limitations of a device can be explained by analyzing its output current-voltage (I-V) characteristics. In the case of FETs, the current swing limits are posed by the input junction forward conduction and device channel pinch-off current values; for the voltage swing, the limits are posed by the ohmic region and breakdown voltage values [Colantonio (2009)]. Consequently, these two limits pose an upper limit to the output power generation of a microwave transistor. The limits in output voltage and current swings are depicted in Figure 24.

In RF engineering, the curve describing the relationship between output current and voltage swings is known as the load line. For maximizing the output power in a given device, it is required to maximize both output voltage swing and output current swing simultaneously. Hence, there is a load of impedance R_{opt} that allows the device to fully exploit the maximum

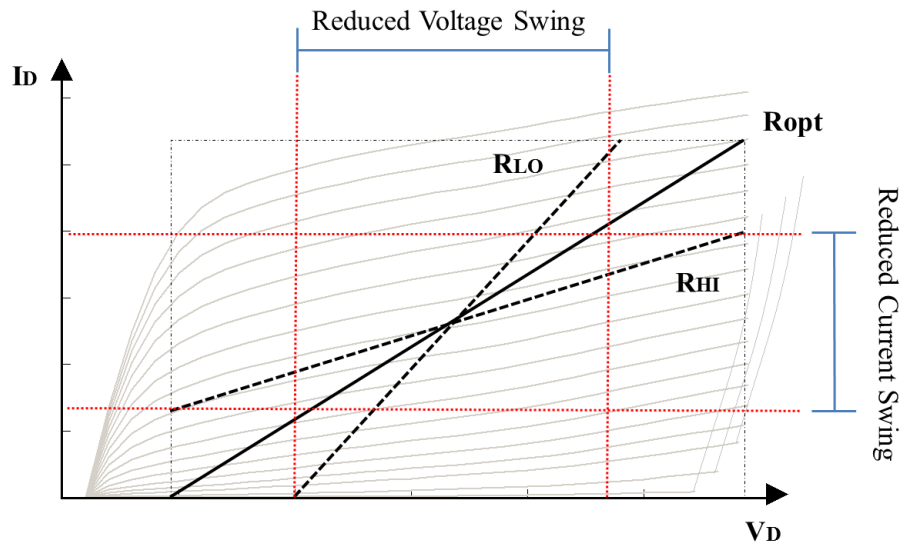


Figure 25. Illustration of the concept of load line for a loading condition for maximum output power. The load lines corresponding to the loading conditions for reduced voltage and current swings are also shown.

current and voltage swings. This latter concept is known as *the power match condition*; the curve labeled as R_{opt} in Figure 25 corresponds to the loading condition for maximum output power.

4.1.2 Cripps' load-line theory

In order to describe in a simple way the variation of output power in a transistor as a function of its loading condition, the simple model of a FET depicted in Figure 26 is considered. The idealized I-V characteristics shown in Figure 26 correspond to a voltage-controlled current source with zero output conductance and constant transconductance. The turn-on (or knee) voltage V_k is assumed to be much less than the device's quiescent voltage.

The previously described device is analyzed by using the circuit shown in Figure 27, where the device is assumed to be perfectly AC coupled to a load through the use of a DC bias circuit. Figure 28 shows the device's output current and voltage waveforms under input sinusoidal excitation and optimum resistive load. For the time being, and for simplicity, a biasing condition of one half the maximum voltage swing and one half the maximum current

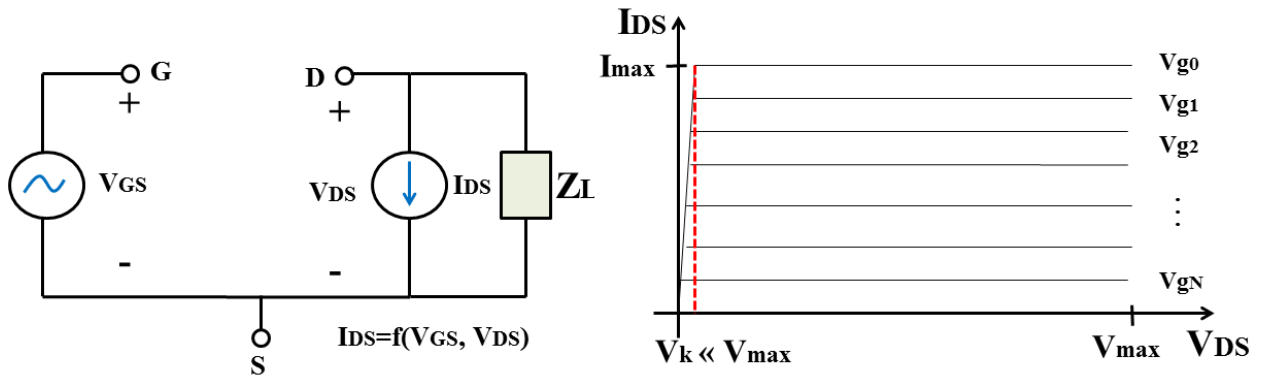


Figure 26. Simplified model of a field effect transistor: a) model and b) I-V curves.

swing is assumed¹.

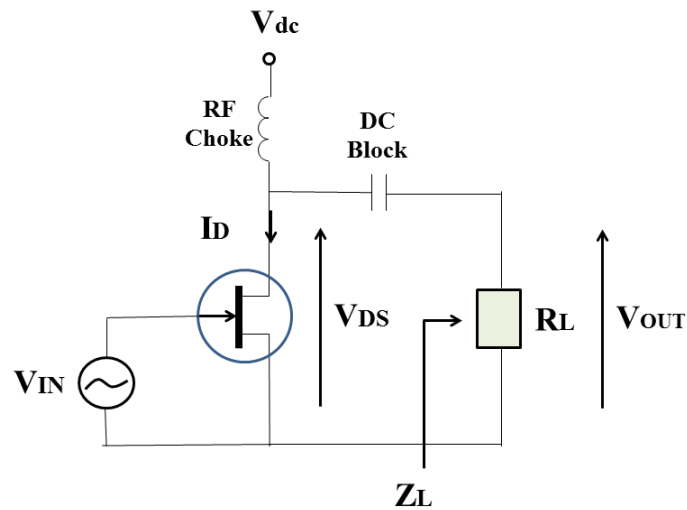


Figure 27. FET device loaded with a load of arbitrary impedance and biased using ideal DC blocking and RF choke networks.

In Figure 28, it can be observed that the current waveform swings from zero to I_{max} , with amplitude $I_{dc} = I_{max}/2$ and the voltage waveform swings from zero to $V_{max} = 2V_{dc}$, with amplitude V_{dc} . Hence, the load for maximum power has a resistance given by the ratio of the RMS value of the voltage and current waveforms,

¹This biasing condition corresponds to the biasing condition of a classical class A amplifier (current conduction angle of 360 degrees). Detailed analysis for optimum resistive load for arbitrary conduction angle may be found in Cripps (2006).

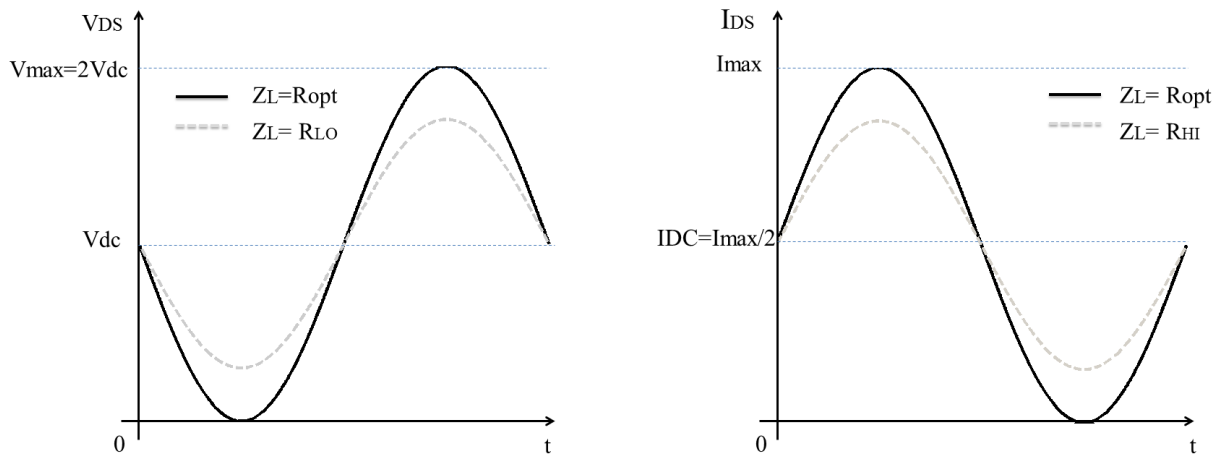


Figure 28. RF waveforms for a typical class-A biasing condition: a) voltage and b) current, at their amplitude reduction due to non-optimum loading conditions.

$$R_{opt} = \frac{V_{dc}}{I_{max}/2} = \frac{V_{dc}}{I_{dc}}. \quad (149)$$

An example of the impedance of this load is plotted in the Smith chart shown in Figure 29.

The RF power delivered to this load is given by

$$P_{opt} = \frac{1}{2} Re \{V_{dc} I_{dc}\} = \frac{1}{2} V_{dc} I_{dc}. \quad (150)$$

Then, let the optimum power P_{opt} be diminished by a factor p , such that the RF power delivered to a resistive load be given as $P_L = P_{opt}/p$. Two forms to allow this power to be produced are: to reduce the current by a factor of p or to reduce the voltage by a factor of p ,

$$P_L = \frac{1}{2} \frac{V_{dc}}{p} I_{dc} = \frac{1}{2} V_{dc} \frac{I_{dc}}{p} = \frac{P_{opt}}{p}. \quad (151)$$

Thus far, we have identified two resistive loads that allow a device to deliver a power P_{opt}/p : a load of resistance value p times lower than the optimum resistance $R_{LO} = R_{opt}/p$ and a load of resistance value p times greater than the optimum resistance $R_{HI} = pR_{opt}$. By using (149)-(150), the optimum power may be expressed as

$$P_{opt} = \frac{1}{2} I_{dc} (I_{dc} R_{opt}) = \frac{1}{2} I_{dc}^2 R_{opt}, \quad (152)$$

$$P_{opt} = \frac{1}{2} V_{dc} \left(\frac{V_{dc}}{R_{opt}} \right) = \frac{1}{2} V_{dc}^2 G_{opt}, \quad (153)$$

where $G_{opt} = 1/R_{opt}$. Then, the power delivered to the loads of impedance R_{LO} and R_{HI} may be expressed as

$$P_L = \frac{1}{2} I_{dc}^2 \frac{R_{opt}}{p} = \frac{1}{2} I_{dc}^2 R_{LO}, \quad (154)$$

$$P_L = \frac{1}{2} \frac{V_{dc}^2}{p R_{opt}} = \frac{1}{2} V_{dc}^2 G_{HI}, \quad (155)$$

where $G_{HI} = 1/R_{HI}$. From (151) and (154)-(155) it can be noted that in the case of a load of impedance R_{LO} , the voltage amplitude is reduced in order to maintain a current amplitude of I_{dc} . Meanwhile, in the case of a load of impedance R_{HI} , the current amplitude is reduced in order to maintain a voltage amplitude of V_{dc} . Figures 25 and 28 show the effect of these two loading conditions in the load-line and RF current and voltage waveforms, respectively. In Figure 29 an example of the location in the Smith chart of R_{opt} , R_{LO} and G_{HI} for different values of p is presented.

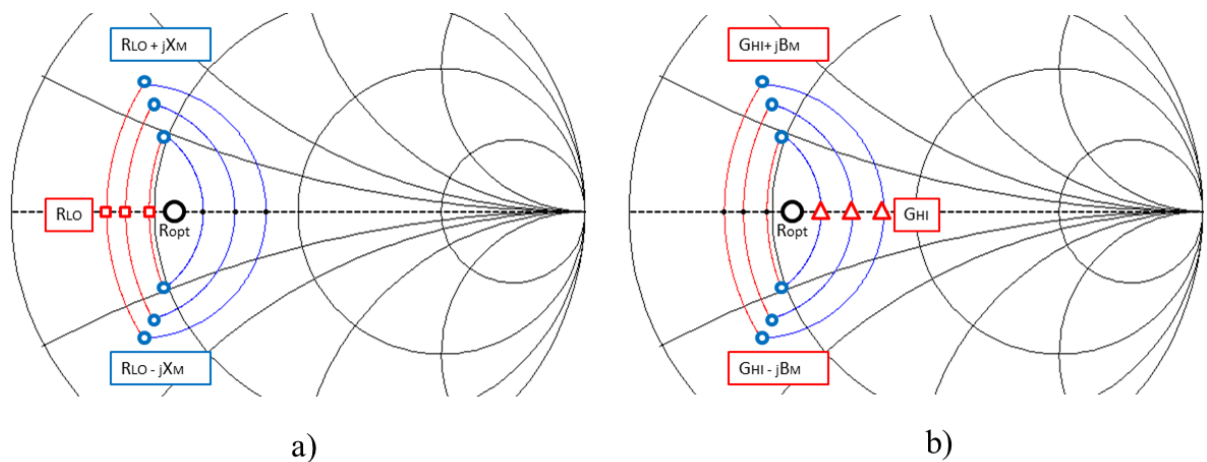


Figure 29. Example of the location of the optimum resistance and the estimation of LP power contours. In a) the addition of a series reactance to a suboptimum resistance is depicted and in b) the addition of a susceptance in parallel with a suboptimum conductance is depicted.

4.1.3 Estimation of the load-pull contours

The three power conditions considered in (150) and (153)-(155), indicate that there is some kind of functional relationship between output power and output loading conditions. The logical next step is to consider loads of complex impedance. This approach is known in the microwave PA research community as the load-pull concept. Meanwhile, the typically observed closed shapes formed by the union in the Smith chart of all the impedances allowing identical delivered output power are known as power LP contours.

In order to analyze the power delivered to loads of complex impedance, a load of impedance $Z_L = R_L + jX_L$ and admittance $Y_L = G_L + jB_L$ is considered. Let define the RMS voltage at and current flowing through this load as V_L and I_L , respectively. The power delivered to the load is then defined as

$$P_L = \frac{1}{2} \text{Re} \{V_L I_L^*\}, \quad (156)$$

where I_L^* denotes the conjugate of I_L . Then, by using the identity $V_L = I_L Z_L$ in (156), the following two expressions may be derived

$$P_L = \frac{1}{2} |I_L|^2 R_L = \frac{1}{2} |V_L|^2 \frac{R_L}{|Z_L|^2}, \quad (157)$$

$$P_L = \frac{1}{2} |V_L|^2 G_L = \frac{1}{2} |I_L|^2 \frac{G_L}{|Y_L|^2}. \quad (158)$$

In order to find a set of loads allowing the power delivered to be constant, one can equate the power delivered to a load of purely resistive impedance R_{LO} to the power delivered to a load of complex impedance $Z_{LO} = R_{LO} + jX_{LO}$. By equating (154) to (157) for a load of impedance Z_{LO} one may obtain

$$\frac{|V_{LO}|^2}{V_{dc}^2} = \frac{R_{LO}^2 + X_{LO}^2}{R_{opt}^2}. \quad (159)$$

Since the voltage at the load cannot be greater than the voltage supplied by the source ($|V_{LO}|/V_{dc} \leq 1$), the following inequality holds

$$R_{LO}^2 + X_{LO}^2 \leq R_{opt}^2. \quad (160)$$

Then, in the limit where $|V_{LO}| = V_{dc}$ one has a maximum value for the load reactance, X_M , given by

$$X_M = \pm R_{opt} \sqrt{1 - \frac{1}{p^2}}. \quad (161)$$

The trajectories formed by the impedances $Z_{LO} = R_{LO} + jX_{LO}$, $|X_{LO}| \leq X_M$, allowing a constant delivered power for different values of p are depicted in Figure 29. It is evident that these trajectories do not form contours, but a piece of them. Thus, a second set of trajectories have to be generated in order to form contours of constant power.

One can equate the power delivered to a load of purely conductive admittance G_{HI} to the power delivered to a load of complex admittance $Y_{HI} = G_{HI} + jB_{HI}$, by equating (155) to (158) for a load of admittance Y_{HI} as

$$\frac{|I_{HI}|^2}{I_{dc}^2} = \frac{G_{HI}^2 + B_{HI}^2}{G_{opt}^2}. \quad (162)$$

Since the current flowing through the load cannot be greater than the maximum current allowed to flow through the device ($|I_{HI}|/I_{dc} \leq 1$), the following inequality holds

$$G_{HI}^2 + B_{HI}^2 \leq G_{opt}^2. \quad (163)$$

Then, in the limit where $|I_{HI}| = I_{dc}$ one has a maximum value for the load susceptance, B_M , given by

$$B_M = \pm G_{opt} \sqrt{1 - \frac{1}{p^2}}. \quad (164)$$

The trajectories formed by the admittances $Y_{HI} = G_{HI} + jB_{HI}$, $|B_{HI}| \leq B_M$, allowing a constant delivered power for different values of p are depicted in Figure 29. It can be noted from (161) and (164), and from the trajectories shown in Figure 29, that the impedance $Z_{LO} = R_{LO} + jX_M$ is identical to the admittance $Y_{HI} = G_{HI} + jB_M$; thus, forming closed contours of constant power in the Smith chart.

It can be observed that the LP contours of constant output power at the current source reference plane, are delimited by the intersection of circles of constant resistance and circles of constant conductance in the Smith chart. This is the reason why the LP power contours observed in practice never behave as circles.

Load-pull contours at the package plane

The analysis presented in the preceding section is aimed to estimate the LP contours of constant output power defined at the plane of the transistor's voltage-controlled current source. Nevertheless, these contours are different from the LP contours commonly observed in practice when characterizing packaged transistors at microwave frequencies. Effects introduced by the device's output capacitance, the bondwires used to connect the transistor's die to the package, or the package parasitics, cause the impedance at the current source to be different from the impedance at the package plane. This causes the LP contours to be dependent on the frequency. In this order, a matter of concern is to estimate the impedance which have to be synthesized by an impedance tuner (Figure 30) at the package plane to have a determined behavior at the transistor's current source plane.

Let Z_L^{CS} be the load impedance seen at the current source plane and Z_L^{PK} be the impedance seen at the package plane (see Figure 30a). As a simple example, the network connecting these two planes is modeled by a parallel capacitance (C_D) accounting for the output device's and package capacitances and a series inductance (L_D) accounting for the bondwires inductance. The ABCD-parameters representation of this network, which is enclosed in dotted lines in Figure 30b, is expressed as [Pozar (2005)]

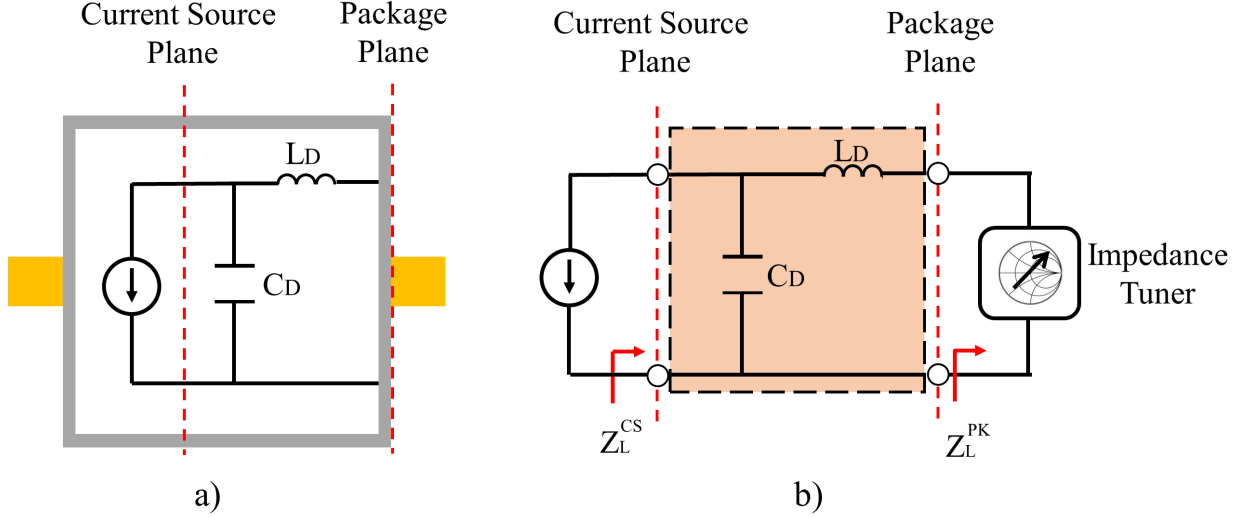


Figure 30. Impedance at the package Z_L^{PK} plane that has to be generated by an impedance tuner to synthesize an impedance Z_L^{CS} at the current source: a) parasitics considered in the analysis and b) equivalent circuit.

$$\begin{bmatrix} A & B \\ C & D \end{bmatrix} = \begin{bmatrix} 1 & Z_{LD} \\ Y_{CD} & 1 + Z_{LD}Y_{CD} \end{bmatrix}, \quad (165)$$

where $Z_{LD} = j\omega L_D$ and $Y_{CD} = j\omega C_D$. By using this ABCD-parameters matrix and calculating the impedance at the input of this network (Z_L^{CS}) when the network is loaded with a load of impedance Z_L^{PK} , one has

$$Z_L^{CS} = \frac{Z_L^{PK} + Z_{LD}}{Y_{CD}Z_L^{PK} + (1 + Z_{LD}Y_{CD})}. \quad (166)$$

Then, by solving (166) for Z_L^{PK} the following expression is derived

$$Z_L^{PK} = \frac{Z_L^{CS}}{1 - Z_L^{CS}Y_{CD}} - Z_{LD}. \quad (167)$$

In order to show in an explicit form the influence of the capacitance and inductance reactances on the determination of the LP contours as the frequency of analysis varies, let assume the following two cases.

1. When only the capacitance is considered ($L_D = 0$), equation (167) reduces to

$$Y_L^{PK} = Y_L^{CS} - Y_{CD}, \quad (168)$$

where $Y_L^{CS} = 1/Z_L^{CS}$ and $Y_L^{PK} = 1/Z_L^{PK}$. The expression shown in (168) indicates that the admittance at the package plane will be determined by subtracting the susceptance of the capacitor from the admittance at the current source plane. For the particular case of the optimum conductance G_{opt}^{CS} at the current generator plane, the admittance at the package plane depends on the capacitance C_D as

$$Y_{opt}^{PK} = G_{opt}^{CS} - j\omega C_D. \quad (169)$$

Equation (169) clearly indicates that a capacitance C_D causes the optimum admittance to move along a circle of constant conductance (G_{opt}^{CS}) in the Smith chart (see Figure 31a). Note that the direction of this movement is not towards the capacitive part of the Smith chart, but in the opposite direction; it occurs because the factor $j\omega C_D$ is being subtracted from G_{opt}^{CS} (the capacitance is embedded).

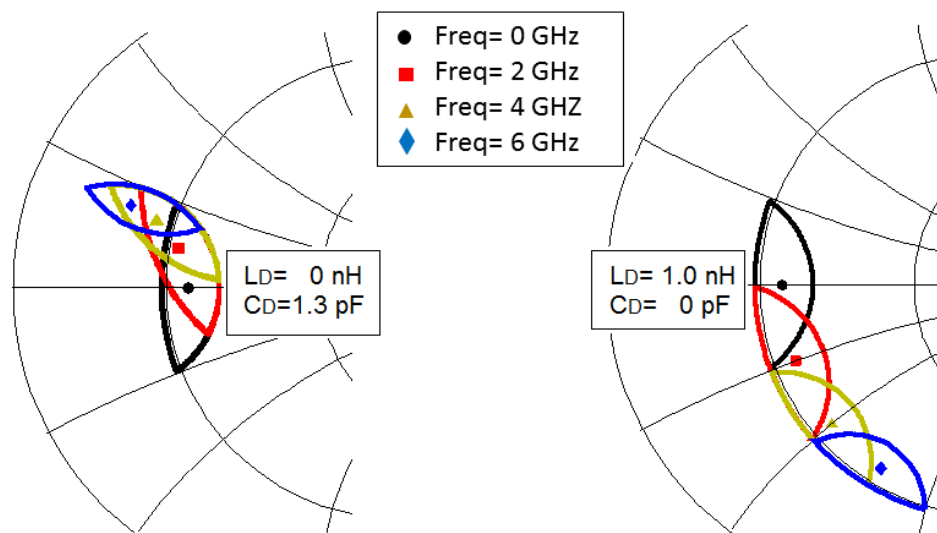


Figure 31. Impedance at the package Z_L^{PK} plane of a transistor when: a) a shunted capacitance of 1.3 pF is considered and b) when a series inductance of 1.0 nH is considered. For compactness, only the impedance for maximum power and the LP contour for 1 dBm of power below the maximum power are shown.

2. When only the inductance is considered ($C_D = 0$), equation (167) reduces to

$$Z_L^{PK} = Z_L^{CS} - Z_{LD}. \quad (170)$$

The expression shown in (170) indicates that the impedance at the package plane will be determined by subtracting the reactance of the inductor from the impedance at the current source plane. For the particular case of the optimum resistance at the current generator plane, the impedance at the package plane depends on the inductance L_D as

$$Z_{opt}^{PK} = R_{opt}^{CS} - j\omega L_D. \quad (171)$$

Equation (171) clearly indicates that an inductance L_D causes the optimum impedance to move along a circle of constant resistance (R_{opt}^{CS}) in the Smith chart (see Figure 31b). Notice that the direction of this movement is not towards the inductive part of the Smith chart, but in the opposite direction; it occurs because the factor $j\omega L_D$ is being subtracted from R_{opt}^{CS} (the inductance is embedded).

While the theory presented in this section gives an insight on the basis of the LP concept and the origin of the LP contours, in practice these contours are obtained through the use of LP measurement systems. In the following section, a description of the most commonly used types of LP systems is presented.

4.2 Load-pull systems

While nowadays significant effort is devoted toward the development of high performance microwave transistors to improve PA efficiency and output power [Bindra (2015)], accurate characterization tools are necessary to evaluate the device's performance in the nonlinear regime [Golio (2010)]. Large-signal characterization of microwave transistors is essential for determining the device's performance in non-linear applications, considering the limitations of

S-parameter in such applications [Ghannouchi (2011, 2013); Hashmi (2013)]. LP is presently one of the most commonly used techniques for carrying out this task.

As presented in the preceding section, for PA design the optimal loading conditions of transistors primarily depends on the transistor's maximum current and voltage waveforms. This is significantly different from the linear case, where the optimal loading conditions (e.g., conjugate match, noise match) are directly identified from S-parameters [Gonzalez (1997)]. In the nonlinear case, LP systems determine the appropriate impedance values experimentally through the use of impedance tuning mechanisms, which vary the load reflection coefficient Γ_{LOAD} while the behavior of the DUT is evaluated in terms of a determined large-signal metric.

The results of the LP characterization of a DUT are commonly reported as contours in the Smith chart; these contours correspond to the level curves of the surface formed by the evaluation of a determined parameter (e.g. P_o , PAE , η_D) versus the variation of the impedance at the device's output plane. Figure 32 illustrates this concept.

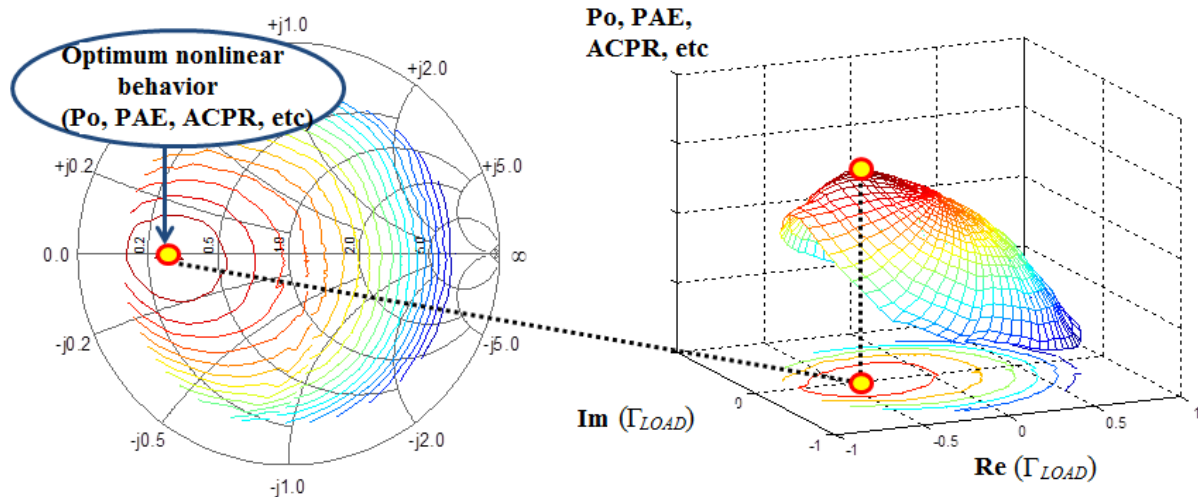


Figure 32. Load-Pull contours as a method for reporting the results of an active device characterization using load-pull systems.

The load of impedance Z_{LOAD} at the output of a DUT, the incident and reflected waves a_2 and b_2 at the DUT's output port, and the reflection coefficient Γ_{LOAD} are related as

$$\Gamma_{LOAD} = \frac{a_2}{b_2} = \frac{Z_{LOAD} - Z_0}{Z_{LOAD} + Z_0}. \quad (172)$$

As expressed in (172), the reflection factor (and the impedance) at the output of a DUT may be varied by varying the ratio of the amplitudes and the difference of the phases of two waves a_2 and b_2 . The wave b_2 emerging from the DUT towards the load is generated by the DUT itself; therefore, the problem to deal with in LP is to find a method by which the wave a_2 entering the DUT's output port is generated. In this respect, LP systems may be classified according to the method by which load impedances are synthesized (i.e., how the wave a_2 is generated).

Load impedance synthesis may be achieved through the use of either passive or active elements [Deshours (1997); Muller (1994)]. Next sections are devoted to discuss the operation along with the advantages and disadvantages of passive and active LP systems used in the characterization of microwave transistors.

4.2.1 Passive load-pull systems

The classical method to synthesize impedances in LP measurement systems is to use passive impedance tuners. Passive tuners, introduced for the first time in [Cusack (1974)], are based on the mechanical movement of a probe along a transmission line, in order to generate complex reflection factors. The probe vary the reflection factor through its movement in the horizontal and vertical directions. The movement of a probe in the vertical direction alters mainly the magnitude of the reflection factor, while its movement in the horizontal direction alters mainly the phase. These impedance tuners are known as passive-mechanical². A generic representation of the working principle of a passive-mechanical tuner is depicted in Figure 33.

²The impedance at the output of a DUT may also be varied by using passive-electronic tuners, using diodes. However, due to the low power-handling capabilities of this type of tuning systems, they are only used in low-power applications (mainly in the noise characterization of active devices).

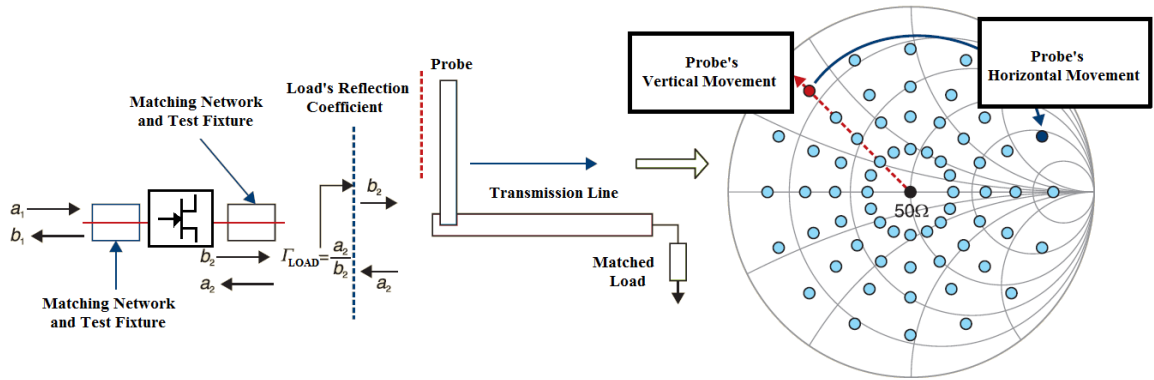


Figure 33. Principle of operation of a passive LP systems and the reflection coefficient synthesis. In this type of tuners, the vertical movements of a probe vary mostly the magnitude of Γ_{LOAD} and the horizontal movements vary mostly the phase of Γ_{LOAD} .

Passive LP systems are capable of working in very high power environments. Nevertheless, due to inherent losses of the elements located between the DUT and passive tuners (e.g., bias-tees, cables, adapters or test fixtures) along with the losses of the tuner itself, passive LP systems are unable to synthesize high Γ_{LOAD} values. This problem is of paramount importance when characterizing power transistors, since these devices manage very high currents, and thus very low impedances, with a corresponding optimum Γ_{LOAD} located on or near the edge of the Smith chart [Hashmi (2011)]. This drawback is also a limiting factor when characterizing devices under harmonic terminations, where loads of very low/high impedance are required [Ferrero (2008); Aboush (2005a)]. These limitations of passive LP systems are overcome by using active tuning systems, as presented next.

4.2.2 Active load-pull systems

Phase-shifting along with attenuator and amplification networks can be used to control the magnitude and phase of the wave a_2 , and thus the magnitude and phase of the reflection coefficient at the output of a DUT. Impedance tuning systems based on this approach are known as active loads and the systems based on this method are referred to as active LP systems.

It is worth mentioning that although some researchers have recently reported advances in the use of this LP approach for characterizing very high power transistors [Hashmi (2013);

Aboush (2005b)], active LP systems are ideally suited for low power and medium power applications. These systems are capable of synthesising any Γ_{LOAD} at the DUT plane, even Γ_{LOAD} values greater than unity. Thus, when using this type of LP systems there is an imminent risk of oscillation in the DUT caused by the LP system³, which can lead to damage of the device being tested.

There are different types of active LP techniques among which open-loop, closed-loop and feedforward are the most commonly used. These three methods are described next.

Open-loop load-pull systems

The open-loop LP technique uses an external RF source, different from the source used to drive the DUT, for generating the wave a_2 at the output of the DUT. Both the source used to drive the DUT and the source in the open-loop at the DUT's output have to be locked to a common reference signal (typically a 10 MHz locking signal) in order to maintain phase coherence between the signal a_2 and the signal b_2 .

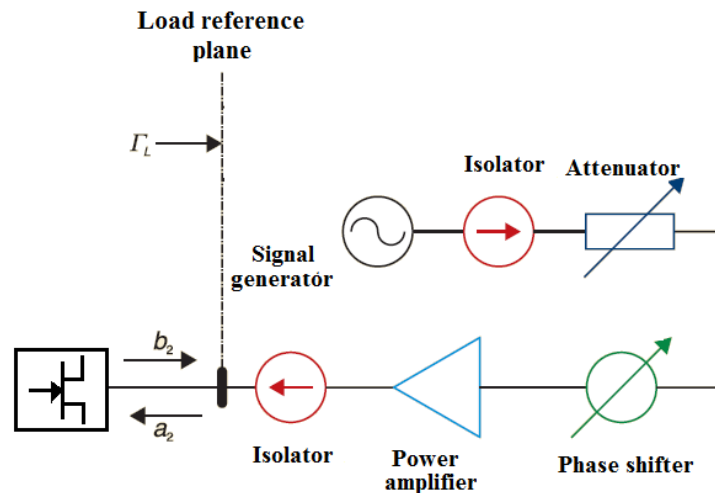


Figure 34. Generic diagram of an active LP system using the open-loop active LP concept.

³Although LP systems are mainly used in the characterization of power transistors for the design of PAs, they can also be used to design oscillators or mixers [Velazquez-Ventura (2003); Roblin (2011)]. In those cases, Γ_{LOAD} values greater than unity are useful.

Figure 34 illustrates the principle of operation of the open-loop LP approach. The amplifier in the open-loop is used to boost the signal emerging from the RF source. The attenuator and phase shifter are used to modify the phase and magnitude of the wave a_2 . Isolators prevent any damage to the loop amplifier and the loop RF source. It is evident that the open-loop LP can synthesize reflection coefficients Γ_{LOAD} of any magnitude, just by changing the magnitude of the wave a_2 . The magnitude of Γ_{LOAD} will be zero when the source in the loop is turned off, or close to zero if the attenuation in the loop is much higher than the gain of the loop amplifier. The magnitude of Γ_{LOAD} will increase as the signal emerging from the active loop increases, either by reducing the attenuation or by increasing the power from the external source.

The magnitude and phase of the signal b_2 emerging from the DUT changes as the DUT's excitation, bias and loading conditions are changed. Thus, synthesizing a determined reflection factor at the DUT output port may become an iterative (and sometimes slow) process, which may necessitate the use of complex converge algorithms [Saini (2010)].

Two drawbacks when using the open-loop technique are related to the harmonic and power scaling of the active loop. When characterizing devices under harmonic terminations, a number of sources identical to the number of harmonics has to be used, all of them locked to a common reference signal. Frequency multipliers can be used to alleviate this limitation by allowing the generation of waves at different commensurate frequencies. Regarding the power, when characterizing high-power devices (managing more than 100 W) under high Γ_{LOAD} conditions, it may be difficult to generate in the active loop a wave of magnitude comparable to the wave generated by the DUT [Hashmi (2011); Aboush (2005b)]; it requires the use of loop amplifiers managing power levels of the order of the power level produced by the DUT.

Feedforward load-pull systems

The original idea of the feedforward LP approach was proposed in [Takayama (1976)]. The operating principle of the feedforward LP approach is depicted in Figure 35. The signal generated by an RF source (and boosted by an amplifier if required) at the input of the DUT is split into two different paths. One path drives the input port of the DUT, while in the other path the signal is varied in magnitude and phase and injected into the DUT's output port as a signal a_2 . Once combined with the signal arising from the DUT b_2 , the equivalent reflection coefficient Γ_{LOAD} results.

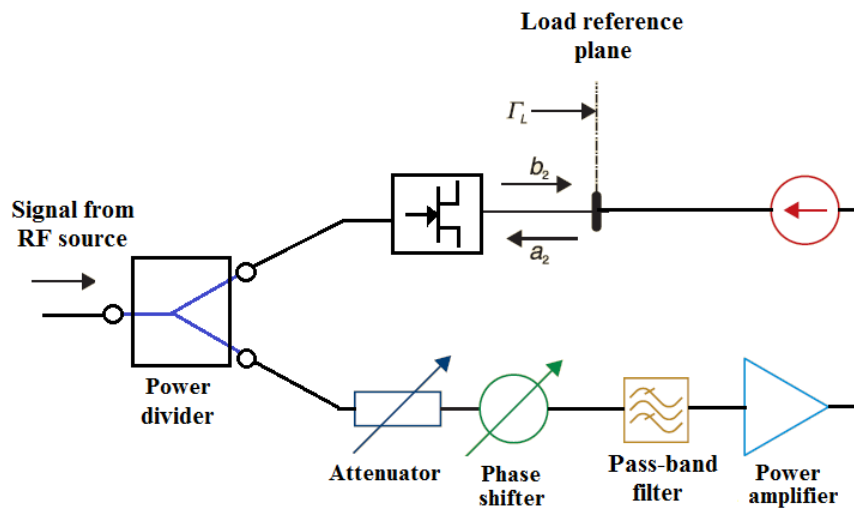


Figure 35. Generic diagram of an active LP system using the feedforward active LP concept.

The operation principle of feedforward LP systems is similar to the open-loop technique. The main difference relies on the origin of the signal a_2 . Since the feedforward LP approach is based on the use of a second path for the signal entering the DUT's output port, this LP approach is also known [Van der Puije (1978)] as the *two-signal path* LP technique.

Closed-loop load-pull systems

The synthesis of reflection coefficients at the output of the DUT may be achieved by sampling the wave generated by the transistor traveling toward the load, controlling its magnitude and

phase, and reinjecting it toward the transistor. This approach, known as the closed-loop LP technique [Bava (1982)], is depicted in Figure 36.

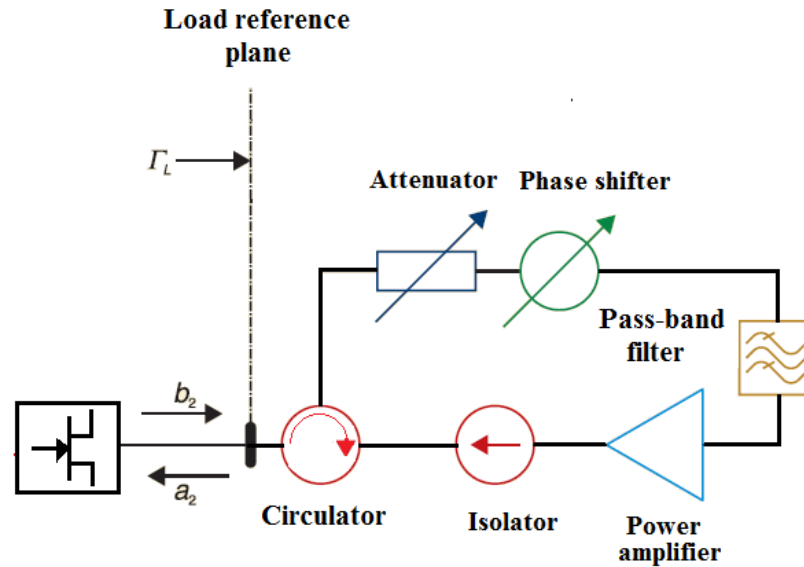


Figure 36. Generic diagram of an active LP system using the closed-loop active LP concept.

Let outline the realization of a closed-loop active LP system. As may be observed in Figure 36, for the realization of a closed-loop LP system it is necessary to use a three-port device (either a circulator or a directional coupler) in the active loop to route the waves b_2 and a_2 in their respective directions. As in the open-loop and feedforward LP systems, the magnitude of the wave injected to the DUT's output is varied through the use of an attenuator and an amplifier located in the loop. Alternatively, a *passive closed-loop* may be used to vary the impedance at the DUT's output by using only the attenuator and phase shifter [Ghannouchi (2010)] in the loop. Depending on the frequency and the attenuator/phase shifter insertion loss, this passive loop may allow synthesizing loads located close to the edge of the Smith chart.

Unlike the open-loop technique, the closed-loop technique does not require external phase coherent sources to maintain phase coherence between the signal a_2 and the signal b_2 ; the waves a_2 and b_2 are coherent by nature. Closed-loop is more similar to the feed-forward

approach; indeed, in some textbooks [Ghannouchi (2013)] the closed-loop technique is referred to as the *feedback LP technique*. The main difference between these two LP techniques relies on the point in the LP system at which the signal injected to the DUT output is sampled: at the input (feedforward) or at the output (closed-loop) of the DUT.

Furthermore, since in the closed-loop technique the signal injected at the DUT output is a modified version of the DUT output signal, it is ensured that the synthesized load impedance is independent of drive level. It avoids the iterative process required in open-loop and feedforward techniques to generate a determined load impedance [Williams (2014)].

The appropriate LP system to be used depends on the type of measurement to be performed. Passive LP systems are mostly used in very high power applications; meanwhile, active LP systems are preferred when low and medium power devices are characterized under high Γ_{LOAD} loading conditions. A special type of LP systems in which the passive and active approaches are combined (hybrid LP systems) have emerged in recent years [Hashmi (2011)]. They are used to alleviate the power requirements from active elements of active LP systems in those cases in which high Γ_{LOAD} values have to be synthesized at the output of high power devices [Ferrero (2008)].

4.2.3 Pre-calibrated and real-time load-pull systems

In the preceding section, a classification of LP systems in terms of the procedures by which the load at the output of a DUT is varied, was presented. LP systems may also be classified as a function of the form by which the measurement setup is calibrated. In this respect, LP measurement systems are classified as pre-calibrated LP systems and real-time LP systems.

Pre-calibrated LP systems

In pre-calibrated LP systems, such as the one depicted in Figure 37, all the impedances presented at the output of the DUT during the LP characterization have to be known prior to measurement process. In this order, pre-calibrated passive impedance tuners have to be

used; it implies using a VNA to determine the S-parameters of the tuner at a set of positions of the probe along the vertical and horizontal axes (see Figure 33).

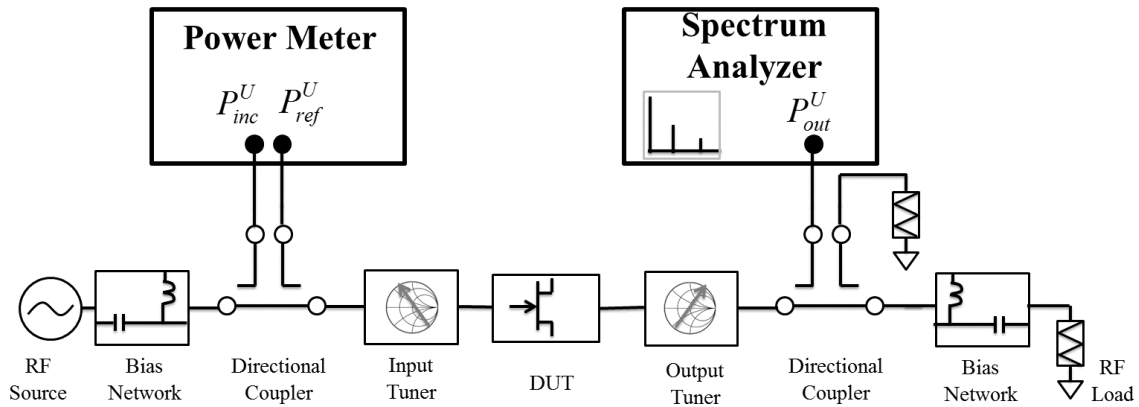


Figure 37. Generic diagram of a LP system using pre-calibrated impedance tuners.

Tuner repeatability is a must in this type of LP systems since it is required that the passive-tuner behaves identically when measured by a VNA and when placed in the LP setup. In addition, since any element located between the tuner and the DUT and between the tuner and the load (e.g., cables, connectors, adapters, test-fixtures or bias-tees) affects the impedance seen by the DUT, all of the elements of the LP system have to be known prior to the measurement.

Pre-calibrated LP systems allow measuring only scalar parameters of a DUT, such as output power, power gain and efficiency⁴, while varying the impedance at its output. In order to measure the power levels at the input and output of a DUT, power receivers (power meters and/or spectrum analyzers) are used, as shown in Figure 37. Since this type of LP systems only allow the use of passive tuning systems, tuners are placed as close as possible to the DUT, in order to achieve the highest reflection coefficient at the DUT's input and output ports. Hence, the power levels measured by the power receivers located at the input ($P_{IN}^U = P_{inc}^U - P_{ref}^U$) and output (P_{OUT}^U) sides of a DUT are not the actual power levels at the DUT plane, but an uncalibrated version of them. In order to determine the power at

⁴Vectorial figures of merit such as amplitude-to-phase conversion of a DUT (AM-PM distortion) or the variation of the DUT's input impedance as a function of the input power cannot be measured.

the DUT ports, the knowledge of the behavior of the passive elements placed between the DUT and the power receivers is used to accurately de-embed their effects [Maury-Microwave (2009)].

The limitations of pre-calibrated LP systems regarding tuner repeatability, pre-characterization of each element of the system, the inability to measure important vectorial figures of merit of a DUT along with the inability to use active load tuning systems are overcome by using real-time LP systems.

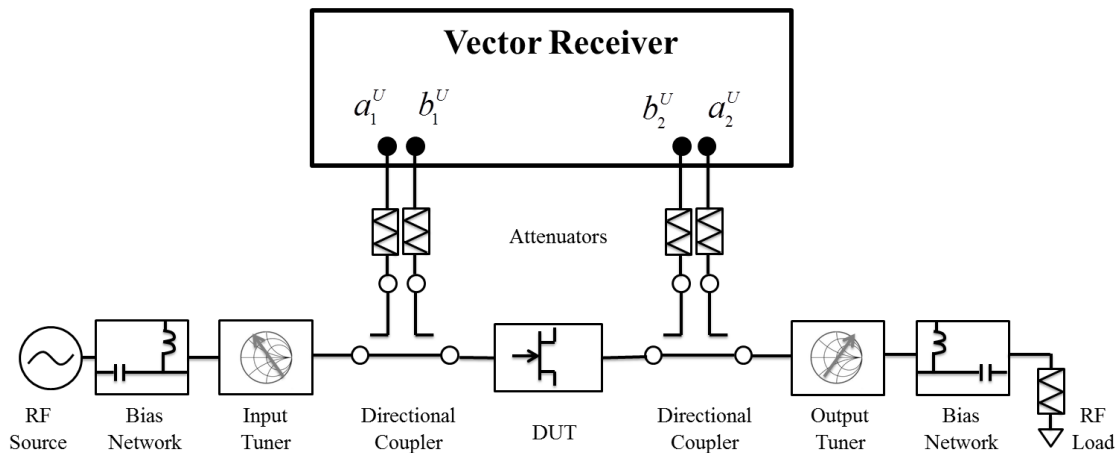


Figure 38. Generic diagram of a real-time LP system.

Real-time LP systems

Real-time LP systems, also known as *vector-receiver load pull systems* [Maury-Microwave (2011)], comprise a signal source (and a boost amplifier if required) to drive the DUT, impedance tuners, directional couplers and a vector-receiver. The vector-receiver is the most important element, it is used to capture uncalibrated ratios of parameters of interest along with the magnitude of the traveling waves at the input and output of a DUT. This information is then used to determine the impedances and the non-linear behavior at the DUT reference plane by using a calibration procedure. Nowadays, state-of-the-art VNAs [Keysight-Technologies. (2015); Anritsu. (2014)] have external access to the internal instrument receivers, which are typically used as a vector receiver in LP measurements.

In real-time LP systems the impedances presented at the DUT's output are determined at the same time the load impedance is varied. In this type of LP systems, neither the impedance tuner nor the elements of the LP system have to be characterized prior to the measurement process. Therefore, tuner repeatability is not a concern in real-time LP systems.

The accuracy of real-time LP measurement systems relies on the calibration of the measurement setup. In order to accurately characterize a DUT, a calibration process (which is independent of the impedance tuner) is used [Ferrero (1993); Pulido-Gaytan (2015a)]. Once calibrated, real-time LP systems allow measuring the impedance at the input of the DUT, the load impedance at the DUT's output and the large-signal behavior of the DUT.

Moreover, unlike pre-calibrated LP systems in which only passive impedance tuners may be used, real-time LP systems allow the use of both passive and active tuning systems. This feature of real-time LP systems is very useful to characterize power transistors, requiring very low impedances for optimum operation.

Although both pre-calibrated and real-time LP systems are widely used in the characterization of power transistors, the accuracy in a LP characterization is enhanced when using real-time LP systems [Ferrero (2001); Maury-Microwave (2011)], provided that they are accurately calibrated. In chapter 5 a complete mathematical formulation of the procedure for calibrating real-time LP systems is presented.

4.3 Load-pull as a tool for power amplifier design

Power amplifier design techniques are commonly categorized into two types. The first category is based on computer aided design (CAD) methods, using nonlinear device models to predict the device's behavior. The second type is based on the use of measurements carried out under nonlinear conditions. In the following subsections these two approaches are summarized.

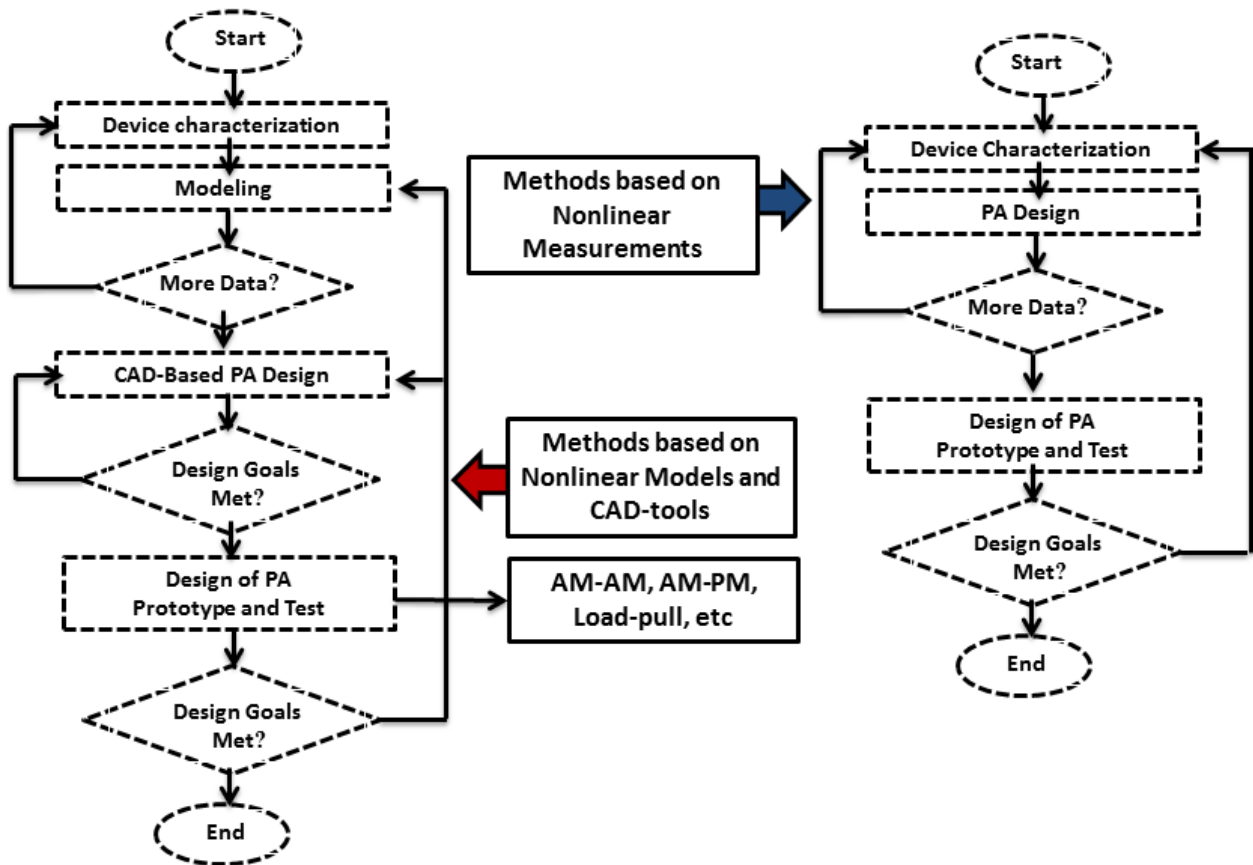


Figure 39. Power amplifier design cycles methods based on device's nonlinear models/CAD-tools and using nonlinear measurements(AM-AM, AM-PM, load-pull) [Ghannouchi (2013)].

4.3.1 Methods based on device's nonlinear models and CAD-tools

While the design of linear microwave circuits using CAD tools has become a standard design approach, the design of nonlinear microwave circuits using CAD tools is still evolving. Methods for PA design based on CAD tools require that a model for active devices be available [Rudolph (2011); Nuttinck (2001)].

Currently, the most commonly used devices for designing PAs for wireless communications are the GaN HEMT, the SiC MESFET and the Si LDMOS transistors. Accurately modeling the large-signal behavior of these devices is a challenging task [Szhau (2013); Dunleavy (2010); Bindra (2015)] and is still an open research topic.

The availability of large-signal measurements is of paramount importance even in PA design using the DUT's model. Once the model of a device has been developed, and before

using it for a PA design, experimental validation of the model has to be carried out using large-signal measurements (e.g., load-pull, AM-AM, AM-PM, etc). The accuracy of the model is iteratively tested and it can be considered as acceptable once the requisite accuracy in the prediction of a determined parameter is achieved.

Accurate measurements of transistors in both the linear and nonlinear regimes are necessary to build reliable models and to verify the model's accuracy [Aaen (2007); Zarate-de Landa (2013)]. Thus, among the considerations for good transistor models are the overall measurement accuracy for development and validation of the models [Dunleavy (2010)].

4.3.2 Methods based on nonlinear measurements

In methods based on nonlinear measurements, transistors are characterized in nonlinear conditions in order to obtain key design parameters of the devices, such as gain, efficiency, load-pull contours, etc. The main advantage of these methods is the time saved discarding the time-consuming development of a device model; in these methods the measured data form the primary basis of the design.

The reliability of these kind of methods relies on the availability of accurate measurement systems. Large-signal measurement systems, such as LP test setups, allow to capture important characteristics of devices, mainly those that can be related to their nonlinear performance. These systems enable first-pass PA design methodologies, considering that the measurements are carried out, and thus the data is collected, under realistic conditions. Figure 39 depicts the design cycle of PAs using methods based on measurements and methods based on CAD-tools. It is evident the reduction in the design cycle when using calibrated nonlinear measurement systems to collect the data for PA design.

Presently, although transistor modeling and computer-aided design of microwave nonlinear circuits have become mature technologies, they have not diminished the interest for transistor LP [Pedro (2015)]. On the contrary, LP techniques have always been, and still are, a hot research topic.

5. Calibration of real-time LP measurement systems

The objective of the characterization of a device using a LP system is the evaluation of its performance under different loading conditions in order to determine the load under which its optimal performance, in terms of a determined metric or set of metrics, may be obtained [Ghannouchi (2013)]. Nevertheless, elements of the measurement setup that allow the LP measurements to be performed introduce errors in the measurement of the impedances and large-signal behavior at the device's plane. Thus, to accurately characterize a device under test (DUT), the measurement setup has to be calibrated. In this chapter, some concepts and mathematical analysis presented in previous chapter are used to develop the calibration procedure of a real-time LP system.

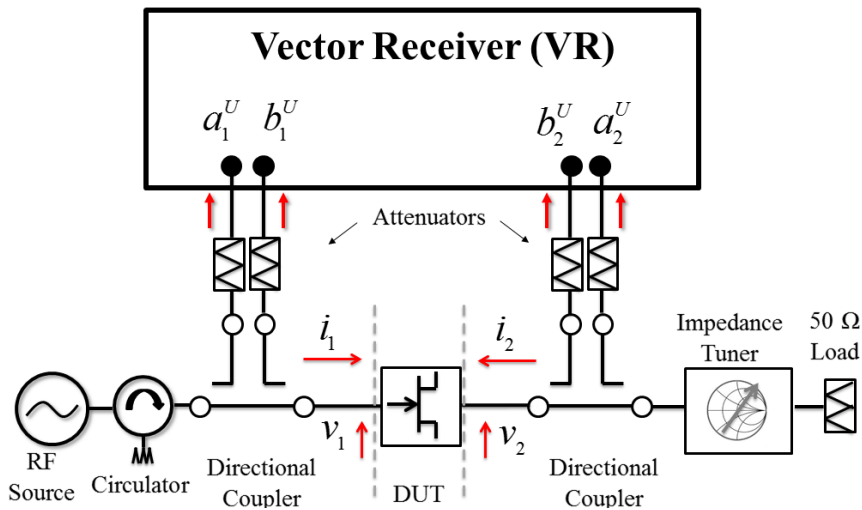


Figure 40. Measurement setup of a real-time load-pull system (neither driver amplifier nor networks for DUT biasing are depicted).

The calibration of a LP measurement setup, such as the one depicted in Figure 40, is divided into two parts: 1) a relative calibration, in which ratios of parameters of interest (e.g., voltages and currents or incident and scattered waves) may be determined, and 2) a power calibration, in which the power levels at the DUT ports are determined. The relative calibration may be carried out by using conventional VNA calibration techniques such as those presented in chapter 3. The power calibration, on the other hand, may be carried out

by using a power meter (PM) connected at the calibration plane [Roblin (2011); Pisani (1996)] as long as the PM can be connected at such plane (e.g., when characterizing coaxial devices). When a PM cannot be connected at the calibration plane (e.g., when the DUT is mounted in a microstrip test fixture or is contacted using coplanar probes) the power calibration is carried out by connecting a PM at a coaxial plane located far from the calibration plane and using a procedure to determine the power at the calibration plane.

In this section a complete mathematical formulation of the calibration procedure of a real-time LP system, that is suitable for the characterization of both coaxial devices and devices mounted on planar structures is presented. Relevant parameters, such as input impedance, load impedance and large-signal gain are considered. By using the ABCD-parameters matrix formalism in the calibration of the LP measurement setup, closed form expressions allowing to evaluate the impact of different VNA calibration techniques on the LP characterization of power transistors are presented.

In order to analyze the calibration of the LP setup depicted in Figure 40, we use the structures shown in Figure 42 and Figure 44 for the analysis of the setup configurations shown in Figure 41 and Figure 43. The calibration procedure described in this section uses the ABCD-parameters formalism for representing the measurements in the vector receiver (VR) and PM used in the calibration. Hence, the analysis is developed in terms of voltages and currents instead of incident and scattered waves [Pulido-Gaytan (2015a)].

5.1 Relative calibration

According to the theory presented in section 2.2, the voltages and currents at the VR ports, v_k^U and i_k^U , $k = 1, 2$, which are defined as a function of the traveling waves at the VR as

$$v_k^U = \sqrt{Z_0} \left(1 + \frac{b_k^U}{a_k^U} \right) a_k^U = \sqrt{Z_0} \left(1 + \frac{a_k^U}{b_k^U} \right) b_k^U, \quad (173)$$

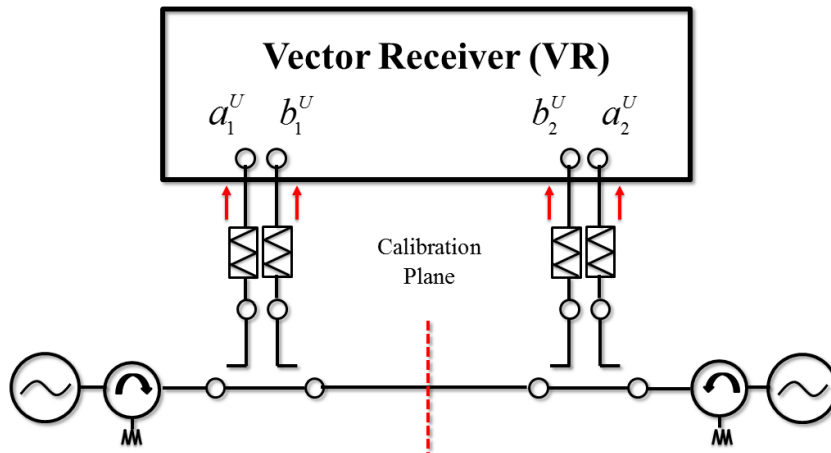


Figure 41. Measurement setup configuration for the relative calibration (networks for DUT biasing are not depicted).

$$i_k^U = \frac{1}{\sqrt{Z_0}} \left(1 - \frac{b_k^U}{a_k^U} \right) a_k^U = \sqrt{Z_0} \left(1 - \frac{a_k^U}{b_k^U} \right) b_k^U, \quad (174)$$

may be related to the voltages and currents at the DUT ports, v_k and i_k , as follows¹

$$\begin{bmatrix} v_1 \\ i_1 \end{bmatrix} = \mathbf{T}_A^{-1} \begin{bmatrix} v_1^U \\ i_1^U \end{bmatrix}, \quad (175)$$

$$\begin{bmatrix} v_2 \\ i_2 \end{bmatrix} = \mathbf{T}_B \begin{bmatrix} v_2^U \\ i_2^U \end{bmatrix}. \quad (176)$$

In (175)-(176), \mathbf{T}_A and \mathbf{T}_B are matrices representing the networks connecting the DUT ports to the VR ports, as shown in Figure 42. According to the theory presented in chapter 3, these matrices may be expressed as

$$\mathbf{T}_A = \mathbf{T}_X \mathbf{T}_Z^{-1} = D_X \begin{bmatrix} \overline{A}_X & \overline{B}_X \\ \overline{C}_X & 1 \end{bmatrix} \begin{bmatrix} -Z_B & Z_A \\ 1 & 1 \end{bmatrix}^{-1}, \quad (177)$$

¹An assumption made in LP is that the elements of the measurement setup are operating linearly, in order ensure that v_k^U, i_k^U are linearly related to v_k, i_k . It holds true for the couplers, bias networks and other passive elements. As far as the VR is concerned, attenuators have to be used to ensure that the instrument receivers are in its linear dynamic range.

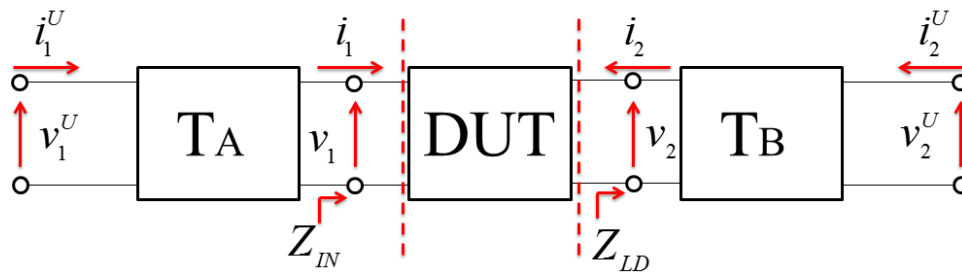


Figure 42. Model for the measurement setup configuration for the relative calibration.

$$\mathbf{T}_B = \mathbf{T}_Z \mathbf{T}_Y = D_Y \begin{bmatrix} -Z_B & Z_A \\ 1 & 1 \end{bmatrix} \begin{bmatrix} \overline{A}_Y & \overline{B}_Y \\ \overline{C}_Y & 1 \end{bmatrix}, \quad (178)$$

where the terms Z_A and Z_B in the matrix \mathbf{T}_Z represent the impedance of one of the calibration structures used in a determined calibration technique. For the sake of clarity, the case in which $Z_A = Z_B = Z$ is first considered.

As presented in chapter 3, the seven terms \overline{A}_X , \overline{B}_X , \overline{C}_X , \overline{A}_Y , \overline{B}_Y , \overline{C}_Y and $D_X D_Y$ are determined by using only information provided by the measurement of the calibration structures corresponding to a calibration technique. Then, by substituting (177) in (175) and (178) in (176), and developing the resultant expressions using $Z_A = Z_B = Z$, the following equations may be derived

$$v_1 = \frac{-Z}{D_X \cdot \Delta_X} [(1 + \overline{C}_X)v_1^U - (\overline{B}_X + \overline{A}_X)i_1^U], \quad (179)$$

$$i_1 = \frac{1}{D_X \cdot \Delta_X} [(1 - \overline{C}_X)v_1^U - (\overline{B}_X - \overline{A}_X)i_1^U], \quad (180)$$

$$v_2 = Z \cdot D_Y [(\overline{C}_Y - \overline{A}_Y)v_2^U - (1 - \overline{B}_Y)i_2^U], \quad (181)$$

$$i_2 = -D_Y [(\overline{C}_Y + \overline{A}_Y)v_2^U - (1 + \overline{B}_Y)i_2^U], \quad (182)$$

where $\Delta_X = \overline{A_X} - \overline{B_X C_X}$. Then, from (179)-(182), the following expressions for the impedance at the input of the DUT and the load impedance at the DUT plane defined as $Z_{IN} = v_1/i_1$ and $Z_{LD} = -v_2/i_2$ are obtained

$$Z_{IN} = -Z \cdot \frac{(1 + \overline{C_X})Z_1^U - (\overline{B_X} + \overline{A_X})}{(1 - \overline{C_X})Z_1^U - (\overline{B_X} - \overline{A_X})}, \quad (183)$$

$$Z_{LD} = Z \cdot \frac{(\overline{C_Y} - \overline{A_Y})Z_2^U - (1 - \overline{B_Y})}{(\overline{C_Y} + \overline{A_Y})Z_2^U - (1 + \overline{B_Y})}, \quad (184)$$

where $Z_k^U = v_k^U/i_k^U$, $k = 1, 2$. Meanwhile, the DUT's voltage gain and current gain, defined as $G_v = v_2/v_1$ and $G_i = -i_2/i_1$, may be expressed as

$$G_v = -\Delta_X \cdot D_X D_Y \cdot \frac{(\overline{C_Y} - \overline{A_Y}) - (1 - \overline{B_Y})Y_2^U}{(1 + \overline{C_X}) - (\overline{B_X} + \overline{A_X})Y_1^U}, \quad (185)$$

$$G_i = -\Delta_X \cdot D_X D_Y \cdot \frac{(\overline{C_Y} + \overline{A_Y})Z_2^U - (1 + \overline{B_Y})}{(1 - \overline{C_X})Z_1^U - (\overline{B_X} - \overline{A_X})}, \quad (186)$$

where $Y_k^U = 1/Z_k^U$, $G_v^U = v_2^U/v_1^U$ and $G_i^U = -i_2^U/i_1^U$.

The commonly used definition for gain in terms of the transmitted and incident waves $G_d = b_2/a_1$, can be determined as

$$G_d = \frac{v_2 - Z_0 \cdot i_2}{v_1 + Z_0 \cdot i_1} = \frac{Z_{LD} + Z_0}{Z_{IN} + Z_0} G_i = \frac{1 + Z_0/Z_{LD}}{1 + Z_0/Z_{IN}} G_v. \quad (187)$$

It may be noted from (183)-(184) that for determining Z_{IN} and Z_{LD} the knowledge of Z is mandatory. Regarding the gain, according to (185)-(186) the voltage gain and current gain do not depend on the knowledge of Z . On the other hand, the gain in terms of incident and transmitted waves G_d depends on Z through its own dependence on Z_{IN} and Z_{LD} . It is worth noting that the power gain G_p , defined as

$$G_p = |G_v|^2 \frac{\text{Re}(1/Z_{LD})}{\text{Re}(1/Z_{IN})} = |G_i|^2 \frac{\text{Re}(Z_{LD})}{\text{Re}(Z_{IN})}, \quad (188)$$

depends on Z through its own dependence on $Re(Z_{IN})$ and $Re(Z_{LD})$, unless the value of Z is purely real.

Relative calibration using nonsymmetrical loads in the TRM technique

In this section a more general formulation to the relative calibration of a LP system, in which Z_A and Z_B are allowed to be either identical or different is presented. As explained in chapter 3, this condition is only encountered when the the relative calibration of a LP system is carried out using the TRM technique implemented using symmetrical or nonsymmetrical loads of arbitrary impedance.

By substituting (177) in (175) and (178) in (176), and developing the resultant expressions, the following expressions for v_k and i_k , $k = 1, 2$, may be derived

$$v_1 = \frac{-Z_A}{D_X \cdot \Delta_X} \left[\left(\frac{Z_B}{Z_A} + \overline{C_X} \right) v_1^U - \left(\frac{Z_B}{Z_A} \overline{B_X} + \overline{A_X} \right) i_1^U \right], \quad (189)$$

$$i_1 = \frac{1}{D_X \cdot \Delta_X} [(1 - \overline{C_X})v_1^U - (\overline{B_X} - \overline{A_X})i_1^U], \quad (190)$$

$$v_2 = Z_A \cdot D_Y \left[\left(\overline{C_Y} - \frac{Z_B}{Z_A} \overline{A_Y} \right) v_2^U - \left(1 - \frac{Z_B}{Z_A} \overline{B_Y} \right) i_2^U \right], \quad (191)$$

$$i_2 = -D_Y [(\overline{C_Y} + \overline{A_Y})v_2^U - (1 + \overline{B_Y})i_2^U]. \quad (192)$$

Note that the expressions for i_1 and i_2 are identical to the expressions previously presented in (180) and (182). The expressions for v_1 and v_2 , on the other hand, take into account possible asymmetry between the loads used as calibration elements in the TRM are identical to the expressions shown in (179) and (181) only if $Z_A = Z_B$.

In this order, the impedance at the input of the DUT and the load impedance at the DUT plane may be expressed as

$$Z_{IN} = -Z_A \cdot \frac{\left(\frac{Z_B}{Z_A} + \overline{C_X}\right) Z_1^U - \left(\frac{Z_B}{Z_A} \overline{B_X} + \overline{A_X}\right)}{(1 - \overline{C_X}) Z_1^U - (\overline{B_X} - \overline{A_X})}, \quad (193)$$

$$Z_{LD} = Z_A \cdot \frac{\left(\overline{C_Y} - \frac{Z_B}{Z_A} \overline{A_Y}\right) Z_2^U - \left(1 - \frac{Z_B}{Z_A} \overline{B_Y}\right)}{(\overline{C_Y} + \overline{A_Y}) Z_2^U - (1 + \overline{B_Y})}, \quad (194)$$

Since the expressions for i_1 and i_2 are independent of the the impedances Z_A and Z_B , the current gain G_i may be expressed as shown in (186). Regarding the voltage gain G_v , it depends on the knowledge of the impedances Z_A and Z_B as follows

$$G_v = -\Delta_X \cdot D_X D_Y \cdot \frac{\left(\overline{C_Y} - \frac{Z_B}{Z_A} \overline{A_Y}\right) - \left(1 - \frac{Z_B}{Z_A} \overline{B_Y}\right) Y_2^U}{\left(\frac{Z_B}{Z_A} + \overline{C_X}\right) - \left(\frac{Z_B}{Z_A} \overline{B_X} + \overline{A_X}\right) Y_1^U}. \quad (195)$$

It differs from the result previously reported in (185), where G_v was found to be independent of the knowledge of the impedance $Z = Z_A = Z_B$.

Regarding the gain expressed as the ratio of the transmitted to incident waves G_d . It depends on the knowledge of the impedances Z_A and Z_B through the dependence of G_v , Z_{IN} and Z_{LD} on Z_A and Z_B .

5.2 Power calibration

Thus far, expressions to determine the impedance at the input of a DUT, its gain and the load impedance at the DUT plane have been derived. Nonetheless, in LP an important concern is to specify the power levels at the input and output of the DUT (i.e., the power level at which the ratios shown in (183)-(188) are defined). In this order, by analyzing the structure shown in Figure 42, the power at the input and output of a DUT may be expressed as

$$P_{IN} = |v_1|^2 \operatorname{Re}(1/Z_{IN}), \quad (196)$$

$$P_{OUT} = |v_2|^2 \operatorname{Re}(1/Z_{LD}), \quad (197)$$

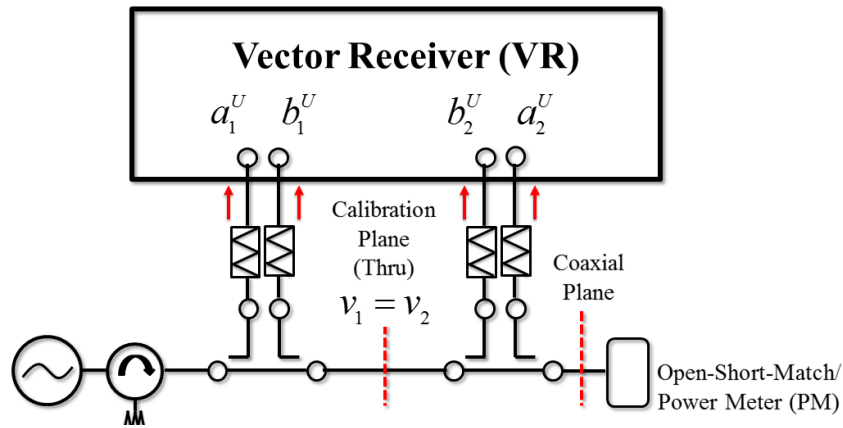


Figure 43. Measurement setup configuration for the absolute power calibration (networks for DUT biasing are not depicted).

where

$$|v_1| = \frac{|Z|}{|D_X|} \left| (1 + \overline{C_X}) - (\overline{B_X} + \overline{A_X}) Y_1^U \right| \frac{|v_1^U|}{|\Delta_X|}, \quad (198)$$

$$|v_2| = |Z| |D_Y| \left| (\overline{C_Y} + \overline{A_Y}) - (1 - \overline{B_Y}) Y_2^U \right| |v_2^U|. \quad (199)$$

From (196)-(199), it is noted that for determining P_{IN} and P_{OUT} it is mandatory to know $|D_X|$ and $|D_Y|$. These terms may be calculated by using the measurement setup configuration shown in Figure 43, as described next.

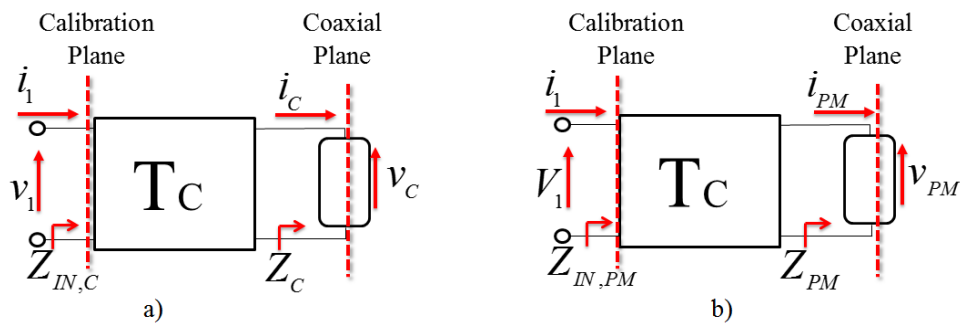


Figure 44. Model for the measurement of the a) coaxial loads and b) the power meter.

Calculation of $|D_X|$ and $|D_Y|$

The procedure for determining $|D_X|$ and $|D_Y|$ consists of: 1) to make a thru connection at the calibration plane, 2) to connect three loads of known impedance at a coaxial plane and 3) to connect a PM at that coaxial plane (Figure 44) [Ferrero (1993)].

When characterizing transistors, the calibration plane is typically set either at the probe-tips when dealing with on-wafer devices, or at the center of a test fixture when dealing with packaged devices. As shown in Figure 44, there is a two-port network connecting the calibration plane to a coaxial plane. When characterizing packaged transistors, this two-port network may include, among other elements, the test fixture, directional coupler, connectors and cables. This network may be represented by an ABCD-parameters matrix T_C .

According to the structure shown in Figure 44a, the voltages and currents at the calibration plane, v_1 and i_1 , may be related to the voltages and currents at the coaxial plane, v_C and i_C , as

$$\begin{bmatrix} v_1 \\ i_1 \end{bmatrix} = \mathbf{T}_C \begin{bmatrix} v_C \\ i_C \end{bmatrix}, \quad (200)$$

with \mathbf{T}_C defined as

$$\mathbf{T}_C = D_C \begin{bmatrix} \overline{A_C} & \overline{B_C} \\ \overline{C_C} & 1 \end{bmatrix}. \quad (201)$$

Since the impedance at the input of the calibration plane, $Z_{IN} = v_1/i_1$, may be determined from (183), the terms $\overline{A_C}$, $\overline{B_C}$ and $\overline{C_C}$ may be determined by using the *OSM* procedure reported in section 3.10, as long as three loads of known impedance, $Z_C = v_C/i_C$, are connected at the coaxial plane.

Once, $\overline{A_C}$, $\overline{B_C}$ and $\overline{C_C}$ are known, let now analyze the connection of a PM at the coaxial plane. First, by analyzing the structure shown in Figure 44b using (200)-(201), the impedance of the PM, Z_{PM} , is calculated as

$$Z_{PM} = \frac{Z_{IN,PM} - \overline{B_C}}{\overline{A_C} - Z_{IN,PM}\overline{C_C}}, \quad (202)$$

where $Z_{IN,PM}$ is the impedance at the input of the calibration plane, when a PM is connected at the coaxial plane (Figure 43).

Then, from the analysis of the structure shown in Figure 44b, using (200)-(201), the following expression may be derived

$$v_1 = D_C (\overline{A_C} + \overline{B_C} Y_{PM}) v_{PM}, \quad (203)$$

where v_{PM} represents the voltage at the PM and $Y_{PM} = 1/Z_{PM}$. Now, let $P_{PM} = |v_{PM}|^2 \text{Re}(Y_{PM})$ be the power measured in the PM. From (203) one can derive the following expression

$$|v_1|^2 = |D_C|^2 |\overline{A_C} + \overline{B_C} Y_{PM}|^2 \frac{P_{PM}}{\text{Re}(Y_{PM})}, \quad (204)$$

where the term $|D_C|^2$ is calculated by assuming that the network represented by the matrix \mathbf{T}_C is reciprocal (the determinant of \mathbf{T}_C equals the unity) as

$$|D_C|^2 = \frac{1}{|\overline{A_C} - \overline{B_C} \overline{C_C}|^2}. \quad (205)$$

Finally, the value of the terms $|D_X|^2$ and $|D_Y|^2$ are calculated by taking advantage of the thru connection made at the calibration reference plane, as presented next. Since a thru connection at the calibration plane is considered, the identity $v_1 = v_2$ holds. Hence, by solving (196) and (199) for $|D_X|^2$ and $|D_Y|^2$, and substituting (204) in the resultant expressions one has

$$|D_X|^2 = \frac{|Z|^2}{|D_C|^2} \frac{|(1 + \overline{C_X}) - (\overline{B_X} + \overline{A_X}) Y_1^U|^2 \text{Re}(Y_{PM}) |v_1^U|^2}{|\Delta_X|^2 |\overline{A_C} Z_{PM} + \overline{B_C}|^2 P_{PM}}, \quad (206)$$

$$|D_Y|^2 = \frac{|D_C|^2}{|Z|^2} \frac{|\overline{A_C} Z_{PM} + \overline{B_C}|^2 P_{PM}}{|(\overline{C_Y} - \overline{A_Y}) - (1 - \overline{B_Y}) Y_2^U|^2 Y_2^U \text{Re}(Y_{PM}) |v_2^U|^2}. \quad (207)$$

Once the power levels at the DUT ports have been determined, the LP measurement system is fully calibrated. Then, for each impedance synthesized by the load tuner, importance figures of merit such as output power, large signal gain along with input and load impedance may be determined.

Other important figures of merit such as drain efficiency

$$\eta_D = P_{OUT}/P_{DC}, \quad (208)$$

and power added efficiency

$$PAE = (P_{OUT} - P_{IN})/P_{DC}, \quad (209)$$

may be calculated as well, as long as the direct current (DC) power dissipated in the device, P_{DC} , is measured using DC voltage and current meters. Contours of constant output power (P_{OUT}), large-signal gain (G_v , G_i , G_d or G_p) or efficiency (η_D or PAE) or some metric of linearity such as $ACPR$ [Darraji (2012)] may be formed.

6. Load-Pull Characterization of Power Transistors

As mentioned in chapter 4, LP systems can be implemented by using either pre-calibrated impedance tuners (non-real-time systems) or real-time tuning and calibration systems. Although non-real-time LP systems are still widely used in both the industry and the academy, the degree of accuracy in the LP characterization of microwave transistors increases when real-time LP systems are used. In this chapter the implementation of a real-time LP system is presented. Experimental results regarding the LP characterization of a packaged GaN-HEMT power transistor using the implemented LP system are presented and analyzed.

6.1 Implementation of a real-time LP measurement system

The real-time LP measurement system depicted in Figure 45 was implemented and a 10 W GaN-HEMT packaged transistor, *Cree, Inc.* CGH40010F [Cree (2015a)], was characterized at 3.5 GHz.

As vector receiver the *Agilent Technologies* PNA-X N5245A was used, having this instrument external access to the instrument receivers. As RF signal source the internal source of the PNA-X was used; alternatively, an external source may be used as long as it is phase-locked to the vector receiver. The signal emerging from the RF source is boosted by a high power amplifier in order to drive the DUT. Circulators set at the input and output of the driver amplifier are used to protect the RF source and amplifier from possible reflections at their outputs.

Strictly, for performing a LP characterization it is not mandatory to use an impedance tuner at the input of the DUT. Nevertheless, an impedance tuner at the DUT's input may be used to match the transistor's input to the source in order to allow maximum power transfer from the source to the transistor. It allows reducing the power from the RF source and driver amplifier required to saturate the DUT.

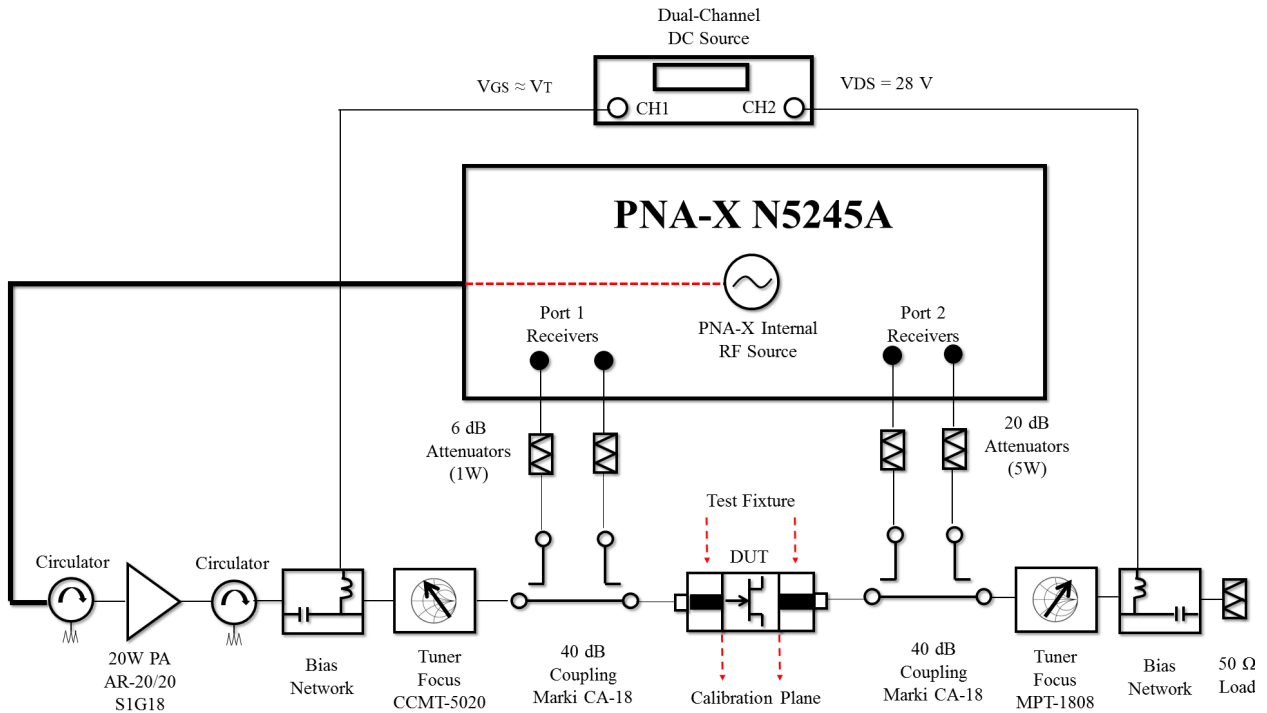


Figure 45. Measurement setup of the implemented passive real-time LP system.

An important aspect to be considered when setting up a LP measurement system is the *power budget* [Betts (2011)]. An estimation of the power level that will be managed in the whole measurement system is used to determine the characteristics of some elements of the setup. Dual directional couplers (40 dB coupling and 0.2 dB insertion loss at 3.5 GHz) were used to allow the vector receiver to measure uncalibrated incident and reflected waves at the DUT's input and output ports. Attenuators may be placed between receivers and couplers' arms to protect the receivers from power levels beyond their safe power limits. High-coupling directional couplers are useful to allow the receivers to operate in their linear dynamic range. Nevertheless, high-coupling could be not beneficial whether very low-power signals are required to be measured, since low-power signals entering the receivers can be affected by noise floor.

The load at the output of the DUT is varied through the use of a mechanical impedance tuner. As presented in chapter 4, low-loss couplers [Teppati (2003)] are useful to enhance the impedance tuning capabilities of the overall LP system [Teppati (2008)]. The insertion

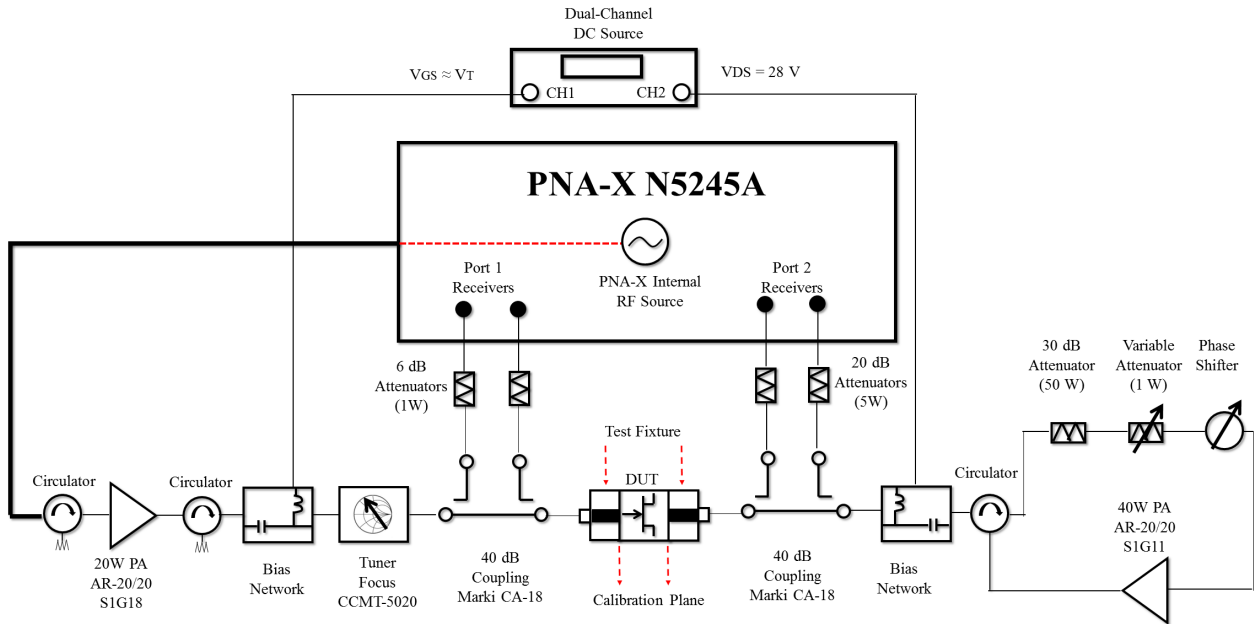


Figure 46. Measurement setup of the implemented closed-loop active real-time LP system.

loss of directional couplers are not a concern whether active tuning systems are used. In this order, the closed-loop active real-time LP measurement system depicted in Figure 46 was also implemented to compare the results obtained using these two approaches for the characterization of the 10 W transistor used as DUT.

The DUT is mounted in a microstrip test fixture comprising $50\ \Omega$ transmission lines and SMA-to-microstrip adapters, as depicted in Figure 47a. The DUT is biased by using a dual-channel DC voltage source through bias networks located at the DUT's input (gate) and output (drain) sides.

The measurement system was calibrated by using the calibration procedure presented in the preceding section. Since different calibration techniques (TRL, TRM, TRRM and LZZ) were used to determine the error terms of the relative calibration part of the calibration procedure, the set of microstrip structures depicted in Figure 47 b-f were fabricated in a substrate RO4003 from *Rogers Corporation* [Rogers (2015)].

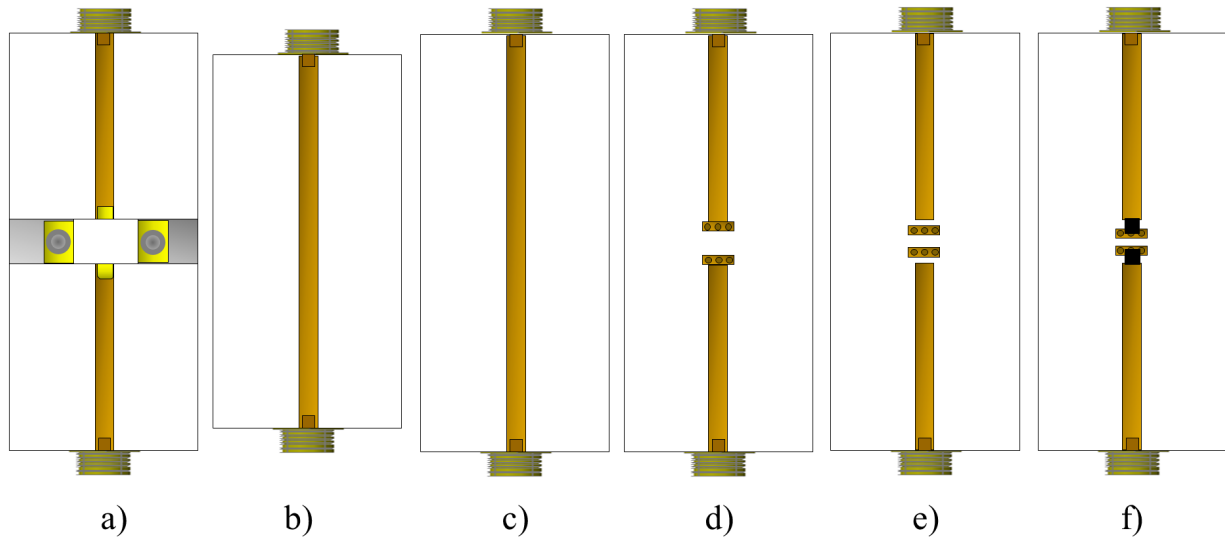


Figure 47. a) Test fixture and calibration structures used to implement the TRL, TRM, TRRM and LZZ techniques: b) thru, c) $50\ \Omega$ transmission line, d) short, e) open and f) $50\ \Omega$ load.

6.2 Characterization of power transistors using LP systems

In this section, the DUT is characterized by using the real-time LP measurement system described in the preceding section. These results were obtained by using the TRL calibration in the relative calibration. In section 6.3 the results obtained using other calibration techniques in the calibration procedure are presented and used to evaluate the impact of different calibration techniques in the characterization of power transistors.

6.2.1 Load-pull contours of constant power, efficiency and gain

First, the accuracy of the calibration of the measurement system is verified. A commonly used form to verify the accuracy in the calibration of a LP system is to measure the large-signal gain of the through connection of the calibration planes (thru) [Ferrero (2001); Bonino (2010); Teppati (2007)], which to be consistent with the theory has to be identical to 1 (0 dB). The power gain is the commonly used parameter for this purpose; nevertheless, according to the analysis presented in section 5.1, there are different forms to define the large-signal gain, namely the ratio of the transmitted to incident waves G_d , voltage gain G_v , current gain G_i and power gain G_p .

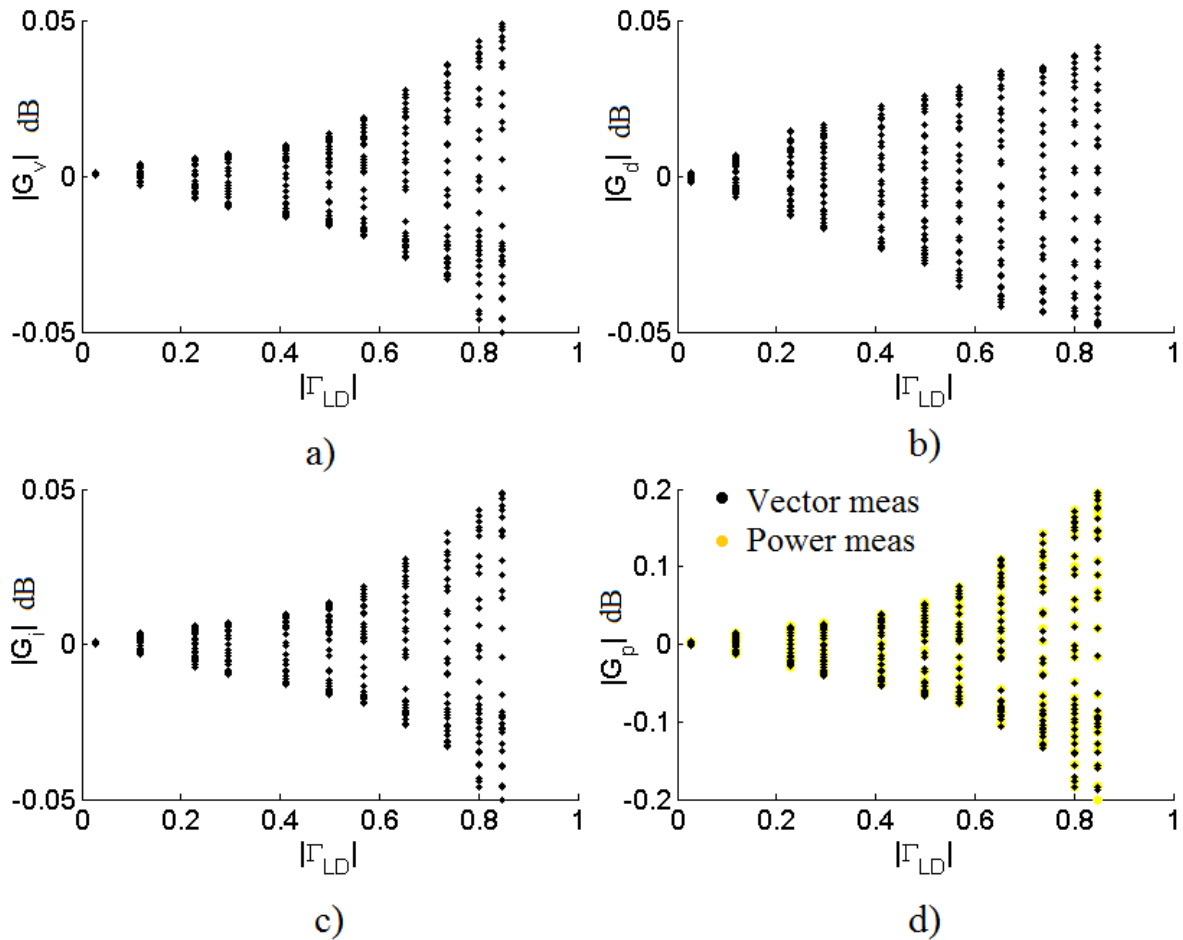


Figure 48. Large-signal gain of a thru: a) voltage gain (G_v), b) ratio of transmitted to incident waves (G_d), c) current gain (G_i) and d) power gain (G_p), as a function of the magnitude of the load reflection coefficient Γ_{LD} .

Figure 48 shows the magnitude of the measured G_d , G_v , G_i and G_p as a function of the magnitude of the synthesized load reflection coefficient, $\Gamma_{LD} = (Z_{LD} - Z_0)/(Z_{LD} + Z_0)$. Note that in all the cases as the value of $|\Gamma_{LD}|$ increases, the difference between the magnitude of the large-signal gain and the expected gain also increases. This is a result commonly observed in practice [Ferrero (2001); Teppati (2012)]. According to several works reported in the literature, it occurs due to uncertainty and residual errors in the relative calibration procedure (i.e., the calculation of the seven calibration terms) and several efforts have been made to mitigate them [Bonino (2010); Teppati (2007); Aldoumani (2014)]. From the author's perspective, the origin of this result may simply be the fact that the measurement system is calibrated under low Γ_{LD} conditions (i.e., during the relative calibration procedure

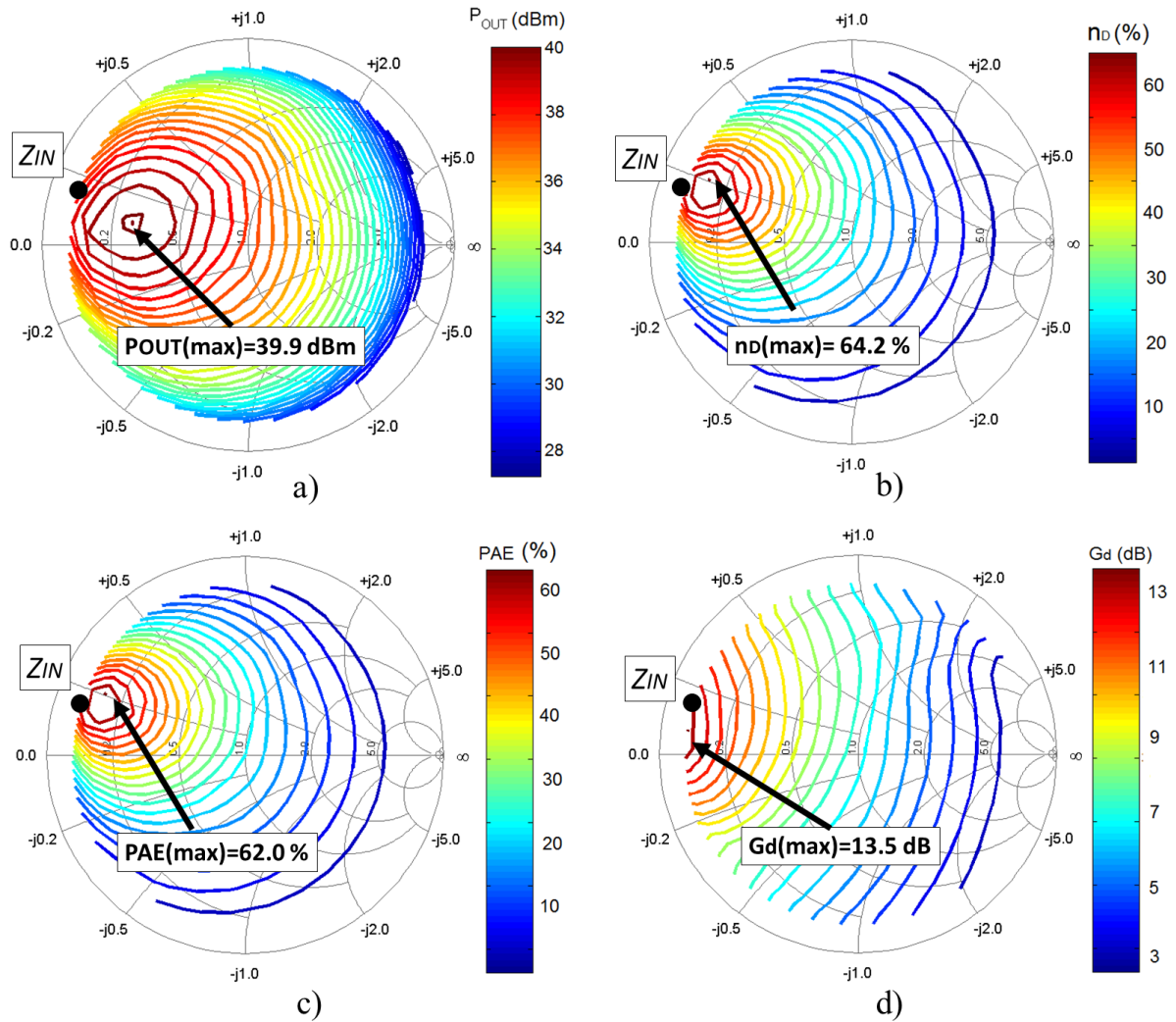


Figure 49. Measured LP contours of constant: a) output power, b) drain efficiency, c) power added efficiency and d) large-signal gain of the transistor used as DUT ($V_{GS} = -2.6$ V; $V_{DS} = 28$ V).

the impedance loading the measurement ports is identical to Z_0) and not under high Γ_{LD} conditions.

Note that G_p may be calculated either from (188) using information provided by the relative calibration (vector measurements) or as the ratio P_{OUT}/P_{IN} from (196)-(197) using information provided by the power calibration (power measurements). To be consistent, both results have to be identical; Figure 48d shows the high correlation between these results.

Once the system is accurately calibrated, a set of impedances distributed along the Smith chart were synthesized using the LP measurement setup depicted in Figure 45 and the large-signal behavior of the DUT ($V_{GS} = -2.6$ V; $V_{DS} = 28$ V) was measured. Measured LP

contours of constant output power (P_{OUT}), drain efficiency (η_D), power added efficiency (PAE) and large-signal gain (G_d) are shown in Figure 49. The location in the Smith chart of the calculated input impedance Z_{IN} is also shown.

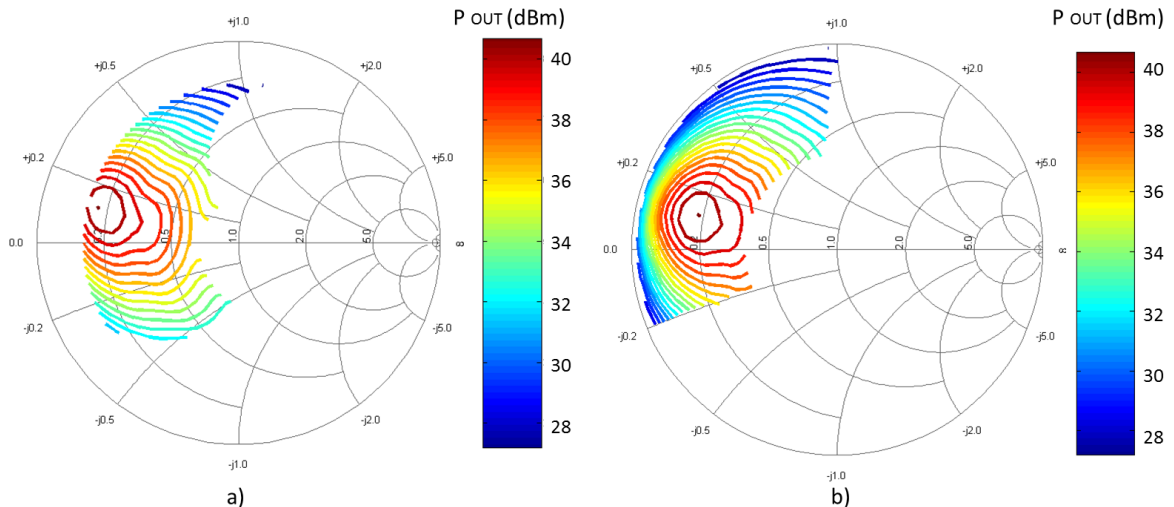


Figure 50. Measured LP contours of constant output power using: a) a passive load-pull system and b) using an active load-pull system of the transistor used as DUT ($V_{GS} = -2.6$ V; $V_{DS} = 28$ V).

Note that the impedances for maximum P_{OUT} , η_D , PAE and G_d belong to a set of load impedance values synthesized using the passive tuner. Therefore, the use of an active LP approach is not strictly required to characterize this DUT at this frequency. Figure 50 shows a set of LP contours of constant output power obtained using a passive LP system shown in Figure 45 and those obtained using the active closed-loop LP system shown in Figure 46. For the transistor used as DUT, the use of an active LP system is not mandatory since those impedances generated by the active system which cannot be generated using the passive system cover an area of the Smith chart that gives not relevant information in the measurement of the contours of constant P_{OUT} .

6.2.2 Large-signal gain under optimal loading condition

An important parameter to consider in the large-signal characterization of a power transistor is its large-signal gain under optimal loading condition, which is a complex quantity. The information provided by the magnitude of the large-signal gain is useful to identify the

power level at which the transistor is operating in its nonlinear regime through its 1 dB compression point [Cripps (2006)]. The angle of the large-signal gain gives an insight into the phase distortion of the device as a function of the input power. Magnitude and angle of the large-signal are directly related to the the *AM-AM* and *AM-PM* distortion of the transistor and, as the LP contours of constant P_{OUT} or η_D , are a parameter commonly used to validate non-linear models of power transistors [Zarate-de Landa (2014)].

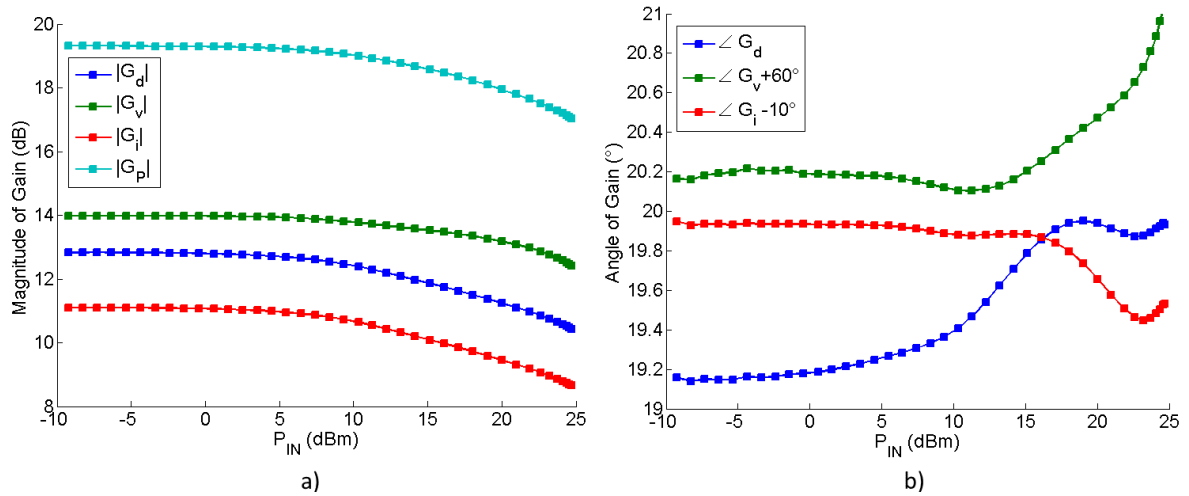


Figure 51. Measured large-signal gain as a function of input power of the transistor used as DUT ($V_{GS} = -2.6$ V; $V_{DS} = 28$ V): a) magnitude, b) angle.

In Figure 51a the magnitude of the voltage gain, current gain, power gain and gain expressed as the ratio of transmitted to incident waves, as a function of the input power are shown. It is noted that the $|G_p|$ is greater than $|G_i|$, $|G_v|$ and $|G_d|$. This is an expected result since these quantities are related as

$$|G_P| = |G_i|^2 \frac{Re(Z_{LD})}{Re(Z_{IN})} = |G_v|^2 \frac{Re(Z_{IN})}{Re(Z_{LD})} = |G_d|^2 \frac{(1 - |\Gamma_{LD}|^2)}{(1 - |\Gamma_{IN}|^2)}, \quad (210)$$

and, as shown in Figure 49, $Re(Z_{IN}) < Re(Z_{LD})$ and $|\Gamma_{IN}| > |\Gamma_{LD}|$. The angle of G_v , G_i and G_d is shown in Figure 51b; this information is useful when two or more devices are required to be combined with a determined phase relationship (e.g., Doherty amplifiers, outphasing amplifiers, balanced amplifiers).

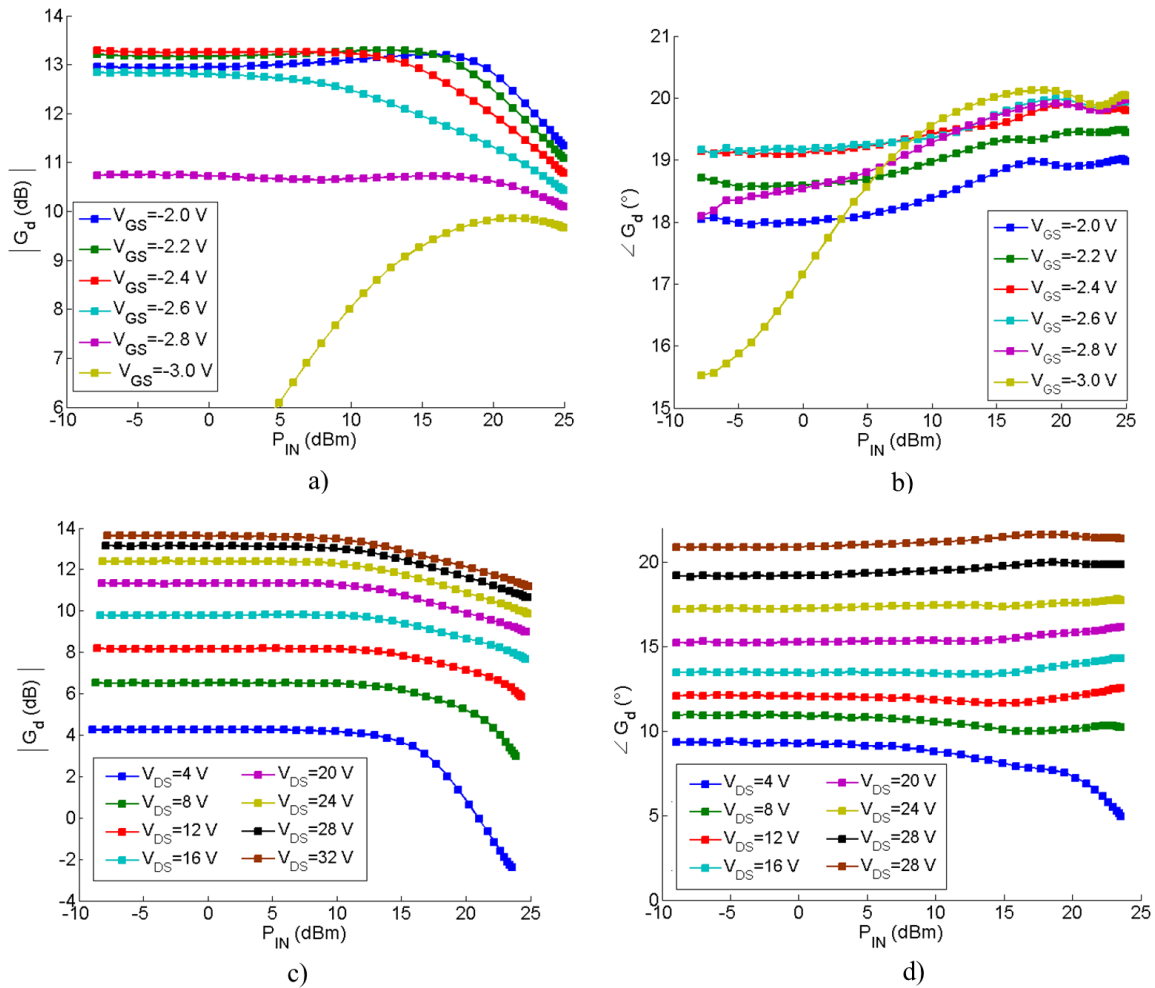


Figure 52. Measured large-signal gain for different bias conditions: a) magnitude and b) angle of $|G_d|$ as a function of V_{GS} , a) magnitude and b) angle of $|G_d|$ as a function of V_{DS} .

As the optimum load impedance, the large-signal gain of a power transistor is a bias-dependent quantity. Figure 52 shows the magnitude and angle of G_d for different bias conditions. The dependence of G_d on the gate-source voltage (V_{GS}) is depicted in Figure 52a-b and its dependence on the drain-source voltage (V_{DS}) is shown in Figure 52c-d. The information provided by these measurements may be useful whether two or more devices operating under different bias conditions are required to be combined.

Whereas the dependence of the magnitude and angle of G_d on V_{DS} and P_{IN} obey to a well-defined behavior (i.e., the greater V_{DS} , the greater the value of $|G_d|$ and $\angle G_d$), the dependence of the magnitude and phase of G_d on V_{GS} and P_{IN} seems obey to a more complex behavior. The large-signal gain is a technology-dependent parameter; modeling the large-signal gain of

GaN-based devices by means of behavioral models [Wood (2014)] is a very complex task and is still an open research topic.

6.3 Evaluation of the impact of calibration techniques on the LP characterization of microwave transistors

In this section the impact of different calibration techniques (TRL, TRM, TRRM, LZZ) on the LP characterization of the microwave power transistor used as DUT in the preceding section is evaluated.

6.3.1 The impact of assuming the line/load used as calibration structures as a non-reflecting element

According to the analysis presented in section 5, in order to determine the most important parameters in LP, it is required to use three different types of data:

1. Uncalibrated ratios of traveling waves and absolute magnitude of traveling waves, which are measured with high degree of accuracy by using a VR.
2. Seven calibration terms partially describing the two-port networks connecting the DUT ports to the VR ports. These seven terms are obtained from the measurement of the calibration structures of a determined calibration procedure and, as shown in chapter 3, their calculation requires minimal knowledge of the electrical characteristics of the calibration structures.
3. The impedance of one of the calibration structures used in a determined calibration technique: the characteristic impedance of a transmission line in the TRL and LZZ, the impedance of a pair of loads in the TRM, or the impedance of a one-port load in the TRRM. These parameters which depend on the type of calibration structures,

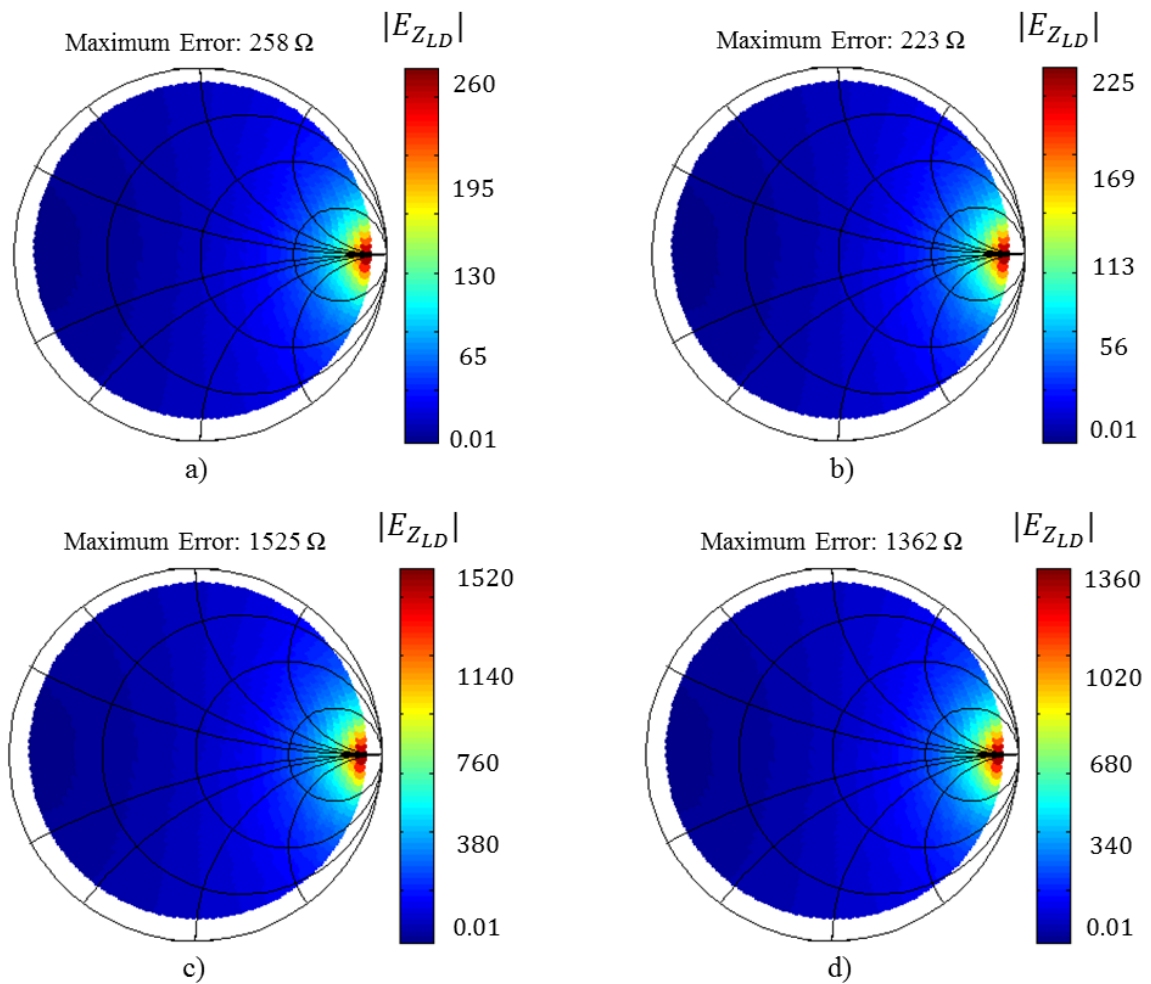


Figure 53. Error in the calculation of Z_{LD} due to assuming the line/load used as calibration structure in the a) TRL, b) LZZ, c) TRM and d) TRRM calibrations as non-reflecting elements.

are generally frequency-dependent and their values have to be known prior to the calibration.

In this order, from the author's perspective, the most important source of errors in the LP characterization of a transistor are errors in the knowledge of the impedance of the transmission line/loads used in the calibration procedure. Let define a metric $E_{Z_{LD}}$ to evaluate the impact of knowing these parameters on the determination of the LP contours. $E_{Z_{LD}}$ is defined as

$$E_{Z_{LD}} = Z_{LD}^{act} - Z_{LD}^{err}, \quad (211)$$

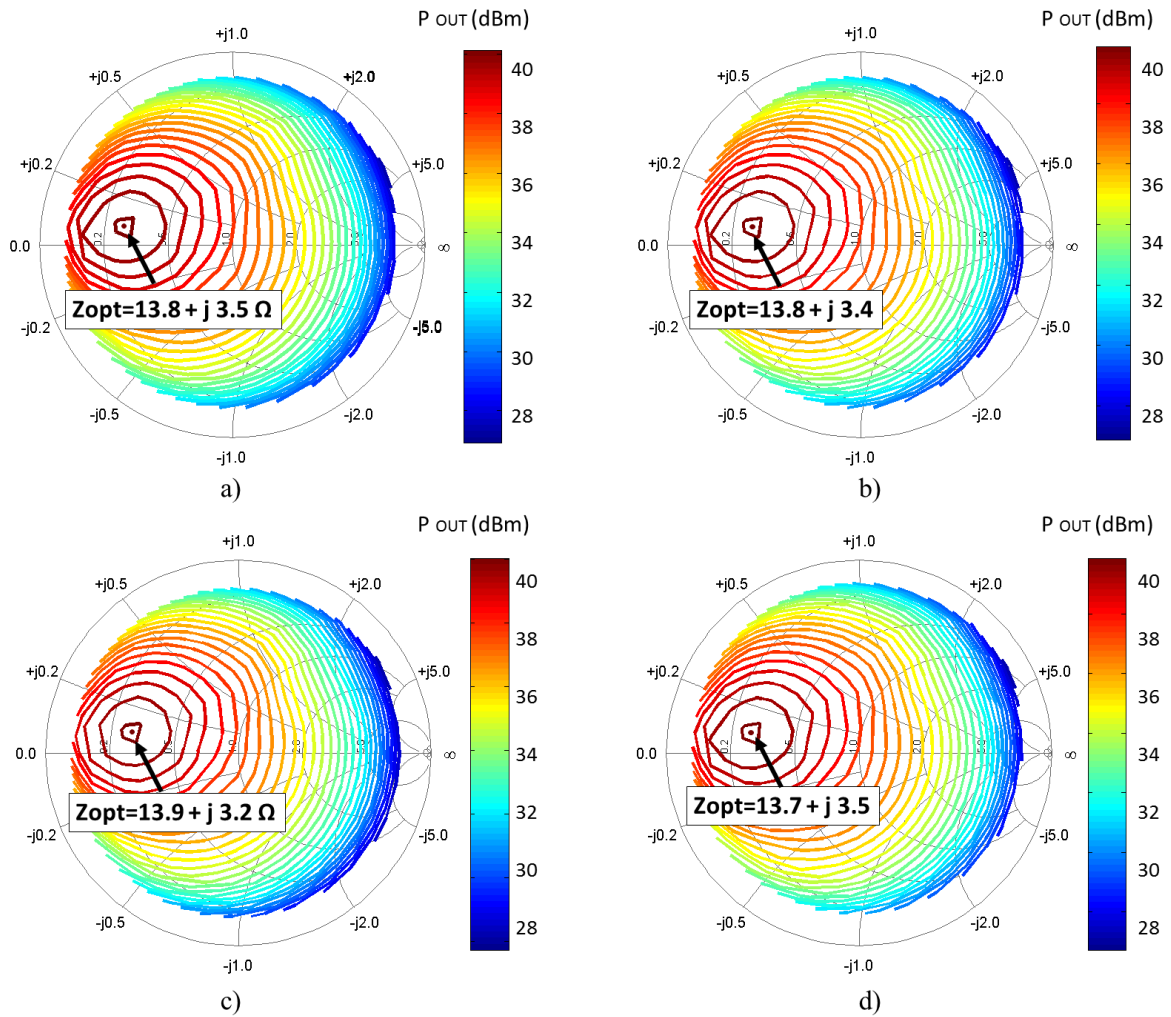


Figure 54. Measured LP contours of constant: a) output power, b) drain efficiency, c) power added efficiency and d) large-signal gain of the transistor used as DUT ($V_{GS} = -2.6$ V; $V_{DS} = 28$ V).

where Z_{LD}^{act} is the load impedance Z_{LD} calculated using the actual value of the impedance of the line/loads used in a calibration technique and Z_{LD}^{err} is the value of Z_{LD} calculated using an erroneous value of these parameters.

In the TRL and LZZ techniques the same 8 mm length transmission line of characteristic impedance $Z_L = 52.5 - j1.5 \Omega$ was used to determine the value of Z_{LD}^{act} . In the TRM and TRRM techniques the same load of impedance $Z_M = 53.5 + j14.0 \Omega$ was used to determine Z_{LD}^{act} ; in the TRM, the load is assumed as symmetrical.

In all the cases Z_{LD}^{err} was considered as the value of Z_{LD} calculated by assuming that the impedance of the line/loads used as calibration structures is purely real and identical to Z_0 .

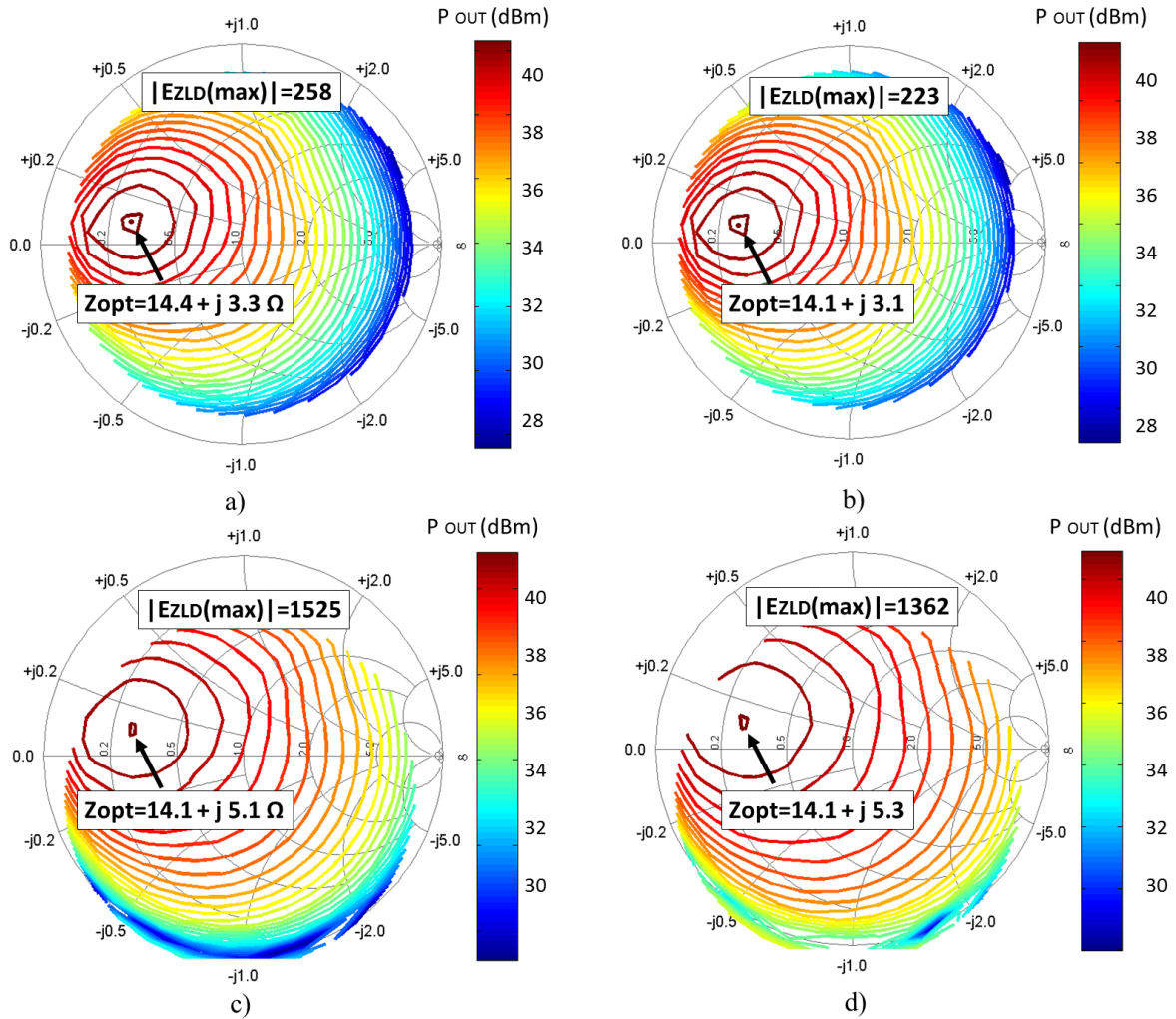


Figure 55. Measured LP contours of constant: a) output power, b) drain efficiency, c) power added efficiency and d) large-signal gain of the transistor used as DUT ($V_{GS} = -2.6$ V; $V_{DS} = 28$ V).

Figure 53 shows the absolute value of the calculated $E_{Z_{LD}}$ as a function of Z_{LD} for different calibration techniques.

An important result to note is the fact that $|E_{Z_{LD}}|$ in all the cases is less in the left-hand side of the Smith chart; this is expected since the left-hand side of the Smith chart covers impedances of lower value than those in the right-hand side of the Smith chart. Power transistors manage high output current levels; therefore, according to the theory presented in chapter 4 power transistors require low output impedance values for optimum operation; it implies that errors in the calculation of the LP contours will be less in the vicinity of the optimum load impedance Z_{opt} than in the area of the Smith chart far from this impedance.

As can be observed in Figure 53, $|E_{Z_{LD}}|$ is greater in the TRM and TRRM. It occurs due to the fact that the difference between Z_M and Z_0 is greater than the difference between Z_L and Z_0 . It suggests that, for these calibration structures, assuming the line as a non-reflecting element introduces less errors in the calculation of Z_{LD} than assuming Z_M as a non-reflecting element. The case in which the impedance of the lines used as calibration structures greatly differs from Z_0 is further analyzed in section 6.3.3.

Figure 54 shows the measured LP contours of constant output power calculated using the TRL, TRM, TRRM and LZZ techniques in the calibration procedure. In the TRL and LZZ techniques, the actual value of Z_L was used; meanwhile, in the TRM and TRRM techniques the actual value of Z_M was used. High correlation between the results obtained using all the aforementioned calibration techniques may be observed.

Figure 55 shows the measured LP contours of constant P_{OUT} calculated by assuming Z_L and Z_M as non-reflecting elements in the calibration procedure. As predicted, errors due to assuming the value of $Z_M = Z_0$ are greater than errors due to assuming the value of $Z_L = Z_0$; moreover, it can be observed that the calculation of Z_{opt} is not significantly affected in all the cases, due to the fact that Z_{opt} is located in the left-hand side of the Smith chart.

In Figure 56 the large-signal gain G_D calculated using different calibration techniques is presented. It may be observed that, provided that the correct value of the impedance of the line (for TRL and LZZ) and load (for the TRM and TRRM) are used in the calibration, the results obtained for all the calibration techniques are very similar. The results obtained when the lines and loads used in the calibration are assumed as non reflecting elements are also shown; the most significative impact of this assumption is observed in the calculation of $|G_D|$ using the TRM and TRRM techniques.

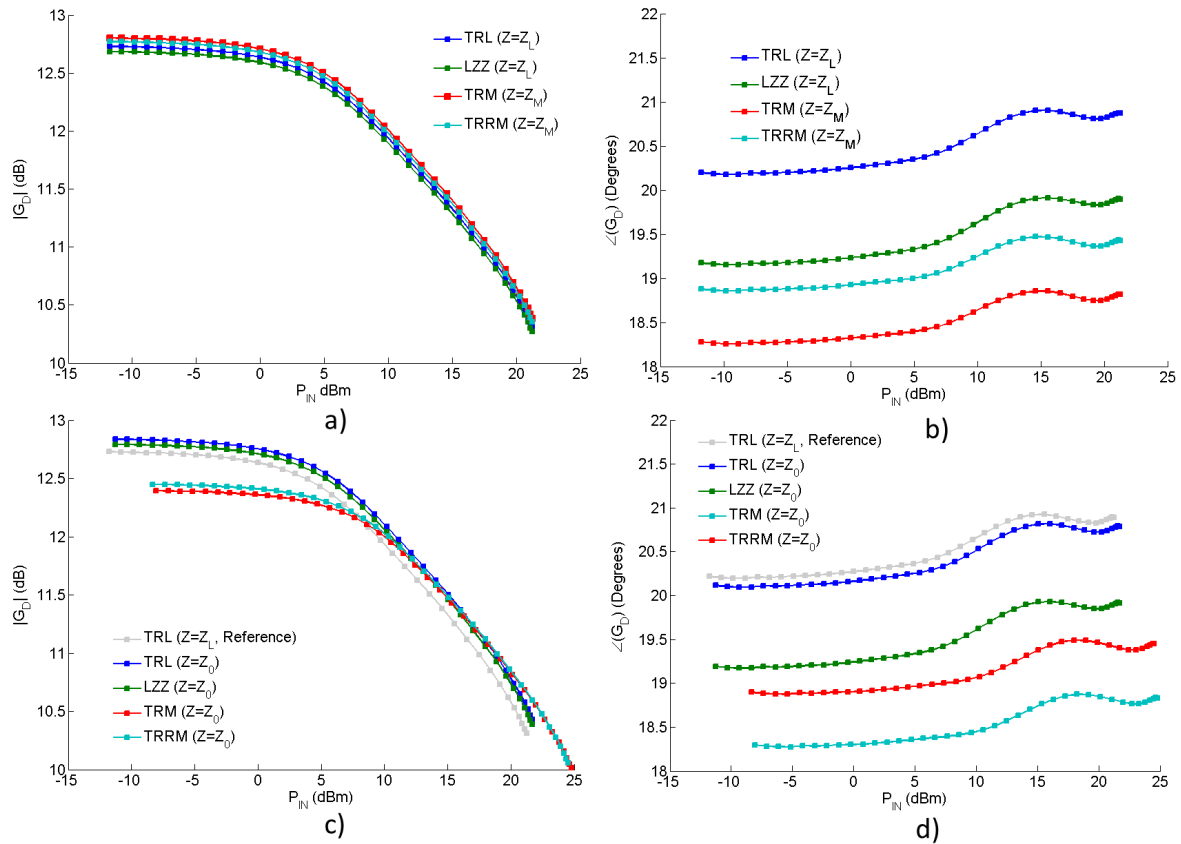


Figure 56. Measured large signal gain calculated using different calibration techniques: a) magnitude, b) phase when the correct values of Z_L and Z_M are used in the calibration. The results obtained when Z_L and Z_M are assumed as non reflecting elements are shown in c) magnitude and d) phase.

6.3.2 The impact of assuming the load used in the TRM calibration as a symmetrical element

In this section the generalized theory of the TRM calibration presented in section 3.6 is used in the calibration of a LP measurement system [(Pulido-Gaytan, 2015b)]. The DUT and test fixture used in the preceding section were used to measure LP contours of constant output power.

The LP measurement system depicted in Figure 45 was calibrated using the TRM technique implemented using as calibration structures: a zero-length thru, a symmetrical highly reflecting load and an asymmetrical load as *match* standard, as shown in Figure 57. The asymmetrical load consist of a load of 50Ω DC resistance at port one and a load of 25Ω DC resistance (two 50Ω loads connected in parallel) at port two; these loads were pre-

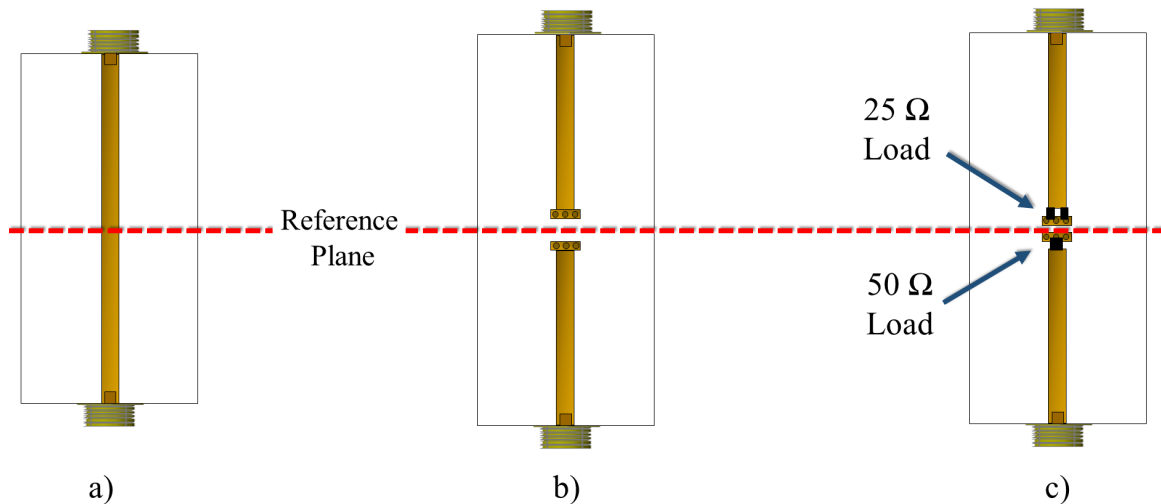


Figure 57. Microstrip structures used to implement the TRM calibration with asymmetrical loads: a) thru, b) reflecting load (short circuit) and c) asymmetrical load. The dotted line indicates that the calibration reference plane is located at the center of the thru.

characterized and their impedance were found to be $Z_{M1} = 53.2 + j13.5$ and $Z_{M2} = 24.2 + j9.8$, respectively, at 3.5 GHz.

Figure 58a shows the LP contours of constant P_{OUT} calculated using the TRL technique (used as reference), whereas the LP contours calculated using the TRM technique taking into account both the asymmetry and frequency-dependence of the loads used as *match* calibration structure (i.e., using $Z_A = Z_{M1}$, $Z_B = Z_{M2}$ in the calibration procedure) are shown in Figure 58b. High correlation between these two results may be observed; thereby, validating the accuracy of the proposed procedure.

Then, in order to show the impact of neglecting the asymmetry and/or frequency-dependence of the load used as calibration structure, the following cases were considered [(Pulido-Gaytan, 2015b)]:

1. First the frequency-dependence of the loads used as *match* standard is neglected, whereas its asymmetry is still taken into account. Figure 59b shows the LP contours of constant P_{OUT} calculated by using the DC resistance of the asymmetrical loads in the calibration procedure ($Z_A = 50$, $Z_B = 25$). These contours greatly differ from the contours shown in Figure 59a, which were calculated by using the actual value of these

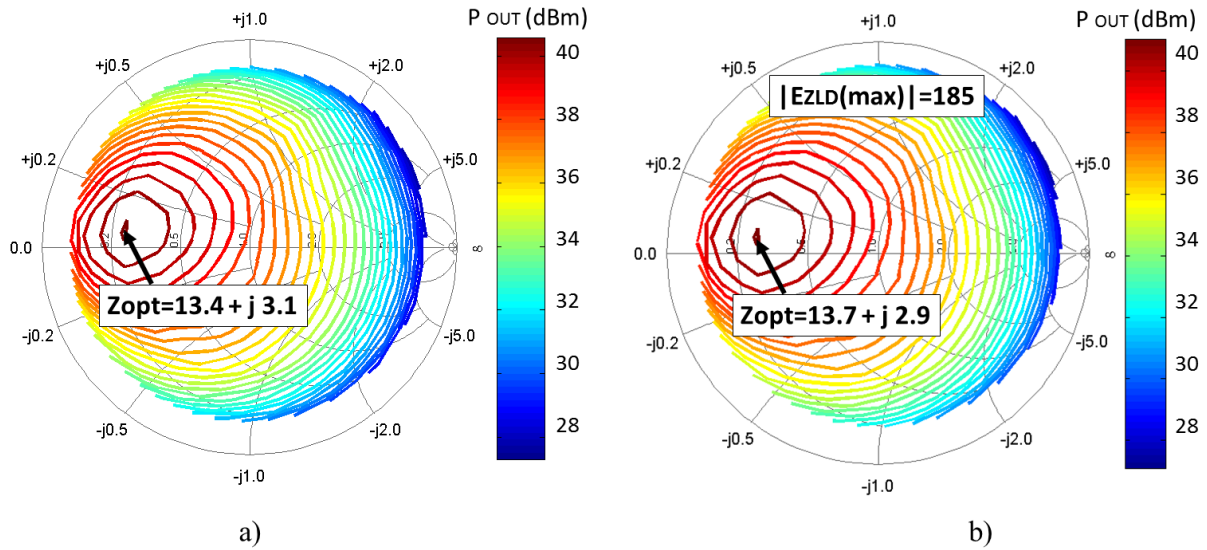


Figure 58. Contours of constant output power calculated using in the relative calibration: a) TRL (used as a reference), b) TRM $Z_A = Z_{M1}$, $Z_B = Z_{M2}$.

loads in the calibration procedure ($Z_A = Z_{M1}$, $Z_B = Z_{M2}$).

2. Then, the impact of neglecting the asymmetry of the loads is evaluated. LP contours of constant P_{OUT} calculated by assuming that the load used as calibration structure is symmetrical and of impedance identical to the load connected at port one ($Z_A = Z_B = Z_{M1}$) are shown in Figure 59c. Meanwhile, the contours calculated by assuming that the impedance of both loads is identical to the load connected at port two ($Z_A = Z_B = Z_{M2}$) are shown in Figure 59e.
3. Finally, both symmetry and frequency-dependence of the loads used as match standard were neglected. Figure 59d and Figure 59f show the LP contours calculated by using in the relative calibration the DC resistance of the load connected at port one ($Z_A = Z_B = 50$) and the DC resistance of the loads connected at port two ($Z_A = Z_B = 25$), respectively.

From the set of results shown in Figure 59 it can be noted that neglecting the asymmetry of the load used as match standard causes a contraction in the size of the impedance map. This contraction is more evident when the loads are assumed to be identical to the load connected at port two than when they are assumed as identical to the load connected at port

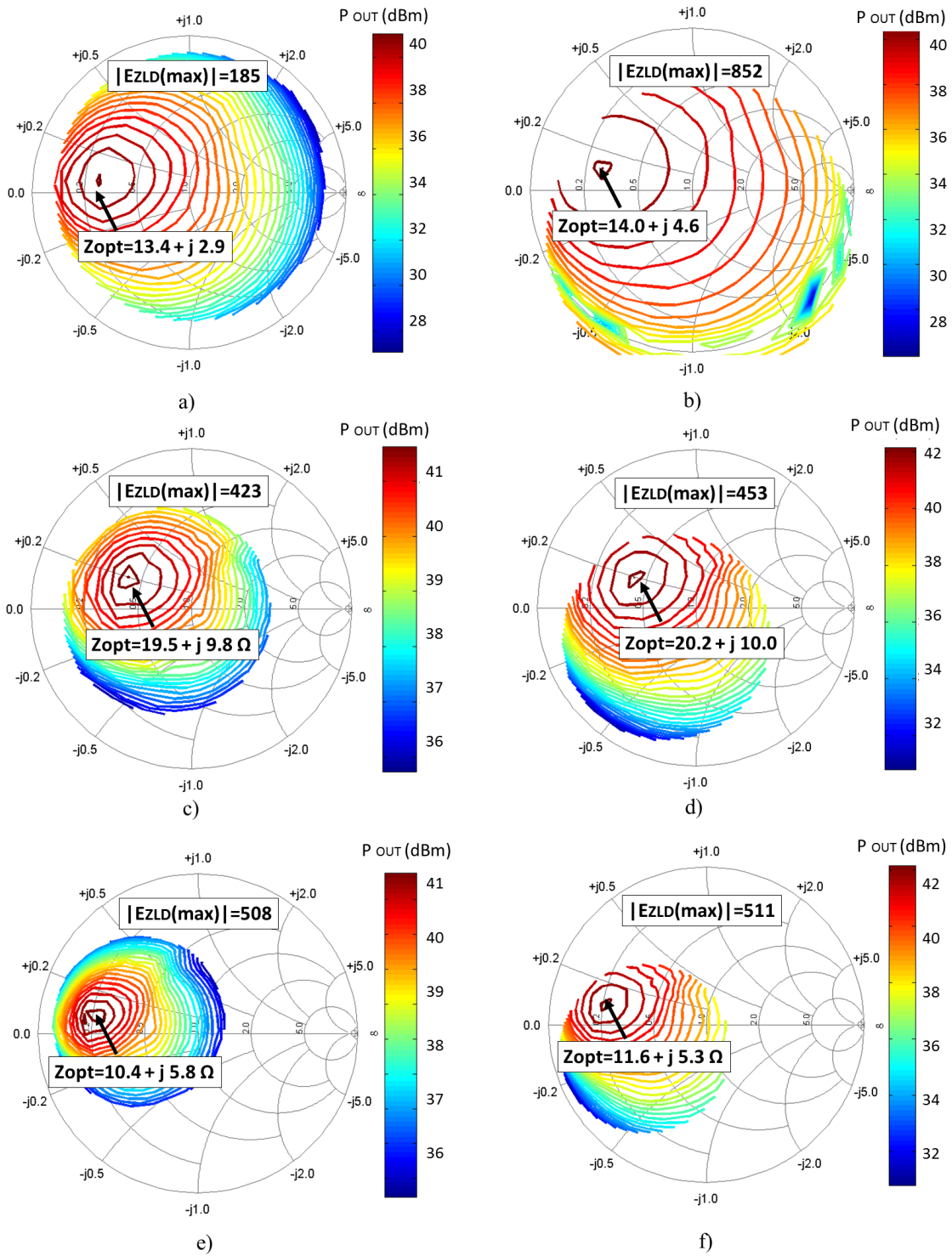


Figure 59. Contours of constant output power calculated using in the relative calibration: a) TRM $Z_A = Z_{M1}$, $Z_B = Z_{M2}$, b) TRM $Z_A = 50 \Omega$, $Z_B = 25 \Omega$, c) TRM $Z_A = Z_B = Z_{M1}$, d) TRM $Z_A = Z_B = 50 \Omega$, e) TRM $Z_A = Z_B = Z_{M2}$, f) TRM $Z_A = Z_B = 25 \Omega$.

one in the TRM. This can be justified by inspection of (194), which after some algebra can be expressed as

$$Z_{LD} = Z_A \cdot \frac{k - \frac{Z_B}{Z_A}}{k + 1}, \quad (212)$$

where $k = (\overline{C_Y Z_2^U} - 1) / (\overline{A_Y Z_2^U} - \overline{B_Y})$. In this expression it may be noted that whether the ratio $\frac{Z_B}{Z_A} = \frac{Z_{M2}}{Z_{M1}}$ is assumed as identical to the unity, the value of Z_{LD} is underestimated, provided that $Z_{M1} > Z_{M2}$ in this example. Moreover, note that this impedance map is further reduced when the load is assumed as symmetrical and of impedance identical to the load connected at port two. This is justified by inspection of (212), where it may be observed that Z_{LD} is scaled by the value of Z_A .

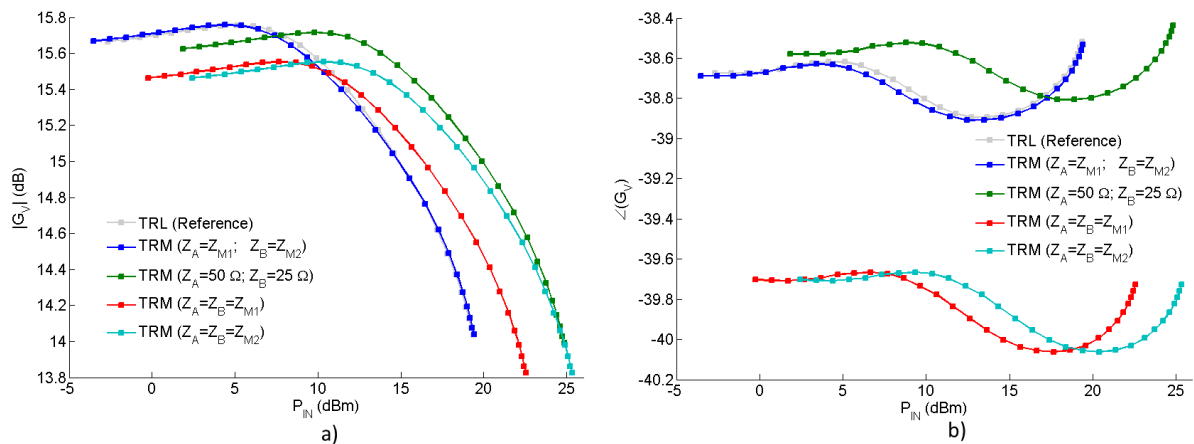


Figure 60. Large-signal voltage gain of the transistor used as DUT calculated using the TRM technique ($V_{GS} = -2.6$ V; $V_{DS} = 28$ V): a) magnitude and b) angle.

In Figure 60 the voltage gain G_v calculated using the TRM calibration technique is presented. It may be observed that, provided that the correct value of the impedance of the loads used as match standards are known, the results obtained are comparable to those obtained using the reference TRL technique. The results obtained when the asymmetry and/or frequency-dependence of the impedance of these structures are not taken into account are also shown.

6.3.3 The impact of knowing the impedance of the line used in the TRL on the LP characterization of power transistors

Thus far, the TRL technique implemented using lines of impedance close to Z_0 has been used in the LP characterization of packaged transistors. The width of the transmission lines used to accommodate power transistors varies according to the transistor power capabilities; the higher the power capabilities, the lower the line's impedance. Test fixtures used to mount those devices utilize wideband impedance transformers to adapt low impedance lines to non-reflecting lines [Aaen (2000); Reynoso-Hernandez (2013)]. As a consequence, the impedance of the lines used as calibration elements in a TRL calibration also vary according to the transistor's power capabilities.

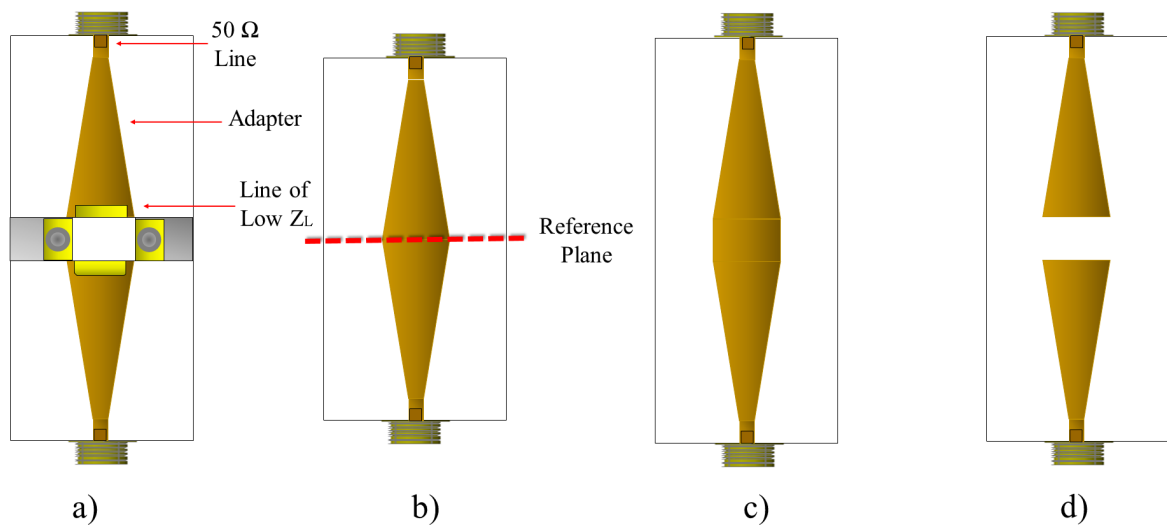


Figure 61. Microstrip structures used to implement the TRL calibration with lines of low impedance: a) DUT in test fixture, b) thru, c) line and d) symmetrical reflecting load (Open circuit). The dotted line indicates that the calibration reference plane is located at the center of the thru.

In this section, the impact of knowing the impedance of the lines used in the TRL calibration on the LP characterization of power transistors is assessed. Relevant parameters, such as input impedance, load impedance and large-signal gain are considered.

The LP measurement system depicted in Figure 45 was used to characterize a 45 W GaN-HEMT packaged transistor, *Cree, Inc.* CGH40045F [Cree (2015b)], at 3.0 GHz. The DUT was mounted in a test fixture comprising wideband impedance transformers that adapt 10 Ω

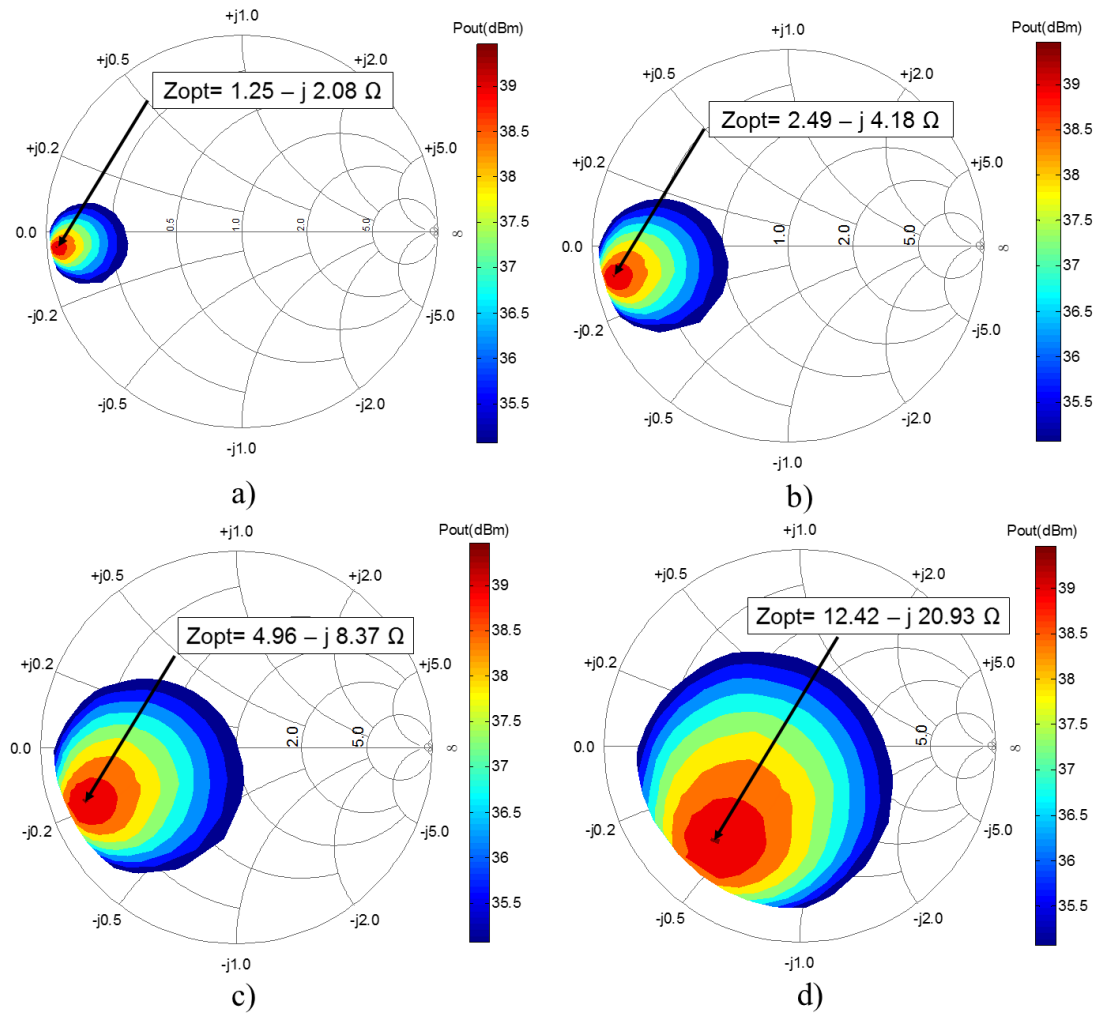


Figure 62. Contours of constant output power of a CGH40045 power transistor ($V_{DS}=20$ V, $V_{GS}=-2.5$ V) using a) $Z_L = 5 \hat{\Gamma}$, b) $Z_L = 10 \hat{\Gamma}$, c) $Z_L = 20 \hat{\Gamma}$, d) $Z_L = 50 \hat{\Gamma}$ in the calibration procedure.

transmission lines to 50Ω transmission lines, as depicted in Figure 61a. The measurement setup was calibrated using the TRL procedure and the output power LP contours of the DUT ($V_{DS}=20$ V; $V_{GS}=-2.5$ V) were measured. The TRL calibration was implemented using as calibration structures a zero-length thru, a symmetrical reflecting load (open circuit) and a transmission line of characteristic impedance close to 10Ω , as depicted in Figure 61b-d. In order to demonstrate in a simple manner the impact of knowing the line's impedance on the LP characterization of the DUT, the actual value of Z_L was assumed to be real and identical to 10Ω .

Figure 62 shows the output power LP contours calculated by using the actual value of Z_L (10Ω) in the calibration procedure along with the contours calculated using three erroneous

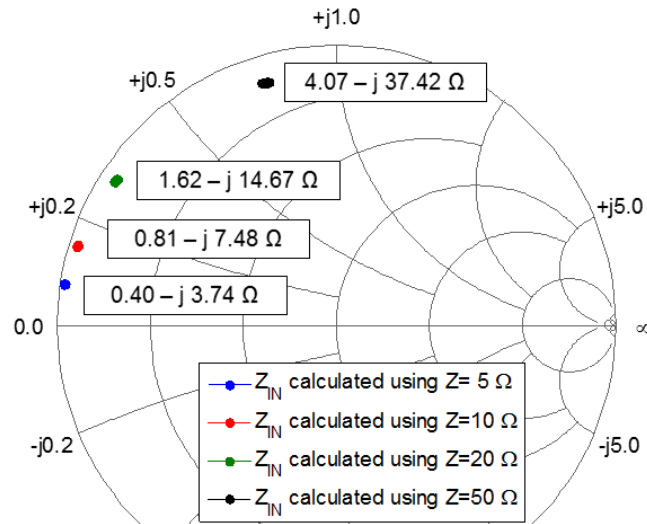


Figure 63. Input impedance of the DUT calculated using different values of Z in the calibration. The load impedance was fixed at $Z_{LD}=Z_{opt}$.

values of Z_L . It may be observed that knowing Z_L is very important in the calculation of the load impedance; an error in the knowledge of Z_L represents a proportional error in the calculation of Z_{LD} . In this order, the optimum impedance (Z_{opt}) is underestimated or overestimated, depending on the error in the value of Z_L . This parameter is very important in the design of PAs since calculating erroneously the value of (Z_{opt}) will result in suboptimum behavior of the transistor in a PA.

Then, the load impedance is fixed at Z_{opt} and the input impedance was measured. Figure 63 shows the input impedance calculated by using the actual value of Z_L in the calibration procedure along with the input impedance calculated using three erroneous values of Z_L . It can be observed that the calculated value of Z_{IN} varies proportionally with the value used for Z_L in the calibration procedure. Z_{IN} is of paramount importance in the design of PAs since it provides PA designers with the information necessary to appropriately design the input matching networks.

Finally, the impact of an error in the knowledge of Z_L in the calculation of the large-signal gain was investigated. Since the calculation of the voltage gain and the current gain is not dependent on Z_L , the gain expressed as the ratio of the transmitted to the incident waves G_d was considered.

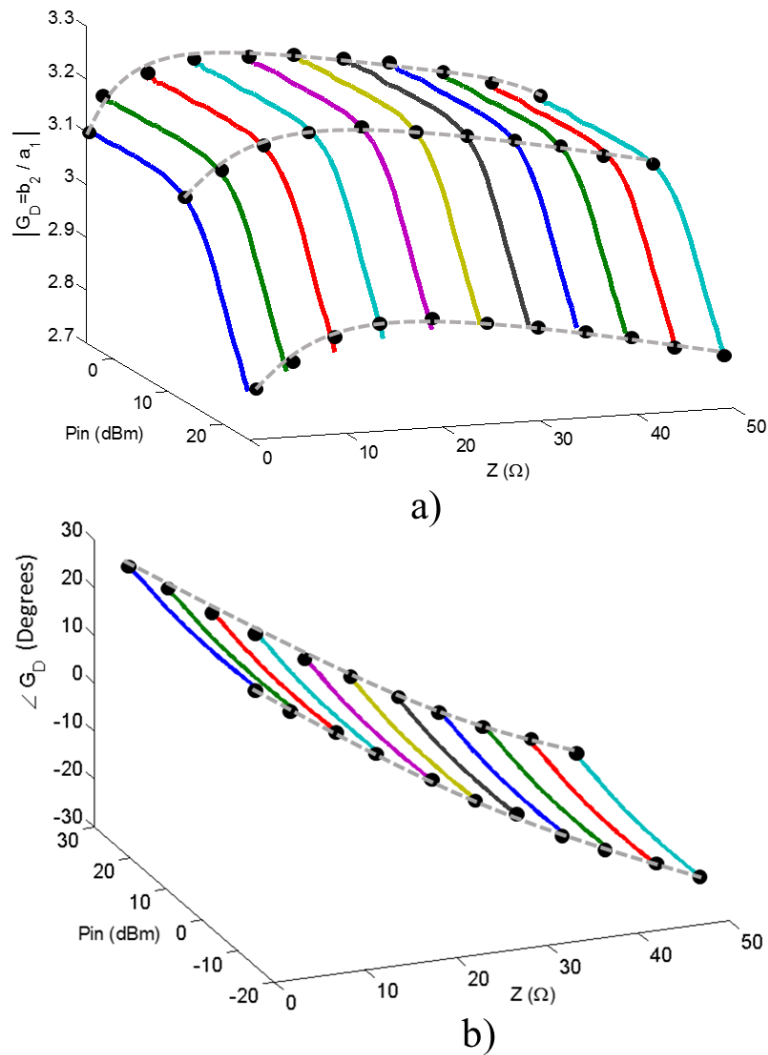


Figure 64. Gain of the DUT calculated using different values of Z in the calibration: a) magnitude and b) phase. The load impedance was fixed at $Z_{LD} = Z_{opt}$.

As presented in section 5, the calculation of G_d depends on Z_L through its dependence on Z_{IN} and Z_{LD} . It does not vary proportionally with Z_L as in the case of Z_{IN} and Z_{LD} . Figure 64 shows the magnitude and phase of G_d calculated using different values of Z_L in the calibration procedure. It may be observed that the calculation of $|G_d|$ does not vary significantly when the value of Z_L is varied. Even if the value of Z_L is considered as 1Ω or as 50Ω , the calculation of $|G_d|$ varies less than 10 % from the $|G_d|$ calculated using the actual value of Z_L . The calculation of the phase of G_d , on the other hand, is greatly affected by errors in the knowledge of the Z_L .

6.4 Design of a power amplifier based on LP measurements

In order to show the usefulness of LP measurements in the design of RF PAs, in this section the design of a class AB power amplifier (PA) using information provided by LP measurements is presented. The same transistor used in the preceding sections (Cree's CGH40010) was used in the design of the PA. LP contours of constant output power and LP contours of constant drain efficiency, as well as the measurement of the input impedance of the transistor, were used as the basis for the PA design.

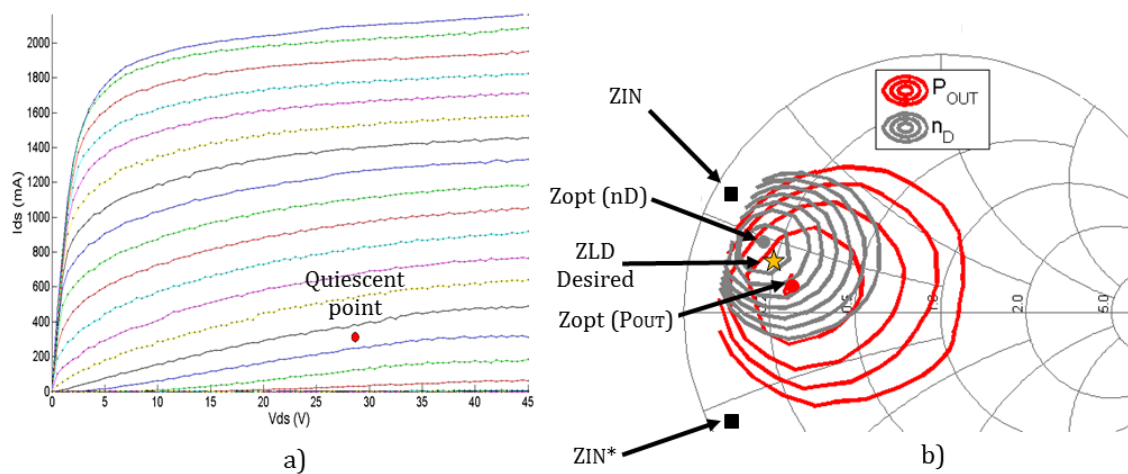


Figure 65. a) I-V curves of the transistor used in the design of the power amplifier. b) LP contours of constant output power and LP contours of constant drain efficiency.

First, a quiescent bias point corresponding to a class AB bias condition ($V_{DS} = 28$ V; $I_{DS} = 200$ mA) was chosen using information provided by the I-V curves of the transistor (Figure 65a). Then, LP contours of constant output power and LP contours of constant drain efficiency were measured for this biasing condition. The load impedance for maximum output power (40.5 dBm) was found to be $Z_{opt(P_{OUT})} = 12.7 + j2.7 \Omega$. Meanwhile, the load impedance for maximum drain efficiency (54 %) was found to be $Z_{opt(\eta_D)} = 7.0 + j9.0 \Omega$. An impedance located between these two impedances $Z_{LD(Desired)} = 9.7 + j5.7 \Omega$, for which an output power of 40.0 dBm and an efficiency of 52 % was achieved, was chosen as the target load impedance. The input impedance for this loading and biasing condition was measured and its value was found to be $Z_{IN} = 2.01 + j11.02 \Omega$.

Input and output matching networks, as long as a biasing network, were designed in the same substrate used to design the calibration structures used in the preceding sections of this chapter (RO4003 from Rogers Corporation).

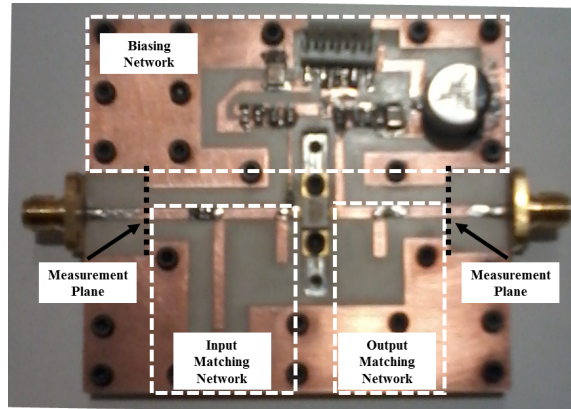


Figure 66. Fabricated power amplifier.

The final amplifier is intended to operate under $50\ \Omega$ input and output loading conditions. In this order, the output matching network was designed to transform a $50\ \Omega$ load into the target impedance $Z_{LD(Desired)}$. Meanwhile, in order to provide maximum power transfer from the RF source to the input of the transistor, the input matching network was designed to transform a $50\ \Omega$ load into the conjugate of the input impedance Z_{IN}^* (conjugate matching).

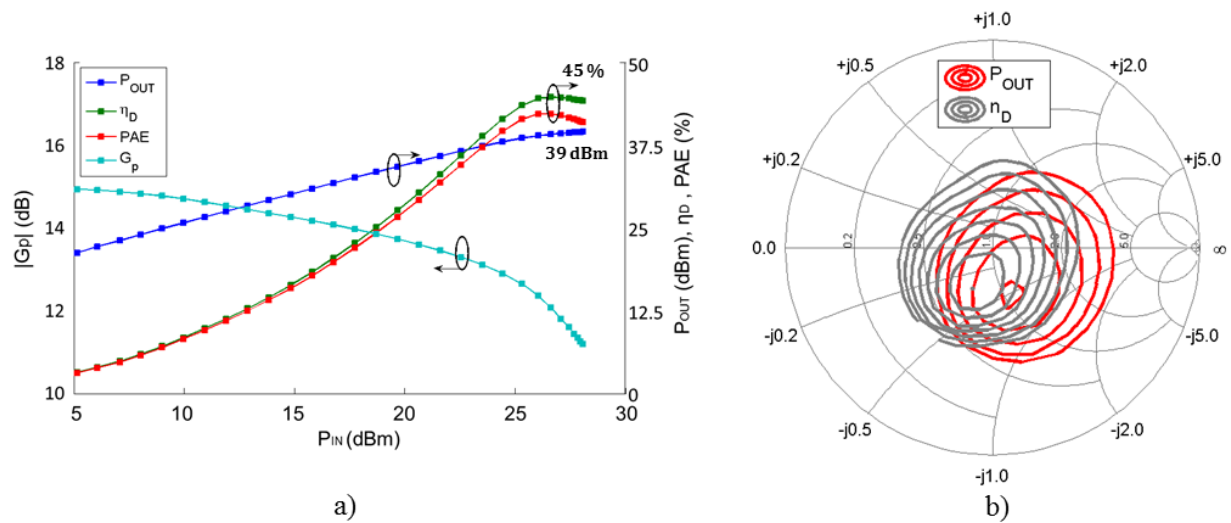


Figure 67. a) Measured performance of the fabricated PA. b) LP contours of constant output power and LP contours of constant drain efficiency of the fabricated PA

In order to measure the performance of the designed PA, the final PA structure was

embedded in coaxial-to-microstrip transitions and $50\ \Omega$ transmission lines as shown in Figure 66. Figure 67a shows the measured performance of the fabricated PA. In order to compare the measured PA performance to the expected PA performance, the reference plane of these measurements was set at the plane of the matching networks, not to the coaxial connectors (Figure 66).

As may be observed, the fabricated PA delivers 39 dBm of output power, 1 dBm of power less than the expected level. An efficiency of 45 %, which is 7 % less than the expected efficiency was also measured. These differences may be mainly attributed to errors in the design and/or fabrication of the matching networks. Load-pull contours of constant output power and constant drain efficiency of the final PA were also measured in order to verify this; in Figure 67b it may be observed that the impedance meeting the best trade-off between output power and drain efficiency slightly differs from $50\ \Omega$.

7. Conclusions and Future work

In this dissertation the impact of different VNA calibration techniques on the LP characterization of microwave power transistors was studied. The most commonly used calibration techniques in both industry and academy, TRL, TRM and TRRM were considered. The line, offset-open, offset-short calibration technique, which one of the contributions of this dissertation, was also considered.

Using the ABCD-parameters formalism, a complete analysis and mathematical formulation of all of the aforementioned calibration techniques was developed. Since the ABCD-parameters are not defined as a function of a reference impedance, it was demonstrated that the unique impedance to which the measurement results should be referred is the measurement system impedance ($Z_0 = 50 \Omega$). Using this mathematical formulation, calibration procedures for all of the aforementioned calibration techniques allowing the use of calibration structures of arbitrary impedance were developed.

The impact of accurately knowing the impedance of one of the calibration structures used in each calibration technique was evaluated. In the case of the TRL and LZZ techniques the impact of knowing the characteristic impedance of the transmission line used as calibration structure was considered. Meanwhile, in the case of the TRM and TRRM techniques, the impact of knowing the impedance of the load used as calibration structure was evaluated. It was mathematically demonstrated that errors in the knowledge of the impedance of the line/load used as calibration structure directly impact the calculation of some parameters of interest in LP, such as the impedance at the input of the DUT, the impedance loading the DUT and the DUT's large-signal gain. Regarding the large-signal gain, it was mathematically demonstrated that the calculation of the voltage gain and current gain do not depend on the knowledge of the line/load used as calibration structure in a determined calibration technique; thus, showing for the first time that these parameters are less sensitive to calibration errors.

Meanwhile, the gain defined the ratio of the transmitted to incident traveling waves does depend on the knowledge of the impedance of a calibration structure.

For most of the experiments shown in this investigation, a 10 W packaged transistor was used. This device was mounted in a test fixture comprising transmission lines of characteristic impedance close to Z_0 and SMA-to-microstrip adapters. For this experiment it was observed that, since the loads used as calibration structures in the TRM and TRRM techniques are more dispersive than the lines used in the TRL and LZZ at microwave frequencies, assuming the loads as non-reflecting elements introduces more errors in the LP characterization of a DUT than assuming the lines as non-reflecting elements.

Transistors capable of managing higher power levels (40 W) were mounted in a test fixture comprising impedance transformers to adapt 50 Ω transmission lines to 10 Ω transmission lines, on which these transistors were mounted. For this kind of devices in which the transmission lines used to calibrate the LP measurement system using the TRL technique are of impedance considerably different than Z_0 , it was shown that errors in the knowledge of the line's impedance are proportional to errors in the calculation of the impedance loading the DUT, and therefore to the determination of the LP contours. When characterizing this kind of devices, assuming the line used in the TRL technique as a non-reflecting element (as in the classical TRL approach) causes an expansion in the calculation of the synthesized impedance map and errors in the calculation of the impedance for optimum operation at the DUT plane are obtained.

The generalized theory of the TRM technique developed in this dissertation allows calibrating a LP measurement system using symmetrical and nonsymmetrical loads of arbitrary impedance. It was demonstrated that assuming the loads used as calibration structures in the TRM technique as symmetrical may cause an expansion or a reduction of the calculated impedance map at the DUT's output plane when these loads are actually symmetrical. Meanwhile, assuming the impedance of these loads as purely real may cause a rotation of the calculated impedance map in those cases in which the loads are of complex impedance.

Future Work

There are a number of applications for LP systems in an RF/microwave research laboratory. The two most important applications for LP systems are the design of power amplifiers and the verification of nonlinear models of microwave transistors.

The LP measurement system of the RF/microwave laboratory of CICESE Research Center is being used for validating the accuracy of nonlinear models of both packaged and on-wafer microwave transistors using both active or passive LP approaches [(Molina-Cesena, 2016)]. A nonlinear model of a power device should predict, among other important quantities, the large-signal gain (magnitude and phase) and the LP contours for a set of bias, frequency and input power conditions.

Regarding power amplifier design, although in this work an example of the design of a power amplifier using LP measurements was presented, the application of LP measurements for designing more complex architectures of power amplifiers/transmitters may be further studied. For example, using a harmonic LP approach, synthesizing the appropriate loads at the fundamental and harmonic frequencies class F, inverse class F or class J amplifiers may be developed. Moreover, combining two or more amplifiers, transmitter architectures such as Doherty, Outphasing or Balanced amplifiers may be developed; these architectures require the individual devices to be combined in a determined fashion, for which knowing their amplitude and phase distortion as a function of input/output power is mandatory.

Further investigation about new architectures for load-pull systems, allowing the time for characterization to be optimized, such as the recently introduced envelope load-pull approach seems to be an interesting area of study. As mentioned in previous chapters, passive LP systems may be pre-calibrated, but their calibration procedure is too slow. Classical active LP systems cannot be calibrated and thus they have to be used in real-time systems. Envelope LP systems are pre-calibrated active LP systems, which can be calibrated considerably faster (seconds) than passive tuners (hours). The measurement of the device behavior is also much

faster than in classical passive and active LP systems. The operating methodology of the envelope LP system is similar to the active closed-loop LP approach; the major difference between these two techniques is the manner in which the traveling wave is modified before being fed back for the synthesis of the desired reflection coefficient at the DUT plane. The envelope LP approach utilizes external control variables, taking place at low-frequency or even DC, for modifying the phase and amplitude of the reflected traveling wave at RF/microwave frequencies. First efforts about this research topic are being conducted in the RF/microwave laboratory of CICESE Research Center [(Malfavaun-Gonzalez, 2016)].

Bibliographic references

- Aaen, P.; Pla, J.A.; Bridges, D.; Shumate, E. (2000). A wideband method for the rigorous low-impedance load-pull measurement of high-power transistors suitable for large-signal model validation. *56th Automatic Radio Frequency Techniques Group (ARFTG) Conference Digest. Boulder, CO, USA.*, pp. 163–169.
- Aaen, P.; Pla, J.A.; Wood, J. (2007). *Modeling and Characterization of RF and Microwave Power FETs*. Cambridge University Press, New York, NY. 326 pp.
- Abouts, Z.; Jones, C.; Knight, G.; Sheikh, A.; Lee, H.; Lees, J.; Tasker, P. (2005a). High power active harmonic load-pull system for characterization of high power 100-watt transistors. *2005 European Microwave Conference.*, pp. 1–4.
- Abouts, Z.; Lees, J.; Benedikt, J.; Tasker, P.J. (2005b). Active harmonic load-pull system for characterizing highly mismatched high power transistors. *IEEE Microwave Theory and Techniques International Symposium (MTT-IMS) Digest. Cherry Hill, NJ, USA.*, pp. 12 – 17.
- Agilent (2011). Specifying Calibration Standards and Kits for Agilent Vector Network Analyzers. *Application Note*.
- Aldoumani, A.; Williams, T.; Lees, J.; Tasker, P.J. (2014). Enhanced vector calibration of load-pull measurement systems. *83rd Automatic Radio Frequency Techniques Group Conference Digest. Tampa, FL, USA.*, pp. 1–4.
- Anritsu. (2014). Vector Star MS4640B Series. *Product Brochure.*, pp. 1 – 32.
- Bava, G.P.; Pisani, U.; Pozzolo, V. (1982). Active load technique for load-pull characterisation at microwave frequencies. *Electronics Letters.*, **18**(4): 178–180.
- Betts, L.; Bepalko, D. T.; Boumaiza, S. (2011). Application of Agilent’s PNA-X Nonlinear Vector Network Analyzer and X-Parameters in Power Amplifier Design. *Agilent Technologies White Paper*.
- Bindra, A. (2015). Wide-Bandgap-Based Power Devices: Reshaping the power electronics landscape. *IEEE Power Electronics Magazine*, **2**(1): 108–116.
- Bonino, S.; Teppati, V.; Ferrero, A. (2010). Further improvements in real-time load-pull measurement accuracy. *IEEE Microwave and Wireless Components Letters*, **20**(2): 121–123.
- Calvillo-Cortes, D.A. (2014). *Energy Efficient and Compact RF High-Power Amplifiers*. Ph.D. Thesis. Delft University of Technology., Delft, The Netherlands. 191 pp.
- Camarchia, V.; Teppati, V. (2007). Microwave measurements part 2: Nonlinear measurements. *IEEE Instrumentation and Measurement Magazine*, **10**(3): 34 – 39.
- Colantonio, P.; Giannini, F.; Limiti, E. (2009). *High Efficiency RF and Microwave Solid State Power Amplifiers*. John Wiley and Sons, United Kingdom. 494 pp.

- Cree (2015a). CGH40010 Power Transistor. *Data Sheet*, pp. 1–15.
- Cree (2015b). CGH40045 Power Transistor. *Data Sheet*, pp. 1–16.
- Cripps, S.C. (1983). A theory for the prediction of GaAs FET load-Ppull power contours. *IEEE Microwave Theory and Techniques International Symposium (MTT-IMS) Digest. Boston, MA, USA.*, pp. 221–223.
- Cripps, S. (2006). *RF Power Amplifiers for Wireless Communications*. Artech House, Norwood, MA, first edition. 456 pp.
- Cusack, J.; Perlow, S.; Perlman, B. (1974). Automatic load contour mapping for microwave power transistors. *IEEE Microwave Theory and Techniques International Symposium (MTT-IMS) Digest. Atlanta, GA, USA.*, pp. 269–271.
- Darraj, R.; Ghannouchi, F.M.; Hammi, O. (2012). Generic load-pull-based design methodology for performance optimisation of doherty amplifiers. *IET Science, Measurement and Technology*, **6**(3): 132 – 138.
- Davidson, A.; Strid, E. (1989). Achieving greater on-wafer S-parameter accuracy with the LRM calibration technique. *34th Automatic Radio Frequency Techniques Group (ARFTG) Conference Digest. Tempe, AR, USA.*, pp. 61 – 66.
- Davidson, A.; Jones, K. (1990). LRM and LRRM calibrations with automatic determination of load inductance. *36th Automatic Radio Frequency Techniques Group (ARFTG) Conference Digest. Monterrey, CA, USA.*, pp. 57 – 63.
- De Groote, F.; Teyssier, J.P.; Gasselings, T.; Jardel, O.; Verspecht, J. (2008). Introduction to measurements for power transistor characterization. *IEEE Microwave Magazine*, **9**(3): 70–85.
- Deshours, F.; Bergeault, E.; Blache, F.; Villotte, J.-P.; Villeforceix, B. (1997). Experimental comparison of load-pull measurement systems for nonlinear power transistor characterization. *IEEE Transactions on Instrumentation and Measurement*, **46**(6): 1251–1255.
- Dobrowolsky, J.A. (1991). *Introduction to Computer Methods for Microwave Circuit Analysis and Design*. Artech House, Norwood, MA. 230 pp.
- Doerner, R.; Rumiantsev, A. (2005). Verification of the wafer-level LRM+ calibration technique for GaAs applications up to 110 GHz. *65th Automatic Radio Frequency Techniques Group Conference Digest. Long Beach, CA, USA.*, pp. 5–9.
- Dunleavy, L.; Baylis, C.; Curtice, W.; Connick, R. (2010). Modeling GaN: Powerful but Challenging. *IEEE Microwave Magazine*, **11**(6): 82–86.
- Engen, G.F.; Hoer, C.A. (1979). Thru-Reflect-Line: an improved technique for calibrating the dual six port automatic network analyzer. *IEEE Transactions Microwave Theory and Techniques*, **27**(12): 987–993.
- Eul, H.; Schiek, B. (1988). Thru-Match-Reflect: one result of a rigorous theory for de-embedding and network analyzer calibration. *Proceedings of 18th European Microwave Conference (EuMC). Stockholm, Sweden.*, pp. 909 – 914.

- Eul, H.; Schiek, B. (1991). A generalized theory and new calibration procedures for network analyzer self-calibration. *IEEE Transactions on Microwave Theory and Techniques*, **39**(4): 724 – 731.
- Ferrero, A. (2011). High power load pull measurements: Today technologies and tomorrow challenges. *78th Automatic Radio Frequency Techniques Group (ARFTG) Conference Digest. Tempe, AZ, USA.*, pp. 1–3.
- Ferrero, A.; Pirola, M. (2008). Harmonic load-pull techniques: An overview of modern systems. *IEEE Microwave Magazine*, **14**(4): 116–123.
- Ferrero, A.; Pisani, U. (1993). An improved calibration technique for on-wafer large-signal transistor characterization. *IEEE Transactions on Instrumentation and Measurement*, **42**(2): 360 – 364.
- Ferrero, A.; Pissani, U. (1992). Two-port network analyzer calibration using an unknown Thru. *IEEE Microwave and Guided Wave Letters*, **2**(12): 505 – 506.
- Ferrero, A.; Teppati, V. (2001). Accuracy evaluation of on-wafer load-pull measurements. *IEEE Transactions on Microwave Theory and Techniques.*, **49**(1): 39–43.
- Focus-Microwave (1994). Basics on Load Pull and Noise Measurements. *Application Note 8*, pp. 1–8.
- Ghannouchi, F.M.; Hashmi, M.S. (2011). Load-pull techniques and their applications in power amplifiers design. *IEEE Bipolar/BiCMOS Circuits and Technology Meeting (BCTM). Atlanta, GA, USA.*, pp. 133–137.
- Ghannouchi, F.M.; Hashmi, M.S. (2013). *Load-Pull Techniques with Applications to Power Amplifier Design*. Springer, New York, NY. 326 pp.
- Ghannouchi, F.M.; Hashmi, M.S.; Bensmida, S.; Helaoui, M. (2010). Loop enhanced passive source- and load-pull technique for high reflection factor synthesis. *IEEE Transactions on Microwave Theory and Techniques*, **58**(11): 2952–2959.
- Golio, M. (2010). *The RF and Microwave Handbook*. CRC, Danvers, MA. 1350 pp.
- Gonzalez, G. (1997). *Microwave Transistor Amplifiers: Analysis and Design*. Prentice hall, Upper Saddle River, NY, second edition. 413 pp.
- Ha, T. T. (2010). *Theory and design of digital communication systems*. Cambridge University Press, United Kingdom. 629 pp.
- Hashmi, M.S.; Ghannouchi, F.M. (2011). Highly reflective load-pull. *IEEE Microwave Magazine*, **12**(4): 96–107.
- Hashmi, M.S.; Ghannouchi, F.M. (2013). Introduction to load-pull systems and their applications. *IEEE Instrumentation and Measurement Magazine*, **16**(1): 30–36.
- Hayden, L. (2006). An enhanced Line-Reflect-Reflect-Match calibration. *67th Automatic Radio Frequency Techniques Group (ARFTG) Conference Digest. San Francisco, CA, USA.*, pp. 143 – 149.

- Heuermann, H.; Rumiantsev, A. (1995). Advanced on-wafer multiport calibration methods for mono- and mixed-mode device characterization. *63rd Automatic Radio Frequency Techniques Group (ARFTG) Conference Digest. Fort Worth, TX, USA.*, pp. 91–96.
- Hiebel, M. (2007). *Fundamentals of Vector Network Analysis*. Rohde and Swartz, Munchen, Germany. 420 pp.
- Hiebel, M. (2008). Vector network analyzer (VNA) calibration: The basics. *Rhode and Swartz Application Note*.
- Keysight-Technologies. (2015). PNA Family of Microwave Network Analyzers. *Configuration Guide.*, pp. 1 – 36.
- Kurokawa, K. (1965). Power Waves and the Scattering Matrix. *IEEE Transactions on Microwave Theory and Techniques*, **13**(2): 194–202.
- Malfavaun-Gonzalez, E.J. (2016). *Caracterización en gran señal de transistores y amplificadores de potencia utilizando un sistema Load-Pull activo*. M.Sc. Thesis (in Process). Center for Scientific Research and Higher Education of Ensenada, Baja California (CI-CESE), Ensenada, Mexico.
- Marks, R. (1991). Multiline method for network analyzers calibration. *IEEE Transactions on Microwave Theory and Techniques*, **39**(7): 92–96.
- Maury-Microwave (2002). A sub 1 ohm load pull quarter-wave prematching network based on a two-tier TRL calibration. *Application Note 5A-036*.
- Maury-Microwave (2009). Introduction to tuner-based measurement and characterization. *Application Note 5C-054*, pp. 1–8.
- Maury-Microwave (2011). Vector-receiver load pull measurement. *Application Note 5A - 051*.
- McCune, E. (2010). Modern cellular wireless signals. *75th Automatic Radio Frequency Techniques Group (ARFTG) Conference Digest. Anaheim, CA, USA.*, pp. 1 – 7.
- Molina-Cesena, M. (2016). *Extracción de las fuentes de corriente de desplazamiento de transistores GaN utilizando un analizador de redes no-lineal*. M.Sc. Thesis (in Process). Center for Scientific Research and Higher Education of Ensenada, Baja California (CICESE), Ensenada, Mexico.
- Muller, J.E.; Gyselinckx, B. (1994). Comparison of active versus passive on-wafer load-pull characterisation of microwave and mm-wave power devices. *IEEE Microwave Theory and Techniques International Symposium (MTT-IMS) Digest. San Diego, CA, USA.*, **24**(9): 1077–1080.
- Nuttinck, S.; Gebara, E.; Laskar, J.; Harris, H.M. (2001). Study of self-heating effects, temperature-dependent modeling, and pulsed load-pull measurements on GaN HEMTs. *IEEE Transactions on Microwave Theory and Techniques*, **60**(6): 2413–2420.
- Pedro, J.C.; Nunes, L.C.; Cabral, P.M. (2015). A Simple method to estimate the output power and efficiency load-pull contours of class-B power amplifiers. *IEEE Transactions on Microwave Theory and Techniques*, **63**(4): 1239–1249.

- Pedro, J.C.; Borges-Carvalho, N. (2002). *Intermodulation Distortion in Microwave and Wireless Circuits*. Artech House, Norwood, MA. 413 pp.
- Pierpoint, M.; Pollard, Roger.D.; Richardson, J.R. (1986). An automated measurement technique for measuring amplifier load-pull and verifying large-signal device models. *IEEE Microwave Theory and Techniques International Symposium (MTT-IMS) Digest*. Cherry Hill, NJ, USA., pp. 625–628.
- Pirola, M.; Teppati, V. (2007). Microwave measurements part 1: Linear measurements. *IEEE Instrumentation and Measurement Magazine*, **10**(2): 14 – 19.
- Pisani, U.; Ferrero, A. (1996). A unified calibration algorithm for scattering and load pull measurement. *Proceedings of the IEEE Instrumentation and Measurement Technology Conference.*, pp. 1250–1253.
- Pozar, D. (2005). *Microwave Engineering*. Willey, New York., third edition. 730 pp.
- Pulido-Gaytan, M.A. ; Reynoso-Hernandez, J.A.; Loo-Yau, J.R.; Maya-Sanchez,M.C. (2015a). The Impact of Knowing the Impedance of the Lines Used in the TRL Calibration on the Load-Pull Characterization of Power Transistors. *86th Automatic Radio Frequency Techniques Group (ARFTG) Conference Digest*. Atlanta, GA, USA., pp. 5–9.
- Pulido-Gaytan, M.A. ; Reynoso-Hernandez, J.A.; Maya-Sanchez,M.C.; Loo-Yau, J.R. (2015b). Calibration of a Real-Time Load-Pull System Using the Generalized Theory of the TRM Technique. *87th Automatic Radio Frequency Techniques Group (ARFTG) Conference Digest*. San Francisco, CA, USA., pp. 1–4.
- Pulido-Gaytan, M.A. ; Reynoso-Hernandez, J.A.; Zarate-de Landa,A.; Loo-Yau, J.R.; Maya-Sanchez,M.C. (2013). Vector network analyzer calibration using a line and two offset reflecting loads. *IEEE Transactions on Microwave Theory and Techniques*, **61**(9): 3417–3423.
- Pulido-Gaytan, M.A. ; Reynoso-Hernandez, J.A.; Zarate-de Landa,A.; Loo-Yau, J.R.; Maya-Sanchez,M.C. (2014). LZZM: An extension of the theory of the LZZ calibration technique. *84th Automatic Radio Frequency Techniques Group (ARFTG) Conference Digest*. Boulder, CO, USA., pp. 5–9.
- Pulido-Gaytan, M.A. ; Reynoso-Hernandez, J.A.; Zarate-de Landa,A.; Loo-Yau, J.R.; Maya-Sanchez,M.C. (2015c). On the implementation of the LZZ calibration technique in the S-parameters measurement of devices mounted in test fixtures. *85th Automatic Radio Frequency Techniques Group (ARFTG) Conference Digest*. Phoenix, AR, USA., pp. 5–9.
- Pulido-Gaytan, M.A. ; Reynoso-Hernandez, J.A.; Zarate-de Landa,A.; Loo-Yau, J.R.; Maya-Sanchez, M.C. (2015d). Generalized theory of the Thru-Reflect-Match calibration technique. *IEEE Transactions on Microwave Theory and Techniques*, **63**(5): 1693–1699.
- Pulido-Gaytan, M.A. (2012). *Investigación e Implementación de la Técnica de Calibración Line-Reflect-Reflect-Match (LRRM)*. Tesis de Maestría. Centro de Investigación y de Educación Superior de Ensenada, Baja California (CICESE)., Ensenada, México. 137 pp.
- Purroy,F.; Pradell,L. (2001). New theoretical analysis of the LRRM calibration technique for vector network analyzers. *IEEE Transactions on Instrumentation and Measurement*, **50**(5): 1307 – 1314.

- Qian, L.; Melde, K. (2007). Broadband on-wafer calibrations comparison for accuracy and repeatability on coplanar waveguide structures. *IEEE Electrical Performance of Electronic Packaging (EPEP) Symposium. Atlanta, GA, USA.*, **1**(1): 315 – 318.
- Rahola, J. (2008). Power Waves and Conjugate Matching. *IEEE Transactions on Circuits and Systems II: Express Briefs*, **1**(1): 1205–1215.
- Reynoso-Hernandez, J.A. (2003). Unified method for determining the complex propagation constant of reflecting and nonreflecting transmission lines. *IEEE Microwave and Wireless Components Letters*, **13**(8): 351–353.
- Reynoso-Hernandez, J.A.; Pulido-Gaytan, M.A. (2015). VNA Calibration Techniques: Theory and Applications. *ARFTG-NIST Short Course on Microwave Measurements. 86th Automatic Radio Frequency Techniques Group (ARFTG) Conference. Atlanta, GA, USA.*, pp. 1 – 48.
- Reynoso-Hernandez, J.A.; Pulido-Gaytan, M.A.; Maya-Sanchez, M.C.; Loo-Yau; J.R. (2012). What can the ABCD parameters tell us about the TRL? *79th Automatic Radio Frequency Techniques Group Conference Digest. Montreal, QB, Canada.*, pp. 1–4.
- Reynoso-Hernandez, J.A.; Pulido-Gaytan, M.A.; Zarate-de Landa, A.; Zuniga-Juarez, J.E.; Monjardin-Lopez, J.R.; Garcia-Osorio, A.; Orozco-Navarro, D.; Loo-Yau; J.R.; Maya-Sanchez, M.C. (2013). Using lines of arbitrary impedance as standards on the TRL calibration technique. *81st Automatic Radio Frequency Techniques Group (ARFTG) Conference Digest. Long Beach, CA, USA.*, pp. 1–4.
- Roblin, P. (2011). *Nonlinear RF Circuits and Nonlinear Vector Network Analyzers: Interactive Measurement and Design Techniques*. Cambridge University Press, New York, NY. 296 pp.
- Rogers (2015). RO4000 Series High Frequency Circuit Materials. *Data Sheet*, pp. 1–4.
- Root, D.; Verspecht, J.; Horn, J.; Marcu, M. (2013). *X-Parameters: Characterization, Modeling, and Design of Nonlinear RF and Microwave Components*. Cambridge University Press, United Kingdom. 219 pp.
- Rudolph, M.; Fager, C.; Root, D.E. (2011). *Nonlinear Transistor Model Parameter Extraction Techniques*. Cambridge University Press., Cambridge, UK. 413 pp.
- Rumiantsev, A.; Ridler, N. (2008). Vector network analyzer calibration. *IEEE microwave magazine*, **21**(3): 86–99.
- Rytting, D. (2004). Network analyzer error models and calibration methods. *Application Note*.
- Safwat, A.; Hayden, L. (2001). Sensitivity analysis of calibration standards for SOLT and LRRM. *58th Automatic Radio Frequency Techniques Group Conference Digest. San Diego, CA, USA.*, pp. 1 – 10.
- Saini, R.S.; Woodington, S.; Lees, J.; Benedikt, J.; Tasker, P.J. (2010). An intelligence driven active loadpull system. *75th Automatic Radio Frequency Techniques Group (ARFTG) Conference Digest. Anaheim, CA, USA.*, pp. 1 – 4.

- Scholz, R.F. ; Korndorfe,F. ; Senapati, B.; Rumiantsev, A. (2004). Advanced technique for broadband on-wafer rf device characterization. *63th Automatic Radio Frequency Techniques Group (ARFTG) Conference Digest. Fort Worth, TX, USA.*, pp. 91–96.
- Secci, F.; Perlow, M.; Perlman, B.S. (1983). A computer controlled microwave tuner for automated load pull. *RCA Review*, **44**(4): 566–583,.
- Simon, H.J. (2010). Method of calibrating a network analyzer. *U.S. Patent No. 7,782,065*, pp. 1–15.
- Simpson, G. (2011). Hybrid active tuning load pull. *77th Automatic Radio Frequency Techniques Group (ARFTG) Conference Digest. Boston, MA, USA.*, pp. 1–4.
- Stancliff, R.B.; Poulin, D.B. (1979). Harmonic Load-Pull. *IEEE Microwave Theory and Techniques International Symposium (MTT-IMS) Digest. Orlando, FL, USA.*, pp. 185 – 187.
- Szhau, L.; Fager, C.; Kuylenstierna, D.; Angelov, I. (2013). LDMOS Modeling. *IEEE Microwave Magazine*, **14**(1): 108–116.
- Takayama, Y. (1976). A new load-pull characterization method for microwave power transistors. *IEEE Microwave Theory and Techniques International Symposium (MTT-IMS) Digest. Cherry Hill, NJ, USA.*, pp. 218 – 220.
- Teppati, V.; Ferrero, A. (2003). A new class of nonuniform, broadband, nonsymmetrical rectangular coaxial-to-microstrip directional couplers for high power applications. *IEEE Microwave and Wireless Components Letters*, **13**(4): 152–154.
- Teppati, V.; Ferrero, A. (2008). Microwave measurements part 3: Advanced non-linear measurements. *IEEE Instrumentation and Measurement Magazine*, **11**(6): 17 – 22.
- Teppati, V.; Ferrero, A.; Parena, D.; Pisani, U. (2007). Accuracy Improvement of real-time load-pull measurements. *IEEE Instrumentation and Measurement Magazine*, **56**(2): 610–613.
- Teppati, V.; Bolognesi, C.R. (2012). Evaluation and reduction of calibration residual uncertainty in load-pull measurements at millimeter-wave frequencies. *IEEE Transactions on Instrumentation and Measurement*, **61**(3): 817–822.
- Tucker, R.S.; Bradley, P.D. (1984). Computer-aided error correction of large-signal load-pull measurements. *IEEE Transactions on Microwave Theory and Techniques*, **32**(3): 296–301.
- Van der Puije, P.D.; Mazumder, S.R. (1978). Two-signal method of measuring the large-signal S-parameter of transistors. *IEEE Transactions on Microwave Theory and Techniques*, **26**(6): 417 – 420.
- Velazquez-Ventura, A.; Lazaro, A.; Pradell-Cara, L.; Comeron-Tejero, A. (2003). Application of CAD load-pull techniques in mixer design. *Microwave and Optical Technology Letters*, **36**(4): 320–323.
- Wartenberg, S. A. (2002). *RF measurements of die and packages*. Artech house, Norwood, MA. 215 pp.

- Williams, T.; Wee, B.; Saini, R.; Mathias, S.; Bossche, M.V. (2014). A digital, PXI-based active load-pull tuner to maximize throughput of a load-pull test bench. *83rd Automatic Radio Frequency Techniques Group (ARFTG) Conference Digest. Tampa, FL, USA.*, pp. 1 – 4.
- Williams, D. F.; Marks, R. B. (1995). LRM probe-tip calibrations using nonideal standards. *IEEE Transactions on Microwave Theory Techniques*, **43**(2): 466–469.
- Williams, D.F. ; Marks, R.; Phillips, K.R. (1991). Translate LRL and LRM calibrations. *Microwaves and Rf*, **62**(8): 78 – 84.
- Wood, J. (2014). *Behavioral Modeling and Linearization of RF Power Amplifiers*. Artech House, Norwood, MA. 362 pp.
- Yifeng,W.; Parikh, P. (2006). High-power GaN HEMTs battle for vacuum tube territory. *Compound Semiconductor.*, **1**(1): 1–3.
- Zarate-de Landa, A. (2014). *Modeling of Microwave Transistors Using Artificial Neural Networks*. Ph.D. Thesis. Center for Scientific Research and Higher Education of Ensenada, Baja California (CICESE)., Ensenada, Mexico. 137 pp.
- Zarate-de Landa, A.; Reynoso-Hernandez, J.A.; Roblin, P.; Pulido-Gaytan, M.A.; Monjardin-Lopez, J.R.; Loo-Yau, J.R. (2013). On the determination of neural network based non-linear constitutive relations for quasi-static GaN FET models. *84th Automatic Radio Frequency Techniques Group (ARFTG) Conference Digest. Columbus, OH, USA.*, pp. 18–21.
- Zarate-de Landa, A.; Pulido-Gaytan, M.A.; Reynoso-Hernandez, J.A.; Roblin, P.; Loo-Yau, J.R. (2012). A neural network approach to smooth calibrated data corrupted from switching errors. *80th Automatic Radio Frequency Techniques Group (ARFTG) Conference Digest. Columbus, OH, USA.*, pp. 29–30.
- Zuñiga-Juarez, E. (2011). *Técnicas de Calibración LRL, LRM y LRRM para Corregir los Errores Sistemáticos del Analizador de Redes Vectorial y su Impacto en la Caracterización de Transistores de Altas Frecuencias*. Tesis de Maestría. Centro de Investigación y de Educación Superior de Ensenada, Baja California (CICESE)., Ensenada, México. 143 pp.
- Zuñiga-Juarez, J.E.; Reynoso-Hernandez, J.A.; Loo-Yau, J.R. (2009). Two-tier L-L de-embedding method for S-parameters measurements of devices mounted in test fixtures. *76th Automatic Radio Frequency Techniques Group (ARFTG) Conference Digest. Boston, MA, USA.*, pp. 1 – 5.